TARGETING CD133 IN ANDROGEN RECEPTOR INDIFFERENT, NEUROENDOCRINE DIFFERENTIATED AGGRESSIVE VARIANT PROSTATE CANCER

A DISSERTATION

SUBMITTED TO THE FACULTY OF THE

UNIVERSITY OF MINNESOTA

BY

PAIGE M. GLUMAC

IN PARTIAL FULFILLMENT OF THE REQUIREMENTS FOR THE

DEGREE OF DOCTOR OF PHILOSOPHY

ADVISOR: DR. AARON LEBEAU

JUNE 2019

Acknowledgements

I would like to express my sincere gratitude to my advisor, Dr. Aaron LeBeau, for his support, guidance, and encouragement over the last four years. He is truly an inspiring mentor and researcher with a glowing enthusiasm for science. I could always count on him to lighten the mood when experiments weren't going as planned and push me to question and explore further when my studies were successful. Additionally, he has been supportive of my personal and professional decisions over the years and I am truly fortunate and grateful to have been trained under his guidance.

I am also very grateful to the members of our lab that have come and gone since my arrival. I would especially thank Dr. Hong Zhou for training me when I first joined the lab. I would also thank Mariya Shapovalova, Hallie Hintz, and Joseph Gallant for their helpful advice, constructive criticism, openness, and companionship during my years in the Aaron's lab. I would also like to thank the members of my dissertation committee, Dr. Hiroshi Hiasa, Dr. Cheuk Leung, and Dr. Scott Dehm, for their guidance and helpful suggestions throughout my graduate career.

I would also like to thank the Department of Pharmacology for their support and encouragement during my time in the Pharmacology Graduate Program. In particular, I would like to thank Dr. Jill Siegfried, Dr. Colin Campbell, and Dr. Kevin Wickman for all of their advice, patience, and assistance during my time in this program.

Abstract

An increasing number of men are developing a lethal, non-androgen receptor (AR) driven form of prostate cancer (PCa) known as aggressive variant prostate cancer (AVPC). Therapeutic options for AVPC are limited, and the development of novel therapeutics is significantly hindered by the inability to accurately monitor the disease through imaging. This underscores the critical need to develop improved imaging agents for AVPC. Targeted imaging agents, such as those developed for prostate-specific membrane antigen (PSMA) have made significant progress in imaging metastatic prostate adenocarcinoma; however, numerous studies have shown that non-AR driven prostate cancer does not express PSMA. Thus, there is an urgent unmet need to identify novel antigens and targeted imaging agents for the detection and monitoring of this lethal form of PCa.

In these studies, we have identified the pentaspan transmembrane glycoprotein, CD133, as a targetable antigen that is overexpressed on the surface of non-AR driven, neuroendocrine-differentiated prostate cancer. Additionally, we have developed a novel antibody, termed HA10 IgG, which was found to bind to a glycosylation-independent epitope on CD133. HA10 IgG was validated in numerous cell lines and demonstrated similar or more accurate binding to CD133 when compared to a frequently used commercial antibody *in vitro*. To assess the imaging potential of HA10 IgG, the antibody was labeled for near-infrared and positron emission tomography imaging. Our CD133 probe was validated in imaging studies and shown to be highly selective for CD133-expressing PCa cells,

suggesting its potential as a non-invasive imaging agent for lethal, non-AR-driven AVPC.

Table of Contents

List of Tables

List of Figures

Abbreviations

ΔNp63: a member of p53 transcription factors family

^{11}C: carbon-11

^{18}F: fluorine-18

^{89}Zr: zirconium-89

^{99m}Tc: technetium-99m

^{99m}Tc-MDP: technetium-99m methyl diphosphonate

ADT: androgen deprivation therapy

AR: androgen receptor

ATCC: American Type Culture Collection

AVPC: aggressive variant prostate cancer

CD133: cluster of differentiation 133

CHGA: chromogranin A

CK: cytokeratin

CRPC: castration-resistant prostate cancer

CSC: cancer stem cell

CT: computed tomography

DRE: digital rectal exam

EBRT: external beam radiation therapy

EC1: extracellular domain 1 (N-terminal domain)

EC2: extracellular domain 2 (extracellular loop 1)

EC3: extracellular domain 3 (extracellular loop 2)

ELISA: enzyme-linked immunosorbent assay

EnzR: enzalutamide resistant

FBS: fetal bovine serum

FDA: U.S. Food and Drug Administration

FDG: [^{18}F]-fluorodeoxyglucose

HIF-1α: hypoxia inducible factor-1α

HSP: heat shock protein

IC1: intracellular domain 1 (intracellular loop 1)

IC2: intracellular domain 2 (intracellular loop 2)

IC3: intracellular domain 3 (C-terminal domain)

IHC: immunohistochemistry

IP: immunoprecipitant

IRB: Institutional Review Board

IRT: internal radiation therapy

MRI: magnetic resonance imaging

NaF: [^{18}F]-sodium fluoride

NIR: near-infrared

NSE: neuron specific enolase

PAP: prostatic acid phosphatase

PCa: prostate cancer

PCBN: Prostate Cancer Biorepository Network

PDX: patient-derived xenograft

PET: positron emission tomography

PROM1: prominin-1

PSA: prostate-specific antigen

PSMA: prostate-specific membrane antigen

qRT-PCR: quantitative reverse-transcriptase polymerase chain reaction

scFv: single chain variable fragment

SN: supernatant

SPR: surface plasmon resonance

TGFβ: transforming growth factor-beta

Theranostic: therapeutic and diagnostic

TMA: tissue microarray

Trop2: tumor-associated calcium signal transducer 2

TRUS: transrectal ultrasound

TURP: transurethral prostate resection

W: pooled washes

CHAPTER I: Background

Impact of Prostate Cancer

Prevalence and Mortality

Prostate cancer (PCa) is the most common non-cutaneous cancer in American men. Approximately 11.6% of men will be diagnosed with PCa within their lifetime and the American Cancer Society currently estimates that there will be approximately 174,650 new cases of PCa in 2019 alone (1). National expenditures for PCa care reached approximately $15.3 billion in 2018, signifying the tremendous personal and economic impact PCa has on society. Despite its high prevalence, PCa is a relatively treatable disease with roughly 98% of patients achieving a 5-year survival (1). Unfortunately, if the cancer has progressed to metastatic disease, the 5-year survival rate drops significantly to a striking 30% (1, 2), indicating the importance of developing better theranostic agents to detect and treat metastatic PCa.

Progression of Prostate Cancer with Response to Therapy

There are three primary stages of PCa progression: 1) localized, 2) regional, and 3) distant disease. Localized PCa is defined as PCa which has not left the confines of the prostate gland. Regional PCa is when the cancer has only spread to neighboring organs such as the seminal vesicles or nearby lymph nodes and distant PCa is described as PCa which has spread to distant sites such as the bones, viscera, and/or distant lymph nodes. Approximately 90% of PCa cases are identified in the localized and regional stages and the average age of diagnosis is approximately 66 years old (2). Since PCa is often a slow growing disease, many

men who are older or present with additional health problems will never receive treatment for their cancer. This is because the treatment for slow growing, local PCa can often times pose more risk to the patient's overall health than the cancer itself (3). The current standard of care in these cases is active surveillance in which the cancer is monitored for signs of rapid progression and metastasis. Monitoring for signs of PCa progression may include prostate-specific antigen (PSA) blood tests, digital rectal exams (DREs), biopsies, and potentially imaging (4-6).

If the initial screening or continuous active surveillance suggests that the PCa is suspected to pose a greater threat than treatment, such as in the cases of a more aggressive pathology or presentation in a younger man, then the first line of treatment is usually surgery, radiation therapy, or a combination of the two. Surgery, often referred to as a prostatectomy, includes direct removal of the prostate gland and sometimes other surrounding tissues that the cancer may have spread to. Alternatively, radiation therapy uses high-energy radiation to kill the remaining cancer cells. There are two main types of radiation therapy, external-beam radiation therapy (EBRT) and internal radiation therapy (IRT). The major difference between these two types of therapy is the location of the radiation source. EBRT uses an externally-located X-ray producing machine to focus radiation onto a specific cancerous region of the body, while IRT requires the implantation of radioactive sources directly into the cancerous regions of the body (3). While surgery and radiation therapy are often curative for most men, approximately 20-30% of patients develop PCa recurrence.

Androgen deprivation therapy (ADT) is the current standard of care for men that present with recurrent and/or metastatic disease and as a neoadjuvant to EBRT for men with localized and/or regional disease (3, 7). Re-activation of the androgen receptor (AR) signaling axis aft ADT is a well-known key player in PCa progression. Androgens, such as testosterone and dihydrotestosterone, bind to AR which promotes dimerization, nuclear translocation, and subsequent gene activation and cancer cell growth (Figure 1) (8). ADT aims to prevent AR signaling by actively reducing the number of circulating androgens that are available to bind to and activate AR (9-11). Most men display a transient reduction of PCa symptoms, including lowered PSA and tumor regression, however, most of these patients eventually progress to castration-resistant PCa (CRPC) which is a hormone-insensitive form of the disease (Figure 2) (12, 13).

CRPC is a biochemical (rising PSA) or clinical (new or larger lesions) progression of the disease despite castrate levels of androgens in the blood. Strategies to combat CRPC often involve cutting off alternate mechanisms of AR signaling using second generation anti-androgens. Two of the most notable second-generation anti-androgens are enzalutamide which directly blocks AR and abiraterone which prevents adrenal gland hormone synthesis. While second generation anti-androgens were initially approved for CRPC, recent Phase II and III trials have documented the success of these agents in nonmetastatic PCa indicating a shift in the treatment landscape (14, 15). Unfortunately, many patients display inherent resistance to these therapies, and others acquire resistance after

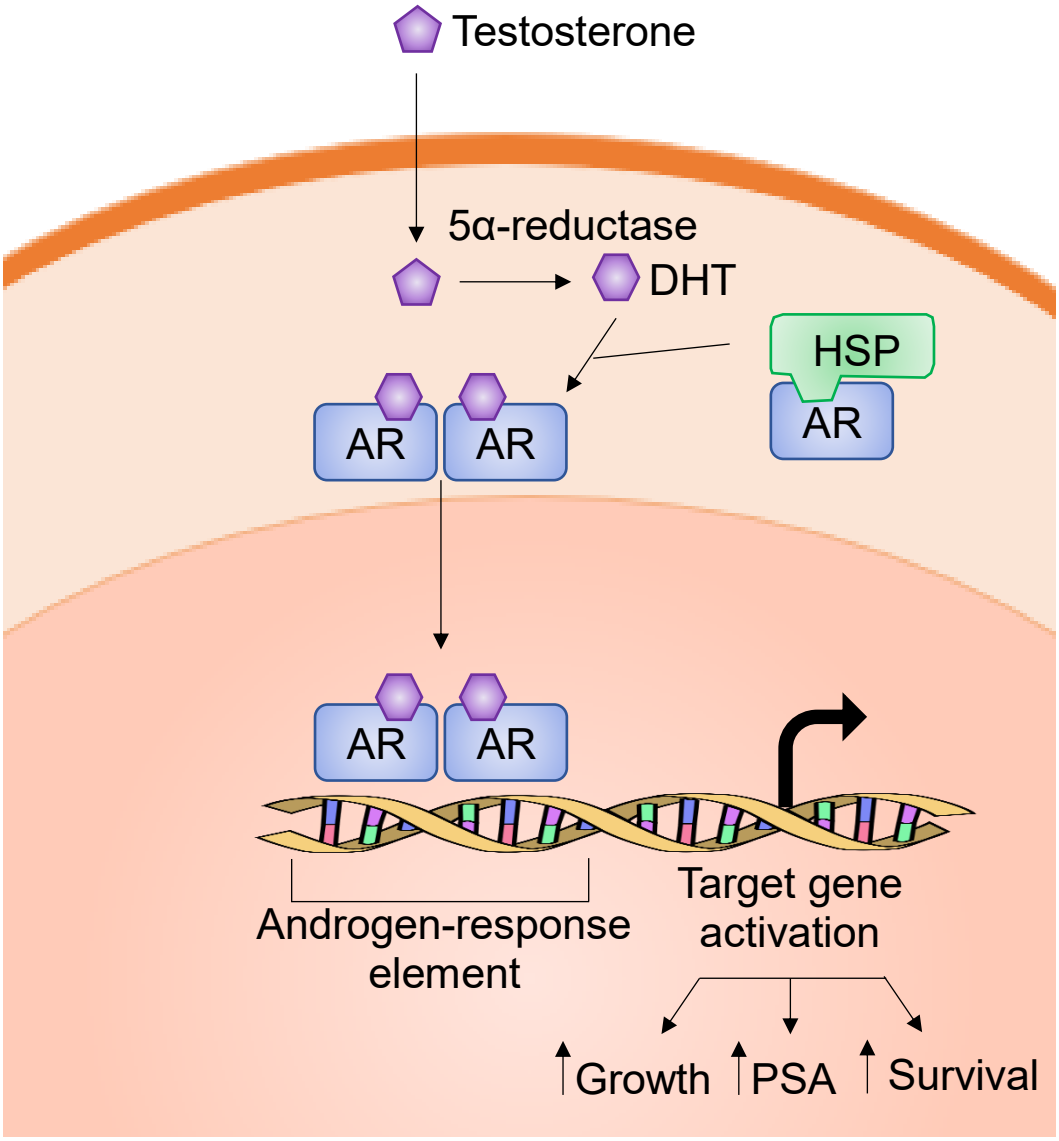

Figure 1. Schematic of the AR signaling axis and PCa progression. Free testosterone or dihydrotestosterone enters the prostate cells and binds to AR. AR dissociates from heat shock proteins (HSPs) and dimerizes to facilitate nuclear translocation. Dimerized AR binds to androgen-response elements in the promoter regions of target genes which leads to biological responses including increased growth, survival, and the production of PSA. This image was reproduced from previous publications (8, 16).

months of use. Additionally, in 2010, the U.S. Food and Drug Administration (FDA) approved the immunotherapy agent, Sipuleucel-T, for treatment of advanced PCa (17). Although Sipuleucel-T did display a mild survival benefit in CRPC patients, there seemed to be very little effect on slowing disease progression (18-20). Similarly, chemotherapy has also been shown to prolong overall survival but is often paired with unpleasant side effects and reduced quality of life. This lethal stage of the disease continuum is known as aggressive variant PCa (AVPC) and can occur with or without AR re-activation (Figure 2).

More specifically, AVPC is a broad-spectrum form of PCa defined as CRPC with at least one of the following features: 1) histologic evidence of small-cell neuroendocrine differentiated PCa (pure or mixed), 2) the presence of exclusively visceral metastases, 3) radiographically predominant lytic bone metastases by plain x-ray or CT scan, 4) bulky (≥ 5 cm) lymphadenopathy or bulky (≥5 cm) high-grade (Gleason ≥ 8) tumor mass in prostate/pelvis, 5) low PSA (≤ 10 ng/mL) at initial presentation (prior to ADT or at symptomatic progression in the castrate setting) plus high volume (≥ 20) bone metastases, 6) presence of neuroendocrine markers on histology (positive staining of chromogranin A (CHGA) or synaptophysin) or in serum (abnormal high serum levels for CHGA or gastrin-releasing peptide) at initial diagnosis or at progression, plus any of the following in the absence of other causes: (a) elevated serum LDH (≥ 2 × ULN), (b) malignant hypercalcemia, (c) elevated serum CEA (≥ 2 × ULN), 7) short interval (≤ 6 months) to androgen-independent progression following the initiation of hormonal therapy

with or without the presence of neuroendocrine markers (21-23). Due to deficiencies in previously used advanced PCa definitions, such as anaplastic, AR-independent, treatment-induced, or neuroendocrine PCa, AVPC has been adopted as a term which includes all of the aforementioned pathologies (22). Despite the fatal prognosis of AVPC, the currently available imaging strategies are often insufficient to accurately detect AVPC lesions and evaluate overall disease progression. The lack of proper diagnostic agents is a major clinical barrier to developing effective therapeutics for this disease. Due to the heterogeneity of AVPC, it has been exceedingly challenging to identify targetable biomarkers that are reliably expressed on the lesions of AVPC patients. Further efforts are urgently needed to identify biomarkers of AVPC and define their relevance in specific AVPC patient populations for improved therapeutic and diagnostic (theranostic) development.

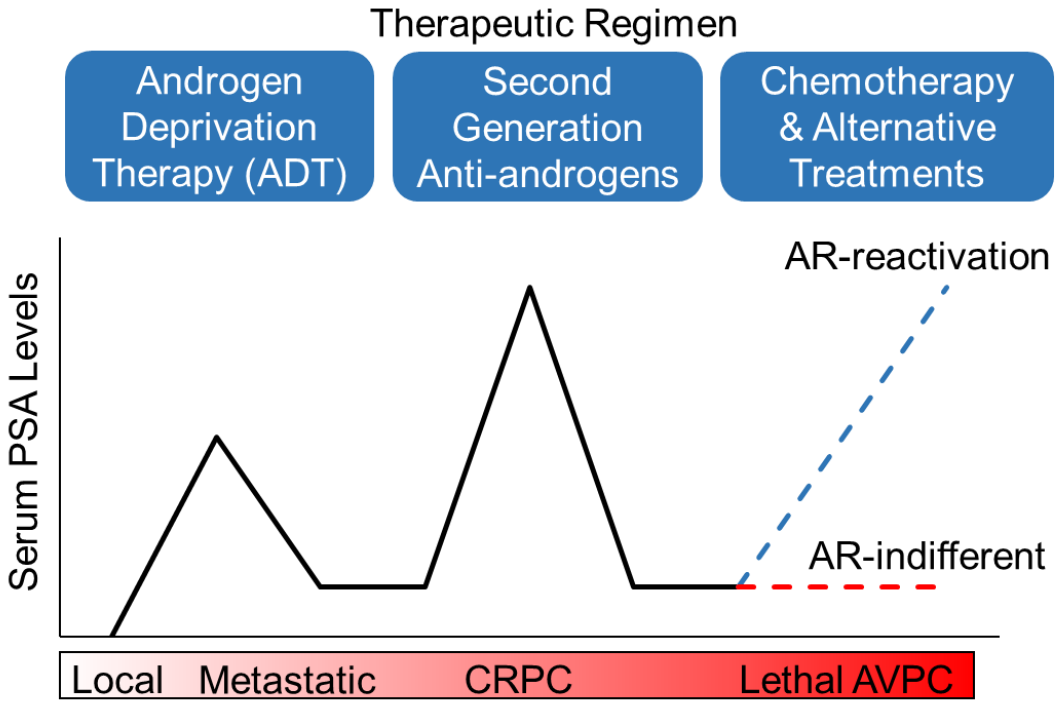

Figure 2. Chart displaying PCa progression with response to therapy. High-risk local or metastatic disease are treated with ADT. While initially responsive, patients eventually develop CRPC. Second generation anti-androgens are given to further prolong lifespan, however, patients eventually acquire resistance to these therapies as well and progress to lethal AVPC. Lethal AVPC can develop with or without AR-reactivation. The only treatment options available for AVPC are chemotherapy and palliative care, neither of which can cure the disease. This image was reproduced from previous literature (24).

Current Detection and Disease Monitoring Approaches

Screening and Staging of Prostate Cancer

Early signs of PCa are often identified by preliminary screening assessments such as the PSA blood test and the DRE. The U.S. Preventative Services Task Force recommends screening for PCa in men between the ages of 50-54 unless there are predefined risk factors that require earlier screening (Table 1). Similarly, regular screening may continue up to the age of 69 on a case by case basis (25, 26). While the use of PSA blood tests and DREs has been highly effective at identifying PCa during the first round of screening, these two tests are also prone to false positives (27-30). PSA is an androgen-regulated protease that is released by the secretory epithelial cells of the prostate gland. In healthy men, the primary function of PSA is to liquify semen during ejaculation and facilitate better sperm transport for reproduction, thus blood PSA levels remain relatively low. However, the basement membrane is often disrupted in PCa which results in significantly more PSA leaking into the blood (31). While high PSA levels are often observed in PCa patients, elevated blood PSA levels may also indicate various non-cancerous conditions as well, such as prostatitis, benign prostatic hyperplasia, urinary tract infections, and even prostate stimulation (32). Correspondingly, DREs are a blind exam in which a physician can manually palpate the prostate through the rectum and thus will not provide enough evidence to confirm a PCa diagnosis. An abnormal DRE exam may include observed nodule formation, asymmetric growth of the prostate, age inappropriate enlargement, or increased signs of

Table 1. Recommended PCa screening ages. This image was reproduced from previous literature (25, 26).

Begin Screening at Age:	Reason:
40	You have a family history of PCa
45	You are of African American decent
50	You have no family history and are not African American
55-69	Discuss with doctor on an individual basis
70+	Screening is not recommended

inflammation (33). When abnormalities are detected through one or both of these preliminary exams, a transrectal ultrasound (TRUS) and biopsy are provided to confirm the PCa diagnosis (26, 34).

The TRUS procedure requires the insertion of a small probe into the rectum which is used to visualize the prostate gland. TRUS is most often used for image guided prostate biopsies, however, it may also be used to measure the size of the prostate and make treatment decisions accordingly (34, 35). For the biopsy, most physicians will take 12 samples from various regions of the prostate to gain an accurate assessment of the overall pathology of the prostate. Pathologists analyze the biopsy samples and determine prostate tissue abnormality using the Gleason scoring system which signifies normal prostate tissue as grade 1 and very abnormal/cancerous tissue as grade 5. To account for heterogeneity within the prostate tissue, a grade is obtained from 2 separate regions of the tissue; the sum of the two grades yields the Gleason score (grade of region 1 + grade of region 2 = final Gleason score). Additionally, the grade of region 1 is the most frequently identified grade throughout the tissue sampled, thus Gleason scores of 3+4=7 are often less aggressive than 4+3=7 (36). Gleason scores can range anywhere from 2 to 10, however, scores below 6 are rarely indicative of PCa (34).

Imaging of Prostate Cancer

Once a PCa diagnosis has been confirmed, imaging tests are often used to assess the extent of cancer spread. CT and magnetic resonance imaging (MRI) may be used to visualize the soft tissues surrounding the prostate if the PCa is

suspected to be regionally located (34), however, both of these conventional imaging modalities are highly limited by their insensitivity for small nodal lesions and inability to detect bone lesions (37). The skeletal system is the second most common site for metastasis of PCa, surpassed only by the lymph nodes. In fact, approximately 80-90% of CRPC patients will develop bone metastases over the course of the disease (38-40). Bone scintigraphy (BS) using technetium-99m methyl diphosphonate (^{99m}Tc-MDP) is the current standard of care for detecting bone metastases in these patients due to its low energy, short half-life, and widespread availability (41, 42). Despite much of the initial success with ^{99m}Tc-MDP, most of the current guidelines using this imaging agent are based on 30-year old studies (37, 43, 44). Additionally, imaging with CT, MRI, and/or ^{99m}Tc-MDP are not sufficient to adequately identify visceral metastases that may be present in AVPC patients and thus are not accurate diagnostic and disease monitoring modalities for PCa patients in this stage of the disease.

Recent studies using positron emission tomography (PET)/CT have indicated that PET imaging may be superior over the current standard of care. The two most common PET radiotracers are [^{18}F]-fluorodeoxyglucose (FDG) and [^{18}F]-sodium fluoride (NaF). While FDG has been highly effective in the diagnosis and monitoring of other cancers (45, 46), it has been deemed unreliable and lacking specificity in PCa and therefore is not frequently used (Table 2) (37). Alternatively, recent meta-analyses have shown that NaF is more specific for bone lesions compared to ^{99m}Tc-MDP and can also detect some nodal lesions in late-stage

Table 2. Current clinical indication of PET radiotracers and their regulatory status.

Tracer	Target	Indication	Regulatory Status
FDG	Glucose metabolism	minimal use in PCa, only used when other tracers are not available	FDA approved, August 5, 2004
NaF	Osteoblastic activity	Known or suspected osseous lesions	FDA Approved, January 26, 2011
^{11}C-choline	Cell membrane metabolism	High-risk staging, biochemical relapse at high PSA levels	FDA approved, September 12, 2012
^{11}C-acetate	Fatty acid synthesis	Useful for monitoring recurrence after focal therapy, unreliable in biochemical recurrence, not as effective as other agents on the market	Under investigation
Fluciclovine	Amino acid transport	High-risk staging, biochemical relapse at high PSA levels	FDA approved, May 27, 2016
FDHT	AR	Early stage disease detection and prognosis	Under investigation
anti-PSMA ligands	PSMA	Multiple stages including biochemical relapse at low PSA	Under investigation

Abbreviations: FDG, [^{18}F]-fluorodeoxyglucose; NaF, [^{18}F]-sodium fluoride; FDHT: [^{18}F]-DHT; PSMA, prostate-specific membrane antigen; AR, androgen receptor; PSA, prostate-specific antigen

CRPC patients, displaying superiority over that current standard of care (42, 47-49). Unfortunately, the widespread use of NaF is substantially restricted due to its lack of availability and reimbursement challenges (50).

Other PET imaging agents have recently been approved or are currently under investigation for PCa detection and monitoring, including ^{18}F/^{11}C-choline, ^{11}C-acetate, [^{18}F]-fluciclovine, [^{18}F]-DHT (FDHT), and prostate-specific membrane antigen (PSMA)-targeted agents (Table 2) (51-55). Three different choline radiotracers are currently available for clinical use (^{18}F-fluoroethylcholine, ^{18}F-fluoromethylcholine, and ^{11}C-choline) although the ^{18}F-choline tracers are still under investigation for FDA approval. PCa cells use choline to synthesize a major constituent of the cell membrane, phosphatidylcholine, making it a promising target for diagnostic imaging (37). Most studies have indicated that choline is highly sensitive and specific for detecting lymph node and skeletal metastases in biochemically recurrent PCa patients, however, it also has a relatively high false positive rate of approximately 20% in nodal disease which is of major clinical concern (37, 56, 57). ^{11}C-acetate works similarly to ^{11}C-choline by exploiting the idea that PCa cells abundantly convert acetate into fatty acids which are then used to produce phosphatidylcholine (37, 58). Despite its similar mechanism of action, a meta-analysis of ^{11}C-acetate in PCa revealed that it was not as sensitive or specific as ^{11}C-choline and will likely not be used over the newer, more effective tracers (59). Fluciclovine, also referred to as FACBC, was recently approved for use in men with suspected PCa recurrence. Fluciclovine is an ^{18}F-labeled leucine

analog that is taken up by PCa cells through amino acid transporters (37, 51). Like the choline and acetate compounds, fluciclovine lacks specificity in early-stage PCa and displays more accurate detection during biochemical recurrence (60, 61). Some studies suggested that fluciclovine is more specific than choline tracers (62, 63), however, the disadvantages of this tracer limit its utility including a high false positive rate and its inability to fully replace BS to detect bone lesions in patients (64). FDHT is a fluorinated DHT molecule that binds directly to AR. Since PCa is primarily driven by AR in its early stages, it makes sense that an AR-targeted imaging agent would allow for better detection of PCa cells (37). Unfortunately, once a patient is treated with an AR antagonist, such as enzalutamide, the imaging agent will be displaced and rendered ineffective (65, 66). Similarly, this agent will not be if AR is not present such as in the case of AR-indifferent AVPC. Additionally, many of the previously mentioned imaging agents have not been tested in AVPC patients and have been shown to display prominent physiological uptake in the visceral organs of many patients (37, 52, 54, 55). Since AVPC patients are prone to metastatic lesions in the viscera, it is critical to develop a targeted diagnostic agent to accurately detect these lesions.

PSMA is a type II integral membrane glycoprotein that has received a lot of interest as a targetable biomarker for individualized PCa imaging and therapy. In general, PSMA has been correlated with metastasis, disease recurrence, and increased overall aggressiveness of the cancer (67, 68). Consequently, numerous efforts have been undertaken to develop PSMA-targeted theranostics for PCa. In

1996, the first anti-PSMA antibody, capromab pendetide or ProstaScint, was approved by the FDA as a diagnostic imaging agent for patients with biopsy-proven PCa who are at high-risk for pelvic lymph node metastasis and post-prostatectomy patients with a rising PSA a high clinical suspicion of metastatic disease (69). Unfortunately, ProstaScint was only able to bind to the intracellular epitope of PSMA which led to only modest clinical improvements over conventional imaging modalities (70, 71). Tremendous efforts have since been made to develop PSMA-targeted ligands that bind to the extracellular domain of the protein. These efforts include the development of the humanized anti-PSMA antibody, J591, which has been successful in multiple diagnostic PET imaging and radioimmunotherapy clinical trials (72-75). To date, zirconium-89 (^{89}Zr) has been the primary radiotracer for assessing the clinical PET imaging capabilities of J591. In fact, a recent study demonstrated that ^{89}Zr-J591 was able to accurately detect more bone and soft tissue lesions than BS, CT, and FDG-PET imaging, demonstrating its superiority over the currently available imaging modalities and radiotracers (76).

The development of PSMA-targeted ligands has laid the foundation for precision medicine in PCa and is working to tailor disease monitoring and treatment strategies to particular characteristics of each individual patient's cancer (77). While PSMA is typically correlated with more aggressive disease, it has been documented that neuroendocrine differentiation in PCa and prolonged ADT usage leads to PSMA suppression (78, 79), both of which are frequent occurrences in

AVPC. Therefore, the identification of new biomarkers of AVPC is necessary to ensure better diagnosis and disease monitoring in these patients.

Current Understanding of CD133 in the Prostate

CD133 Structure and Function

Cluster of differentiation 133 (CD133) is a 97-kDa pentaspan transmembrane glycoprotein that contains an extracellular N-terminal domain (EC1), five transmembrane segments which separate two small intracellular loops (IC1 and IC2), two large extracellular loops (EC2 and EC3), and an intracellular C-terminal domain (IC3) (Figure 3) (80). The two extracellular loops contain nine putative N-glycosylation sites; five on EC2 domain and four on EC3 domain (81). Glycosylation of CD133 yields a 120 kDa protein and alters the overall tertiary structure and stability of CD133 (82-84). Additionally, a few commercially available antibodies have been developed for CD133, however, most of them display poor efficacy in various assays. The two most commonly used antibodies, CD133/1 and CD133/2, only work in certain assays and bind to glycosylated epitopes which will be further addressed in Chapter II. Therefore, even these antibodies have limited utility in research and are not recommended for preclinical or clinical use.

The CD133 gene, Prominin 1 (PROM1), is located on chromosome 4 in humans and chromosome 5 in mice and is only approximately 60% homologous from primates to rodents (84, 85). Transcription of human CD133 is driven by five alternative promoters, three of which are located on CpG islands and are partially regulated by methylation. These promoter regions often result in alternative splicing of CD133 mRNA, resulting in CD133 isoforms with potentially unique roles (83, 86-88).

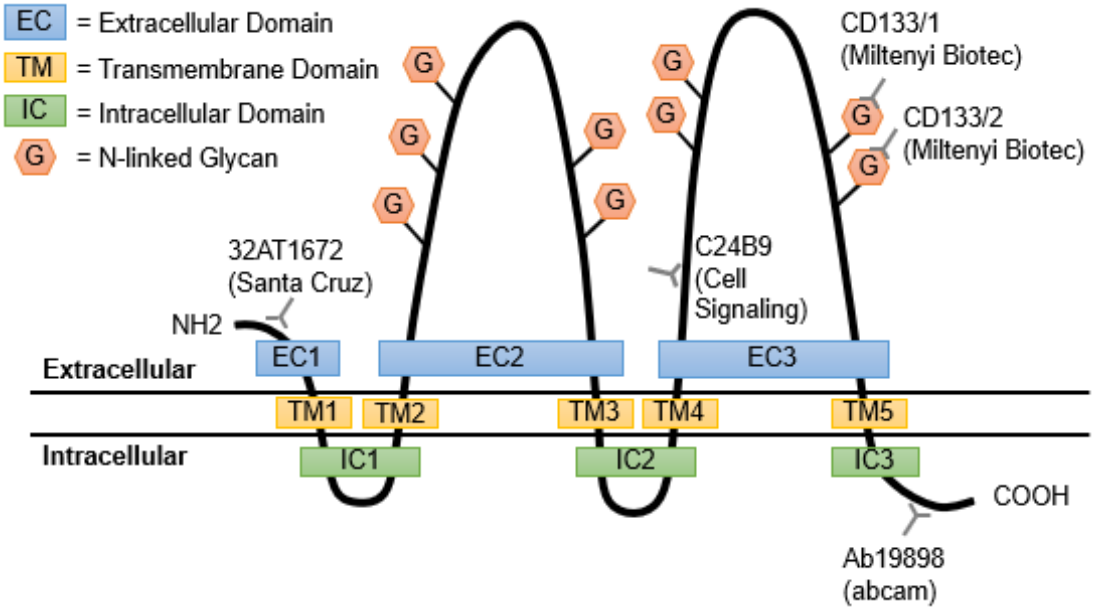

Figure 3. Schematic of the CD133 topology and putative epitopes of commercially available CD133 antibodies. The five transmembrane glycoprotein contains two large extracellular loops (EC2 and EC3), which comprise a total of nine N-linked glycan residues. The commonly used CD133/1 and CD133/2 epitopes are located on the EC3 region of CD133 and have the potential for epitope masking or antibody inaccessibility due to changes in glycosylation patterns.

The physiologic function of CD133 in normal biology and the progression of cancer remains elusive. CD133 is known to be preferentially localized in plasma membrane protrusions and microvilli, suggesting its involvement in membrane organization (89, 90). The subcellular localization of CD133 allows it to bind directly to cholesterol-containing lipid rafts where it can be involved in various signaling cascades (91, 92). Observations from CD133 knockout mice support the presumed role of CD133 as a scaffolding protein by showing that a lack of CD133 caused a defect in outer segment morphogenesis of the photoreceptor cells. While these mice remained viable and fertile, they experienced significant retinal degeneration and blindness (93). Other studies have additionally suggested a potential role of CD133 in determining cellular fate or maintaining stem cell-like properties (94-97), however, the precise molecular mechanisms for this are still unclear.

CD133 has primarily been described in the literature as stem cell marker of both normal and cancer stem cells (CSCs) in various cancers, including PCa (98-100). Many different molecular mechanisms have been investigated to better understand the modulation of CD133 in both normal and CSCs, but the data is highly contradictory. Studies from both normal and CSC lines have indicated that CD133 antibody reactivity is reduced when cells are in the G_1/G_0 portion of the cell cycle as opposed to the G_2/M phase of the cell cycle, suggesting some level of cell cycle dependence related to CD133 expression (101). Hypoxia in the stem cell and tumor microenvironment has also been shown to promote CD133 expression

via hypoxia inducible factor-1α (HIF-1α) upregulation (102-105). Similarly, a study using human glioma cells demonstrated that pharmacologically induced mitochondrial dysfunction produced an increase in CD133 protein expression, suggesting that hypoxia may also be perturbing the mitochondrial membrane potential to regulate CD133 post-transcriptionally (106). It has also been suggested that CD133 may play an important role in cellular glucose metabolism through modulation of the cytoskeleton (107). In parallel to these roles, a recent study also discovered a mechanism by which CD133 inhibited transferrin uptake (108). Since transferrin is involved in supplying iron to the cell and iron is required for efficient oxygen transport, the CD133-transferrin-iron network may provide a potential mechanism for a better understanding of CD133 modulation under hypoxic conditions.

Several reports have also begun to highlight potential signaling pathways involved in CD133 expression. The role of CD133 as inductor of Wnt/β-catenin signaling has been previously reported in CSCs (109-111). In particular, suppression of CD133 was associated with a loss of β-catenin nuclear localization and a reduction in canonical Wnt signaling (109, 110). Similar results were also reported in normal $CD133^{pos}$ renal cells, suggesting that CD133 may be a functional protein and/or a marker of differentiation status (112). Additionally, the deacetylase, HDAC6, has been shown to physically interact with CD133 in mammalian cells (111). This association stabilized β-catenin, whereas inhibition of either CD133 or HDAC6 resulted in increased β-catenin acetylation and

degradation and correlated with decreased proliferation and tumorigenesis, suggesting another potential role for targeting CD133 for cancer therapy. CD133 has also been implicated as an important regulator of PI3K/Akt signaling in CSCs (113-115), however, due to the complexity of the biological role of CD133, most studies focus on its use as a cell surface marker for the detection of somatic stem cells and CSCs. The functional role of CD133 is even less clear in the context of cancer, as it is ubiquitously expressed in numerous malignant and non-malignant tissues (116).

CD133 in the Healthy Prostate

In the healthy human prostate, CD133 was first identified as a stem cell marker in a rare population (~1%) of basal cells that expressed $\alpha_2\beta_1$ integrin (Figure 4). This $CD133^{pos}/\alpha_2\beta_1^{high}$ cell population was able to reconstitute prostatic-like acini with secretory activity when transplanted into male nude mice, validating their stemness and suggesting a hierarchical structure (117). Similarly, CD133 was used in combination with other cell surface markers to identify prostate stem cells in the proximal region of mouse prostate lobes which also preferentially expressed the basal marker CK14, but not the luminal marker CK18 (118). To validate the stemness of these cells, single $CD133^{pos}/Lin^{neg}/Sca\text{-}1^{pos}/CD44^{pos}/CD117^{pos}$ stem cell grafts were transplanted into the renal capsule of nude mice and 14 out of 97 (~14.4%) of the engraftments were capable of prostate development. The above studies support the idea that CD133 expression marks a particular basal stem cell population by reflecting a hierarchically organized phenotype.

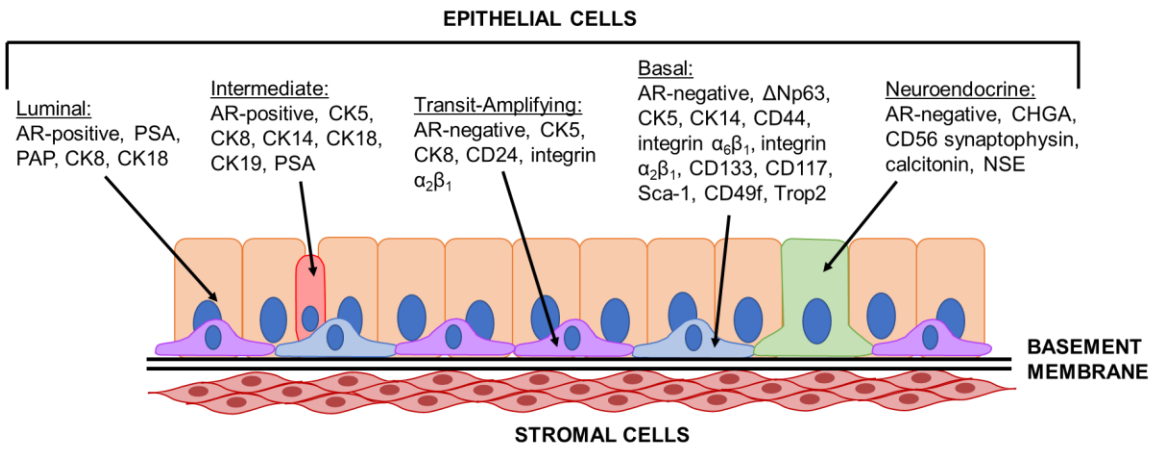

Figure 4. Schematic of the different cell types in the prostate and their identifying markers. The epithelial compartment is composed of three basic cell types: basal, luminal, and neuroendocrine cells; and two intermediate phenotypes. Basal cells are non-secretory cells located along the basement membrane of the epithelium and are characterized by the following markers: ΔNp63 (119), CK5 and CK14 (120, 121), CD44 (122), integrin $\alpha_2\beta_1$ (117), integrin $\alpha_6\beta_1$ (123, 124), CD133 (117), CD117 (118), Sca-1 (118, 125), CD49f, and Trop2 (126). Basal cells give rise to secretory luminal cells by transitioning through intermediate states. Two intermediate phenotypes have been described: (1) transit-amplifying cells which are non-secretory and exhibit a more basal-like phenotype and (2) intermediate cells which are secretory and exhibit a more luminal-like phenotype. Both, transit-amplifying and intermediate cell types may express CK5 and CK8, however, only transit-amplifying cells have been shown to express CD24 to distinguish them from low-differentiated basal cells (127) and only intermediate cells have been shown to express CK19 to distinguish them from luminal cells (128). Luminal cells are secretory columnar cells that express high AR, CK8 and CK18, and PAP (129). Neuroendocrine cells are very rare cells located in the luminal layer and represent less than 1% of the prostatic epithelium. They are non-secretory, differentiated cells that express CHGA, CD56, synaptophysin, calcitonin, and NSE (130, 131). This figure has been adapted from diagrams in related literature (132-134).

This hypothesis was supported and accepted for many years, however, more recent findings have indicated the presence of CD133 in luminal epithelial cells in both human and rodent models (135-137). A study documented that $CD133^{pos}$ and $CD133^{neg}$ cells contributed equally to prostate epithelial homeostasis, bringing into question the accuracy of CD133 as a true stem cell marker (138). Based on the evidence in the prostate alone, it appears to be clear that not all $CD133^{pos}$ cells are stem cells and that some $CD133^{neg}$ cells may also possess stem-like properties. Several additional studies support this hypothesis by demonstrating that CD133 was expressed in differentiated epithelial cells in a variety of other organs including the pancreas (139, 140), liver (141, 142), colon (116, 143), sweat glands (144), salivary and lacrimal glands (144, 145), uterus (144), and kidneys (146). Altogether, these studies indicate that the overall expression of human CD133 expands beyond stem cell populations and although it appears to negatively correlate with cell differentiation, it is likely not a regulator of stemness in most tissues (143). Rather, it is more likely that CD133 is a general marker of the apical or apico-lateral membrane of the glandular epithelium (144, 147). Furthermore, it is important to note that no stem cell population from any tissue type has been isolated to clonal purity on the basis of CD133 alone.

CD133 in Prostate Cancer

CD133 was first investigated as a PCa stem cell marker using the same cell surface markers for identifying normal stem cells in the prostate. One study identified PCa stem cells by isolating a population of cells from 40 patient biopsies

which was $CD44^{pos}/\alpha_2\beta_1^{high}/CD133^{pos}$ (148). This particular cell population was postulated to be a CSC population based on its ability to self-renew, proliferate extensively, and invade *in vitro*. The $CD44^{pos}/\alpha_2\beta_1^{high}/CD133^{pos}$ exhibited a self-renewal capacity that was 3.7-fold greater than the $CD133^{neg}$ population. Additionally, $CD133^{pos}$ cells from primary and metastatic prostate tumors showed increased proliferative potential and invasiveness compared to $CD133^{pos}$ cells derived from benign prostate tissues. CD133 has also been used to identify CSCs in PCa cell lines though the isolated $CD133^{pos}$ cells regenerate phenotypically heterogeneous populations. For example, a CWR22Rv1 culture propagated from freshly sorted $CD133^{pos}$ cells (>98%) revealed that only 6.15% of cells remained $CD133^{pos}$ after two weeks in culture (149).

Based on the evidence of rare CD133 expression in somatic stem cells of the prostate, it was hypothesized that these $CD133^{pos}$ CSCs populations resulted from mutated normal stem cells and thus were derived from basal cells. Several early studies supported this theory by showing that the $CD133^{pos}$ cell populations exhibited known basal cell identifiers summarized in Figure 4, although the most frequently recognized of these basal cell markers is often negative androgen receptor expression (AR^{neg}). In these studies, the $CD133^{pos}$ cells had the ability to proliferate and differentiate into AR^{pos} cell populations, reflecting the relevance of CD133 to a hierarchically organized phenotype. However, another study demonstrated that isolated $CD133^{pos}$ PCa cells were AR^{pos} and exhibited significant growth inhibition when exposed to high-dose androgens, suggesting

that these $CD133^{pos}$ CSCs may be derived from a malignantly transformed intermediate cell rather than normal basal stem cells (149).

Conversely, some studies have indicated that $CD133^{pos}$ and $CD133^{neg}$ cell populations from immortalized primary human PCa tissues demonstrated similar tumorigenicity when inoculated into NOD/SCID mice and that the $CD133^{neg}$ cells generated significantly more prostaspheres *in vitro* (150). Thus far, $CD133^{pos}$ CSC populations have only been shown to represent roughly 1-5% of the total cell population in PCa cell lines (149). However, it has been suggested that $CD133^{pos}$ populations could be enriched *in vitro* through chemotherapy or radiotherapy, postulating that these cells exhibit at least some level of chemo/radioresistance (151). A study evaluating the circulating tumor cells from 12 metastatic CRPC patients established that the $CD133^{pos}$ cells exhibited higher proliferative potential than their $CD133^{neg}$ counterparts in 10/12 patients (152), suggesting that $CD133^{pos}$ cells do have enhanced potential for cell division despite chemo/radiotherapy. Due to the inconsistent evidence supporting CD133 as a PCa stem cell marker, it is still unclear whether CD133 plays a direct role in PCa stem cell maintenance or if it is simply correlated to more aggressive disease.

Goals of Research

Tumor heterogeneity is a hallmark of AVPC lesions and a well-documented clinical challenge in developing new and improved theranostic agents. Recent studies have focused on incorporating a precision medicine-based approach to detecting and treating PCa by using specific imaging and therapeutic agents that are targeted to the patient based on their tumor pathology. PSMA-targeted theranostics have laid the foundation for the development of targeted agents for the detection and treatment of specific phenotypes of PCa, but they are limited in their ability to target $PSMA^{neg}$ lesions, which are frequently found in the lethal AVPC stage of PCa progression. As such, new targetable biomarkers are urgently needed to continue improving the diagnosis, disease monitoring, and therapeutic options for lethal AVPC.

Recent studies on CD133 have indicated that it may play a role in the progression of PCa as it is often identified in more aggressive stages of the disease which also happen to display higher levels of chemo/radioresistance. To date, the investigation of CD133 as a stem cell and CSC marker has dominated the CD133 literature, but the verdict is still out as to whether CD133 plays a true role in the stemness of the cell population. **The focus of this dissertation is to investigate CD133 as a biomarker of aggressive PCa and develop a novel antibody to detect CD133 in preclinical PCa models.**

Due to the limitations of previously commercialized antibodies binding to inaccessible or glycosylated epitopes of CD133, Chapter II focuses on the

identification of a novel single chain variable fragment (scFv), termed HA10, which detects a glycosylation independent epitope of CD133. In addition to the validation of HA10, this chapter also includes a case study describing CD133 expression during PCa progression and suggests the significance of targeting CD133 in lethal AVPC patients. In Chapter III, CD133 expression in a particular AVPC phenotype is defined using a high-throughput analysis. Furthermore, HA10 is converted into a full-length IgG, termed HA10 IgG, and used to image preclinical models of PCa. Chapter IV concludes my research by elucidating the impact of targeting CD133 as a biomarker in AVPC and discussing the future directions of this research.

CHAPTER II: Development and Characterization of a Novel anti-CD133 Single Chain Variable Fragment (scFv)

Introduction

PCa is a prevalent disease that afflicts men in the western world greater than any other malignancy. The inability of therapies to eliminate PCa in a subset of patients and the recurrence of disease many years post-radical prostatectomy is indicative of the existence of cancer stem/initiating cells. In the healthy prostate, a subset of slow-growing AR^{neg} basal cells possess an unlimited ability to self-renew and differentiate into neuroendocrine cells and transit-amplifying cells that ultimately yield the AR-expressing secretory cells that populate the majority of the glandular epithelium (153). One model suggests that cancer stem/initiating cells arise from these normal stem cells within the basal layer of the prostate epithelium after they have accrued mutations that promote carcinogenesis (154). Complicating the study of stem cells is their low abundance in the heterogeneous prostate epithelium. The pentaspan transmembrane protein, CD133, has been used extensively as a marker to identify and isolate prostate stem cells and cancer/stem initiating cells (99, 100, 155). Possessing an extracellular N-terminal domain (EC1), two large heavily glycosylated extracellular loops (EC2 and EC3), and often existing as different splice variants, the biological function of CD133 is unknown (84, 156). Identified originally as an antigen present on the surface of hematopoietic stem cells in 1997 (157, 158), the expression of CD133 has been documented in normal and CSCs from a number of diverse tissue and cancer types (100, 117). Underscoring its association with stem cells in the prostate, basal cells isolated from benign prostate tissue that expressed $\alpha_2\beta_1$

integrin and CD133 were able to regenerate a fully differentiated prostate epithelium in vivo (117). Additionally, purported PCa stem cells expressing a $CD133^{pos}/\alpha_2\beta_1{}^{high}/CD44^{pos}$ phenotype were isolated from human tumor biopsies and demonstrated tumorigenic properties (159).

Investigating the functional role CD133 plays in the development of the adult prostate and in the initiation and progression of cancer is hindered by several factors. Very few cell lines uniformly express endogenous CD133. PCa cell lines and non-immortalized prostate epithelial cells do possess a minor population of CD133-expressing cells (~1–5%) (149). When the $CD133^{pos}$ cells are isolated and expanded in culture, CD133 expression is lost returning to the original minor population (155). Reliable antibodies for the detection and isolation of CD133 also do not exist—this has been a significant limitation in investigating the biology of CD133 (85, 160). The two most commonly used antibodies for the isolation and analysis of CD133, AC133 (epitope CD133/1) and AC141 (epitope CD133/2), both recognize glycosylated epitopes (155). During the lifetime of a protein, glycosylation motifs can be pared or lost altogether making them inconsistent epitopes for analysis (85, 161). Several investigators have documented that the AC133 epitope disappears upon CSC differentiation even though CD133 protein and mRNA are still present (83, 162, 163). Further illustrating the paucity of high-quality antibodies for CD133, studies have found discordant CD133 expression by IHC using different CD133 antibodies tested in sections of the same tissues (85, 160, 164). The dynamic nature of the glycosylation motifs on the extracellular

domains of CD133 coupled with the lack of a sensitive antibody suggest that CD133-expressing cell populations may be more abundant than previously imagined in tissues, but those cell populations are not detectable by the current CD133 antibodies.

In this study, we detailed the characterization of a novel antibody for CD133 that was identified from a human antibody phage display library. Our antibody, termed HA10, was found to bind to a glycosylation-independent epitope on the protein backbone of CD133. Using our antibody, we were able to detect CD133 expression in cell lines by flow cytometry and in formalin fixed paraffin embedded tissue sections. In several instances, HA10 was able to detect CD133 expression that was not identified by the commercially available AC133 antibody. In concordance with previous studies, little CD133 expression in healthy prostate and prostate adenocarcinoma sections was observed. We did, however, make a novel finding documenting extensive CD133 expression in AR^{neg} LuCaP patient-derived xenograft (PDX) models and in a liver biopsy from a patient with AR^{neg} that also expressed the neuroendocrine marker, CHGA.

Materials & Methods

Cell Culture

All cancer cells lines used in this study were purchased from American Type Culture Collection (ATCC) except for the CWR-R1^{CD133} cells which were a generous gift from Dr. Donald Vander Griend, University of Chicago (165). Cells were maintained in their respective recommended media, supplemented with 10% FBS (Gibco), 1% antibiotic-antimycotic (Gibco), and 1% glutaMAX (Gibco) at 37°C and 5% CO_2. Additionally, enzalutamide resistant (EnzR) cell lines were supplemented with 10 μM enzalutamide (APExBIO) at all times. The cell lines were authenticated using short-tandem repeat profiling provided by the vendor and routinely monitored for mycoplasma contamination. The PC3^{CD133} knock-in cell line was generated using PROM1 Lentifect Purified Lentiviral Particles (LPP-M0038-Lv105–200-S, GeneCopoeia). PC3 cells were seeded at 5×10^4 cells/well in a 24-well plate using heat-inactivated FBS. Once cells became 70–80% confluent, transduction was performed according to the manufacturers protocol using 7 μg/mL Polybrene (H9268–5G, Sigma-Aldrich) and 10 μL of lentivirus for 24 h. Following overnight incubation, transduced cells were reseeded into three wells of a six-well plate and incubated for 48 h. Transduced clones were stably selected with 3 μg/mL puromycin for the duration of culture.

Phage Display Biopanning

A fully human naïve scFv phage display library was used to identify clones against native human CD133. Recombinant human CD133 (NBP2-59787PEP,

R&D Systems) was biotinylated using EZ-link™ NHS-PEG_4-Biotin (Thermo Fisher) at a 20-fold mM excess of biotin to protein. The biotinylated CD133 was captured using Dynabeads™ M-270 Streptavidin (Invitrogen) in 100 ng/µL of 1% BSA in PBS (137 mM NaCl, 2.7 mM KCl, Na_2HPO_4, 10 mM, KH_2PO_4 2 mM pH 7.4) with constant inversion for 30 min. The scFv phage display biopanning protocol was carried out as previously described in Kim *et al*. (166). The biopanning protocol was repeated three times to enrich for positive binders to glycosylated recombinant CD133 and one additional round with deglycosylated CD133.

Quantitative RT-PCR

RNA was prepared from each cell line (~2 × 10^6 cells) using an RNeasy kit (Qiagen). RNA was synthesized to cDNA using the High Capacity RNA-to-cDNA kit (Applied Biosystems). For each gene, Taqman qRT-PCR was performed using the Taqman Universal PCR Master Mix (Applied Biosystems) and the following Taqman Gene Expression Assay probes: CD133-Hs01009257_m1 PROM1 for experimental samples and 18s ribosomal 1 (reference gene) Hs03928985_g1 RN18S1 for a normalization control. All qPCR was performed on a StepOnePlus Real-Time PCR system instrument (Applied Biosystems). Each reaction was performed in triplicate and the data were analyzed using the comparative Ct method (fold change = $2^{-\Delta\Delta Ct}$) as previously described by Schmittgen *et al*. (167). All data are presented as mean ± SEM.

ELISA

ScFvs were produced from 288 individual clones using 5 mM IPTG induction in a microtiter plate format. The scFvs that leaked into the cell culture media were screened for binding to native and deglycosylated CD133 by ELISA. Deglycosylation of CD133 was accomplished using PNGase F (Promega) according to the manufacturer's protocol. MaxiSorp® plates (Nunc) were coated with 50 µL of 5 µg/mL of captured CD133 (some experiments used deglycosylated or truncated forms of CD133) in 1% BSA in PBS overnight at 4°C. The unbound CD133 was removed and wells were washed three times with PBS and blocked with 2% BSA in PBS for 1 h at room temperature. The wells were washed three times with PBS and the supernatants of scFv induced cultures were added to each well and incubated at room temperature for 1 h. The wells were washed three times with PBS and the scFv was detected with anti-HA antibody conjugated to peroxidase (Roche) in 1% BSA in PBS and Turbo TMB reagent (Pierce). Reactions were stopped with 15 µL of 2.5 M H_2SO_4 and the absorbance was measured at 450 nm using a microplate reader. Confirmed positive clones for CD133, irrespective of glycosylation status, were sequenced to identify unique clones.

ScFv Expression and Purification

Unique clones were inserted into pET-22b(+) vectors (Novagen) according to the manufacturer's protocol. Expression of each clone was carried out in SHuffle® T7 Competent *Escherichia coli* K12 cells (NEB). A single colony from each clone was selected and cultured overnight at 37°C in 5 mL of 2xYT broth

containing 100 μg/mL ampicillin. The 5 mL overnight cultures were used to inoculate 1 L cultures of 2xYT broth containing 100 μg/mL ampicillin. Cells were cultured at 30°C until the OD_{600} reached 0.5–0.7. Protein expression was induced by the addition of 1 mM IPTG and 0.4 M sucrose and cultured for an additional 16–18 h at 25°C. Cells were harvested by centrifugation at 6000g for 10 min and the periplasmic *E. coli* fraction was extracted via osmotic shock. Harvested cell pellets from each liter of culture were resuspended in 20 mL of 1× TES (0.2 M Tris, pH 8, 0.5 mM EDTA, 0.5 M sucrose) and 20 mL of 1× EDTA-free protease inhibitor (Pierce) solution. Each cell suspension was incubated for 30 min on ice with agitation every 10 min. Cells were centrifuged and the supernatant was collected as periplasmic fraction 1. This protocol was repeated to the cell pellet to obtain periplasmic fraction 2. The two periplasmic fractions were combined and 1 M $MgCl_2$ (200 μL) and 5 M imidazole (600 μL) were added prior to purification. The periplasmic fractions were filtered through a 0.45 μm filter and purified by Ni^{2+} affinity chromatography as follows. A 5-mL HisTrap HP column (GE Healthcare) was equilibrated with 20 mM $NaPO_4$, 0.5 M NaCl, 40 mM imidazole, pH 7.4. The clarified periplasmic fraction was loaded onto the column and washed with equilibration buffer for 10 column volumes and bound protein was eluted with 20 mM $NaPO_4$, 0.5 M NaCl, 500 mM imidazole, pH 7.4 Eluted scFvs were collected, concentrated using a 10 kDa centrifugal filter, and buffer exchanged into D-PBS using a Sephadex G-25 PD-10 desalting column (GE Healthcare). Each scFv was subject to analysis by reducing and non-reducing SDS-PAGE and

protein concentrations were measured based on absorbance at 280 nm using a NanoDrop™ One UV-Vis Spectrophotometer (Thermo Fisher).

IgG Production

The heavy chain and light chain variable domains of the HA10 sequence were cloned separately into pFUSE2ss derived rabbit IgG expression vectors (invivogen) and co-transfected into HEK293T (Life Technologies) cells for 72 h. Following incubation, the serum was collected, filtered through a 0.45 µm filter, and purified using a 1 mL HiTrap Protein A HP column (GE Healthcare). The column was equilibrated with 20 mM sodium phosphate, pH 7.4. The serum was loaded onto the column and washed with equilibration buffer for 10 column volumes and bound protein was eluted with 0.1 M citric acid, pH 3. Eluted IgGs were collected, concentrated using a 50 kDa centrifugal filter, and buffer exchanged into D-PBS, and analyzed as described above.

Surface Plasmon Resonance

SPR measurements were obtained using a BIAcore T100 instrument. The native recombinant CD133 protein was captured on a CM5 sensor chip by amine coupling at pH 4.5 to a final immobilization density of ~680 resonance units (RU). Un-reacted sites were blocked with 1M ethanolamine. A control flow cell without immobilized CD133 protein was prepared for reference subtraction. Dilutions of HA10 in running buffer (10 mM HEPES, 150 mM NaCl, 0.005% Tween 20, pH 7.4 [HBS-T] or 50 mM phosphate, 100 mM NaCl, 0.01% Tween 20, pH 6) were injected over the chip for 200 s followed by a 600 s dissociation in running buffer. The chip

was regenerated with a 30 s injection of 10 mM glycine, pH 2.5, and two 45 s injections of HBS-T. The flow rate used for all methods was 30 L/min. Binding affinities were derived by analysis of the generated sensograms using the Biacore T100 evaluation software. The equilibrium RU observed for each injection was plotted against protein concentration and fit to a steady-state affinity model included in the evaluation software for determination of the equilibrium binding affinity (K_D).

ScFv-Fluorphore Conjugation

A total of 0.5 mg of HA10 was labeled with a 3-fold molar excess of Alexa Fluor® 488-NHS ester (Life Technologies) dissolved in DMSO under alkaline conditions (pH 9.0) using 1 M sodium bicarbonate. The conjugation reaction was performed for 90 min at room temperature with gentle agitation. Unbound Alexa Fluor® 488 was removed by performing a buffer exchange into D-PBS using a Sephadex G-25 PD-10 desalting column (GE Healthcare). Labeled HA10 was concentrated using a 10 kDa centrifugal filter and the protein concentration and degree of labeling were determined as follows:

Protein concentration (M) = $[(A_{280} – (A_{494} \times 0.11)) \times \text{dilution factor}] / [\text{Molar extinction coefficient (M)}]$

Moles dye per mole protein = $[A_{494} \times \text{dilution factor}] / [71{,}000 \times \text{protein concentration (M)}]$

Flow Cytometry

Cells were harvested by incubation with TrypLE for 3 min at 37°C. 1×10^6 cells were labeled with either 1 μM HA10, 0.1 mg/mL of commercialized CD133/1 (AC133, #130–105-226) purchased from Miltenyi Biotec, or 0.1 mg/mL of an IgG control (#130–092-213, Miltenyi Biotec) for 30 min at 4°C. Cells were washed two times and resuspended in flow cytometry staining buffer (eBioscience). Cell samples were analyzed on a FACSCalibur flow cytometer (Becton-Dickinson) and at least 10,000 viable cells were gated and analyzed with FlowJo software.

Immunoprecipitation

Cell lysates were prepared using non-denaturing 1% triton X-100 lysis buffer with protease and phosphatase inhibitors. The concentrations of cell lysates were determined using an RCDC assay. Purified HA10 (2 μg) was incubated with 0.5 mg of cell lysate overnight at 4°C to facilitate antibody conjugation. Protein A/G Plus-Agarose beads (#sc-2003, Santa Cruz Biotechnology) were added to the lysate-antibody mixture and incubated for 3 h at 4°C. The immunoprecipitant was washed three times with D-PBS and captured proteins were eluted using 40 μL of 1× laemmli buffer. The sample was boiled at 95°C for 5 min and centrifuged at 100×g for 5 min to remove majority of the agarose beads from the precipitant. The eluate was analyzed by SDS-PAGE followed by subsequent western blotting using the commercialized AC133 antibody (Miltenyi Biotec) as well as mass spectrometry using a Linear Ion Trap mass spectrometer (Thermo Scientific) and PEAKS proteomics software package.

Immunohistochemistry

The LuCaP tissue microarray (TMA) was acquired from the Prostate Cancer Biorepository Network (PCBN). The LuCaP TMA was constructed with each PDX model in triplicate. Patient biopsies for analysis were acquired using a University of Minnesota Human Subjects Division approved Institutional Review Board (IRB) protocol for tissue acquisition (IRB#1604M86269) and with patient consent. The healthy prostate tissue and adenocarcinoma TMAs were obtained from the BioNET Tissue Procurement Facility at the University of Minnesota. The samples for these TMAs were all arranged in duplicate. The patient samples for the TMA were originally acquired using an approved IRB protocol for tissue procurement. Unstained sections (4 μm) were de-paraffinized and rehydrated using standard methods. For antigen retrieval, slides were incubated in 6.0 pH buffer (Reveal Decloaking reagent, Biocare Medical) in a steamer for 30 min at 95–98°C, followed by a 20 min cool down period. Endogenous peroxidase activity was quenched by slide immersion in 3% hydrogen peroxide solution (Peroxidazed, Biocare Medical) for 10 min followed by TBST rinse. A serum-free blocking solution (Sniper, Biocare Medical) was placed on sections for 30 min. Blocking solution was removed and slides were incubated in primary antibody diluted in 10% blocking solution/90% TBST. The following primary antibodies and concentrations used were: CD133 HA10 antibody, rabbit monoclonal (1:100); androgen receptor SP107 (Sigma), rabbit monoclonal (1:200); chromogranin A PB9097 (Boster Biological Technology) rabbit polyclonal (1:1000); CD133/1 (AC133) (Miltenyi) mouse

monoclonal (1:25). Slides were rinsed in TBST buffer followed by detection with Novalink polymer (Leica Biosystems) according to manufacturer's directions. All slides then proceeded with TBST rinse and detection with diaminobenzidine (DAB) (Covance). Slides were incubated for 5 min followed by TBS rinse then counterstained with Harris Hematoxylin for 1 min. Slides were then dehydrated and cover slipped. An independent pathologist reviewed the stained slides and assigned a qualitative staining intensity score of negative, weak, moderate, and strong. The staining patterns were described as rare (0–25% cells positive), variable (25–75% positive), and uniform (>75% positive).

Statistical Analysis

A one-way ANOVA using GraphPad Prism 7 was used to calculate statistics for PROM1 mRNA expression from qRT-PCR experiments. Each cell line was compared to the calibrator (PPT2) to determine statistically significant levels of CD133 mRNA expression. All other assays were carried out 2–3 times and data replication were observed in repeated experiments.

Results

Antibody Identification

A human scFv antibody phage display library with a diversity of 8×10^9 was initially screened for three rounds against glycosylated recombinant CD133. Biopanning was performed using biotinylated CD133 attached to magnetic streptavidin coated beads to ensure that the protein retained some three-dimensional structure. An additional round of biopanning was performed with CD133 that had been deglycosylated by PNGase F treatment to enrich for clones against a glycosylation-independent epitope. After the fourth round, 288 independent clones were screened by ELISA using fully glycosylated CD133. Of those clones, 122 showed high ELISA signals and 14 clones cross-reacted with deglycosylated CD133. Sequence analysis of the 14 clones discovered 8 unique antibodies. One scFv, designated HA10, expressed well in *E. coli* (~2 mg/L) and was selected for further characterization studies. After purification, the majority of the purified product was composed of scFv, however, some dimerized and oligomerized products were also present (Figure 5A), which is in accordance with previously documented scFv preparations (168, 169). Subsequent SPR analysis determined that the monovalent HA10 scFv possessed a K_D of 3 nM for fully glycosylated CD133 (Figure 5B). Additionally, the epitope of HA10 was found to reside on the extracellular domain 2 (EC2) of CD133 by ELISA using recombinant biotinylated fragments of each extracellular domain (Figure 5C). In contrast, both of the commercially available antibodies, AC133 and AC141, are known to bind to

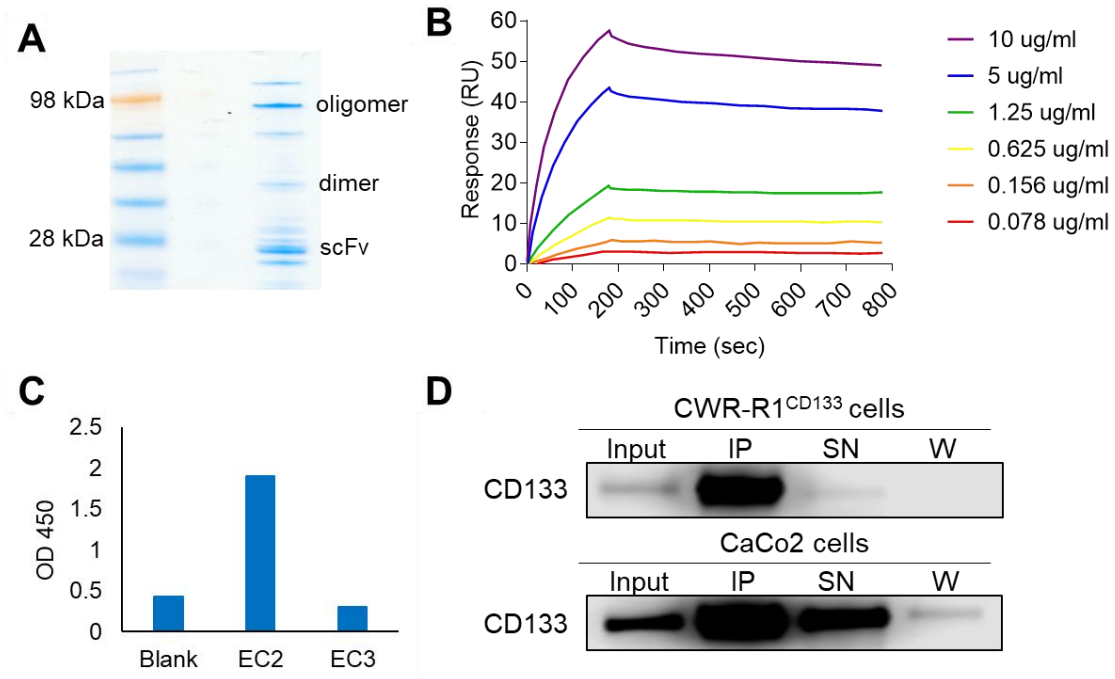

Figure 5. Validation of HA10 binding to CD133. A) SDS-PAGE gel of purified HA10 scFv displays some dimer and oligomer formation. **B)** SPR measurements of immobilized CD133 interacting with 3, 6, 25, 50, 200, and 400 nM of purified HA10 are shown, demonstrating potent binding to native recombinant CD133 with a K_D = 3 nM **C)** ELISA assay of HA10 with purified recombinant CD133 extracellular loops (EC2 and EC3) shows that HA10 binds to an epitope located on the EC2 domain of CD133. Detection of HA10 binding was performed using a peroxidase conjugated HA-tag antibody and Turbo TMB reagent. OD_{450} measurements were obtained on a microplate reader and a control blank well containing no immobilized protein was used to assess background absorbance **D)** To further confirm the binding of HA10 to CD133, CD133 was immunoprecipitated from two $CD133^{pos}$ cell lines, CWR-$R1^{CD133}$ and CaCo2 (colon cancer) using HA10. Western blot analysis with the Miltenyi Biotec CD133/1 (AC133) antibody and mass spectrometry of the immunoprecipitant were used to confirm the identity of CD133. IP, immunoprecipitant; SN, supernatant; W, pooled washes.

glycosylated epitopes on the extracellular domain 3 (EC3). Immunoprecipitation with HA10 revealed binding to CD133 in the colon cancer cell line, CaCo2; and the PCa cell line, CWR-R1^{CD133} which was engineered to express CD133 (Figure 5D).

Lentiviral transduced and naturally expressing CD133^{pos} cell lines were next analyzed by flow cytometry and western blot to compare the binding of HA10 scFv to the AC133 antibody which targets the CD133/1 epitope on EC3. First, CD133 gene expression analysis was used to evaluate mRNA levels of PROM1, which encodes for CD133. The artificially expressing cell lines, PC3^{CD133} and CWR-R1^{CD133}, displayed significantly higher levels of PROM1 compared to the remaining cell lines. Additionally, the naturally expressing cell lines: E006AA-hT, E006AA-hT-EnzR, PPT2, and CaCo2 showed 100-1000-fold more PROM1 compared to the CD133^{neg} cell lines (Figure 6A). Despite the high mRNA levels in the artificially expressing cell lines, flow cytometry and western blotting revealed that CD133 protein expression was similar to the colon cancer cell line, CaCo2, which serves as a positive control (Figures 6B and 6C). As seen by the negligible shift in the histograms, insignificant staining was only observed in the CD133^{neg} parental PC3 and CWR-R1 cells, confirming the lack of cross-reactivity of HA10 with other human proteins. Conversely, PC3^{CD133} and CWR-R1^{CD133} cell lines were specifically labeled by both HA10 and AC133 at almost equivalent levels. Both antibodies were next tested with the naturally expressing CaCo2 cell line and the recently identified CD133^{pos} PCa cell line, PPT2 (170). HA10 showed comparable staining in CaCo2 cells and stained 21.5% more of the PPT2 cell population than

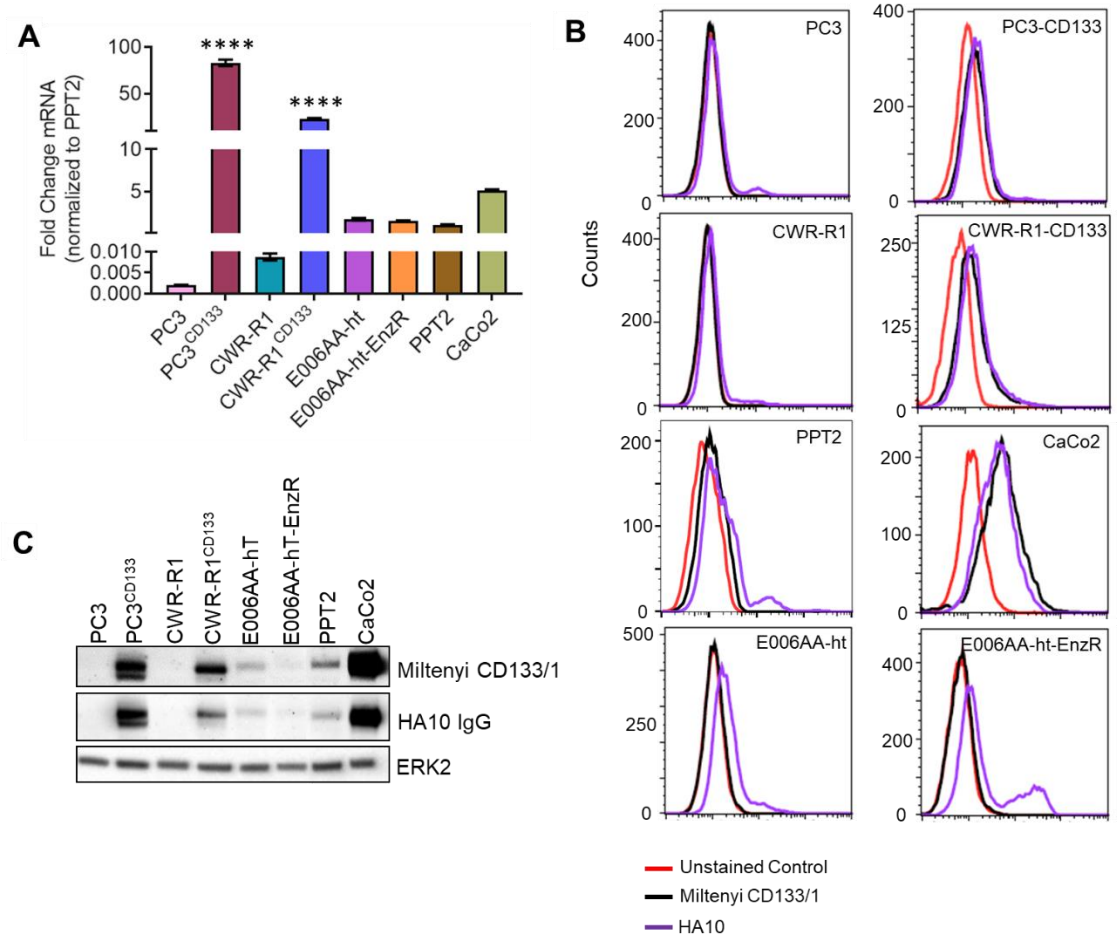

Figure 6. Analysis of CD133 expression in various cell lines. A) High levels of PROM1 mRNA expression were observed in the artificially ($p<0.0001$) expressing PCa cell lines. Despite being insignificant, total PROM1 mRNA expression in the naturally-expressing cell lines were comparable to the positive control, CaCo2, whereas CD133 mRNA expression levels in the $CD133^{neg}$ prostate cancer cell lines were roughly 0.001–0.1% of the remaining cell lines when analyzed by qRT-PCR. **B)** Flow cytometry was used to compare the specificity and staining intensity of HA10 (purple line) and the Miltenyi antibody CD133/1 (AC133) (black line) on these various CD133-expressing live cells. Both antibodies were compared to an unstained control (red line) to identify any non-specific binding. Staining profiles on the negative and transduced cell lines suggest comparable performance, however, higher staining profiles were observed in naturally expressing cell lines with HA10 compared to the AC133 antibody. **C)** Comparable detection was observed in all cell lines by western blot.

AC133. Additionally, since African Americans are known to exhibit more aggressive PCa, the African American PCa cell lines, E006AA-hT and E006AA-hT-EnzR, were assessed for CD133 expression. Similar to the PPT2 cells, staining was only observed with HA10 in a small population of cells, while AC133 was unable to detect CD133 expression on the cell surface (Figure 6B). When the same cell lines were analyzed by western blot, the antibodies were comparable in signal across all cell lines (Figure 6C). Interestingly, there is a small population of E006AA-hT-EnzR cells identified using HA10 in the flow cytometry analysis that is not detected via western blot, which may be due to changes in structure or epitope alterations from the lysis procedure. However, these results ultimately suggest that HA10 may be more effective at detecting CD133 in naturally expressing $CD133^{pos}$ cell populations, potentially due to the effects of CD133 glycosylation, epitope masking, or protein truncation.

Antibody Staining in Fixed Tissues

The variable heavy and light chains of HA10 scFv were cloned into rabbit IgG scaffold vectors for expression in a mammalian system. After purification, the rabbit IgG version of HA10 was used by IHC to detect CD133 in formalin-fixed paraffin embedded sections from subcutaneous CWR-$R1^{CD133}$ and $PC3^{CD133}$ xenografts. HA10 detected strong uniform of CD133 with >75% of the cancer cells stained in the transduced models with no appreciable staining observed in the parental sections as anticipated (Figures 7A-7D). Mock tissue sections of $PC3^{CD133}$ cells embedded in paraffin also demonstrated specific staining for CD133

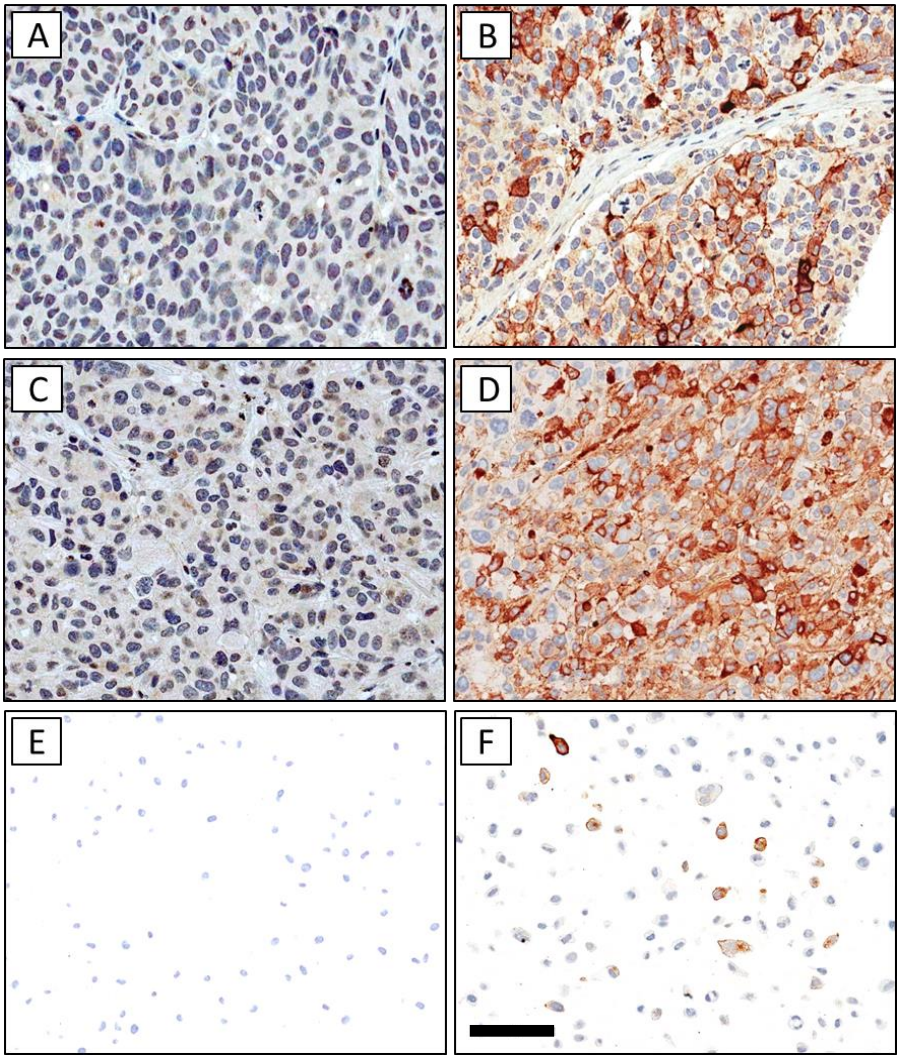

Figure 7. IHC validation of HA10. Staining with HA10 is depicted in FFPE xenograft sections derived from parental cell lines and cell lines engineered to express CD133. No immunoreactivity was present in a parental R1 section (A) but was in the engineered $R1^{CD133}$ section (B). Staining was not observed in a parental PC3 section (C) while strong uniform staining was in the $PC3^{CD133}$ section (D). Mock tissue sections of the PC3 cells were made consisting of fixed cells embedded in paraffin and then sectioned (E and F). CD133 was absent in PC3 parental cell mock tissue section (E). The mock tissue section of the $PC3^{CD133}$ cells did show positive staining (F). Scale bar, 60 μm.

compared to the non-transduced control cells (Figures 7E and 7F). After the IHC protocol was optimized, a panel of healthy human tissues were stained with HA10 to assess CD133 distribution (Figure 8). Staining was largely absent in healthy human tissues, except for weak and variable staining in colon. The presence of CD133 in the colon and in colon cancer has been documented before (171).

Tissue microarrays of healthy prostate tissue and adenocarcinoma (Gleason 6–9) were next analyzed for CD133 expression using HA10. Immunoreactivity was found in very few of the healthy and diseased sections. Out of the 150 healthy prostate sections, the presence of CD133 was observed in only 12 sections (8%). All of the CD133 was located in the prostate epithelium with no detectable staining in the stroma (Figure 9). Positivity was greatest on the apical side of luminal cells. Staining was not uniform across luminal cells, however, with cells adjacent to $CD133^{pos}$ cells often showing no immunoreactivity (Figure 9A). Basal cell staining was only observed in one healthy prostate section (Figure 9B) while another section displayed complex epithelial staining that may have included basal cells (Figure 9C). CD133 immunoreactivity was almost equally as sparse in the prostate adenocarcinoma sections with only 10 out of 110 (9%) sections demonstrating immunoreactivity (Figure 9D). The staining was confined to the apical side of luminal cells with no basal staining observed in the sections that were surveyed. The presence of CD133 in the adenocarcinoma sections did not correlate with Gleason Grade, PSA level, or progression free survival.

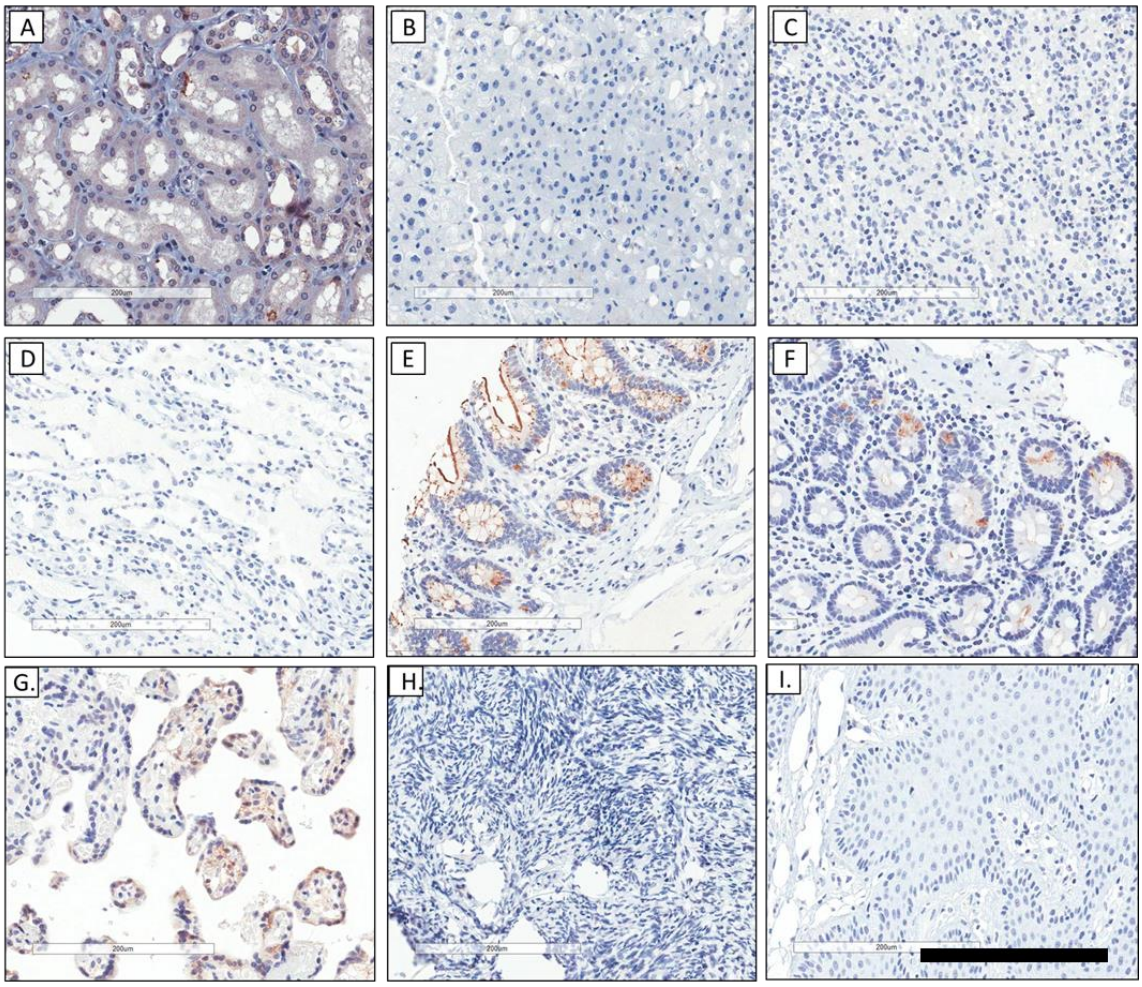

Figure 8. HA10 staining in healthy tissue. A) kidney, **B)** liver, **C)** spleen, **D)** lung, **E)** illium, **F)** small intestine, **G)** placenta, **H)** ovaries and **I)** skin. Scale bar, 200µm.

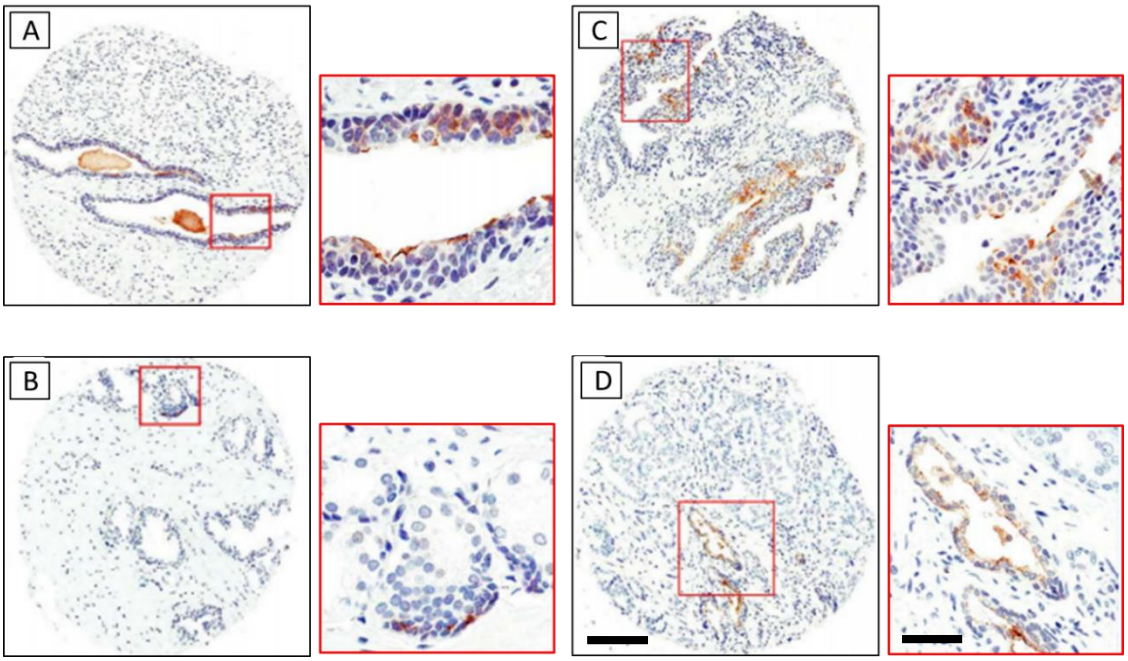

Figure 9. CD133 staining in the healthy prostate and prostate adenocarcinoma using HA10. The presence of $CD133^{pos}$ cells was rare in healthy tissue with 12/150 (8%) of the sections displaying immunoreactivity (A-C). **A)** Non-uniform staining of luminal cells was present in the glandular epithelium of a healthy prostate. **B)** A collection of basal cells in the glandular epithelium demonstrating the presence of CD133. **C)** An example of complex epithelial staining in a healthy prostate section. **D)** CD133 staining of luminal cells in an adenocarcinoma section Gleason 4 + 3. Only 10/110 (9%) of the adenocarcinoma sections had detectable CD133 present. Scale bars, 200 µm for the wide view and 60 µm for the magnification.

In order to more fully interrogate the potential expression of CD133 in heterogeneous primary and metastatic PCa, we stained a TMA constructed of the LuCaP PDX models (Figure 10). Out of the 42 LuCaP PDX models, only three (LuCaP 49, 145.1, and 145.2) were immunoreactive resulting in a uniform staining pattern akin to the engineered $PC3^{CD133}$ and CWR-$R1^{CD133}$ xenografts. No staining was detected in any of the LuCaP sections using an optimized protocol for the commercially available AC133 antibody. The $CD133^{pos}$ LuCaP models were all AR^{neg} and express at least one marker of neuroendocrine differentiation (CHGA or synaptophysin), as did their originating tumors. We did not observe any CD133 positivity in sections of the other AR^{neg} LuCaP model with neuroendocrine differentiation features, LuCaP 93.

Clinical Case Study of CD133 Expression

A liver biopsy was obtained from a PCa patient who underwent treatment at the University of Minnesota Masonic Cancer Center. The patient was originally diagnosed with aggressive PCa (Gleason 4 + 5, T3bN1M0, PSA of 45 ng/mL) and underwent a transurethral resection of the prostate (TURP). Shortly afterwards, a CT scan of the abdomen and pelvis showed bilateral pelvic lymphadenopathy and ADT consisting of lueprolide and bicalutamide was initiated. After 1 year of ADT, the patient's PSA had dropped to 2.8 ng/mL. Progression on ADT was observed after 25 months of treatment by an increase in PSA to 87 ng/mL and the development of extensive skeletal metastases. The patient then started on treatment with abiraterone and prednisone. After a year on this regimen, his PSA

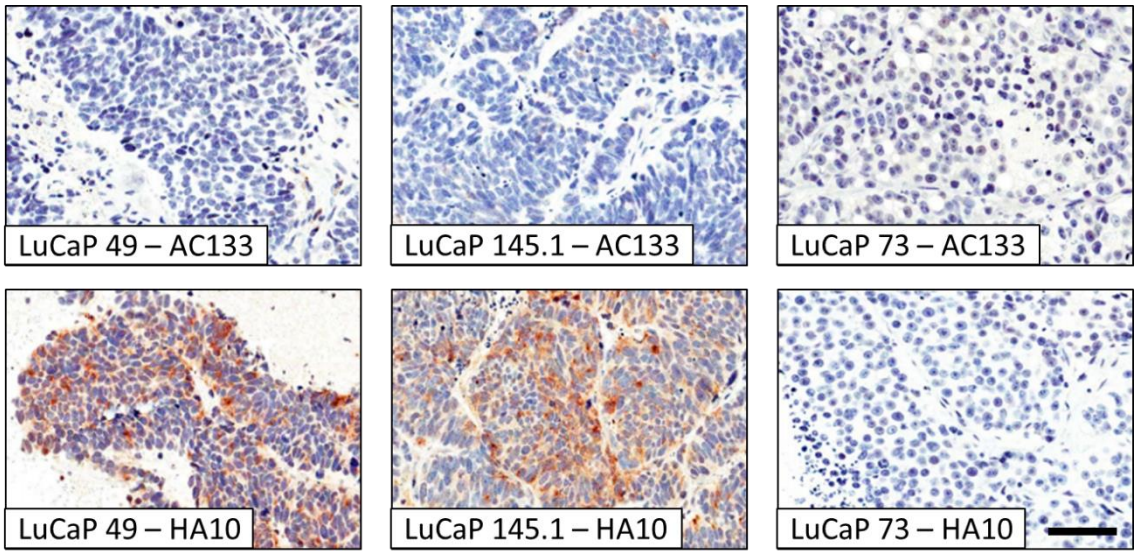

Figure 10. CD133 expression in LuCaP PDX models using HA10 and the Miltenyi antibody CD133/1 (AC133). None of the LuCaP PDX models were found to be positive for CD133 using the AC133 antibody. The neuroendocrine prostate cancer-derived models LuCaP 49 and LuCaP 145.1 did show staining for CD133 using HA10. Staining with HA10 was not observed in any of the other LuCaP PDX models, including AR positive LuCaP 73 shown at the lower right. Each image is representative of three replicates for each model. No variability was observed between the replicates. Scale bar, 100 μm.

had decreased from 87 to 17 ng/mL, however, a CT scan found extensive liver metastasis (Figure 11A). Biopsies of the liver lesions were found to be positive for CD133 based on staining with HA10 (Figure 11B). Strong CD133 staining was largely uniform across the tumor foci standing in stark contrast to the apical staining pattern observed in the healthy prostate and adenocarcinoma sections. Subsequent IHC analysis found that the liver metastases were also negative for AR expression (Figure 11C) and positive for the neuroendocrine marker, CHGA (Figure 11D). A TURP section from this patient stained with HA10 found no CD133 expression in the original primary disease (Figure 11E). The patient initially responded well to chemotherapy with carboplatin and taxotere, but progressed rapidly after 8 months developing extensive visceral metastases in the presence of declining PSA. A liver biopsy acquired after resistance to carboplatin and taxotere occurred was subsequently found to be positive for CD133 demonstrating moderate staining intensity with >50% of the tumor cells positive (Figure 11F). No sections from this patient were stained with AC133 due to scarcity of the samples.

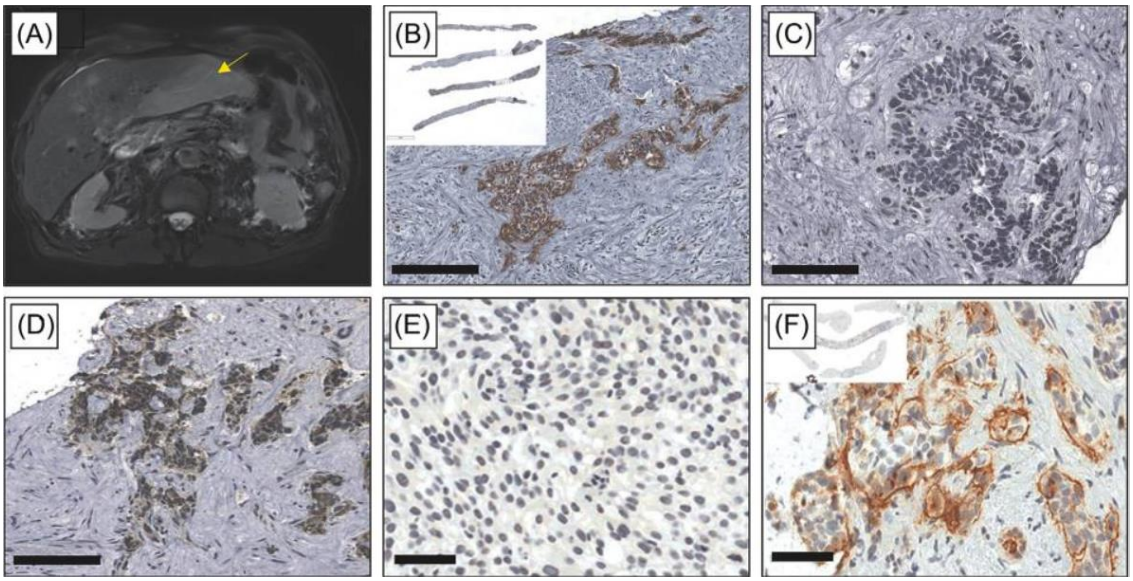

Figure 11. Case study of a patient with aggressive prostate cancer. A) CT scan of diffuse liver metastases that appeared in the presence of declining PSA after the patient failed treatment with Zytiga (abiraterone). **B)** Strong staining for CD133 was detected in the liver metastases using HA10. **C)** No staining for the AR was observed in the liver metastases using an antibody specific to the N-terminal domain of the AR. This antibody would detect both full-length AR and AR splice variants. **D)** Staining was observed for the neuroendocrine differentiation marker, CHGA, in the liver metastases. **E)** An original TURP specimen from the patient depicting poorly differentiated Gleason 4 + 5 cancer stained for CD133. Note the complete absence of CD133. **F)** Liver biopsy from the patient after failing treatment with carboplatin and taxotere documenting moderate staining for CD133. Scale bars, (B-D) 200 μm and (E-F) 60 μm.

Discussion

For many years, hybridoma technology has been the preferred method for identifying monoclonal antibodies against target antigens (172). This technology has allowed for the discovery of thousands of monoclonal antibodies that are used as laboratory reagents, nuclear imaging probes, and antibody-based therapeutics in the clinic. Though it has been successful, there are several limitations of hybridoma technology. Recent studies have suggested that less than a quarter of all commercially available antibodies actually bind to their target antigen or work for their intended application (173, 174). Hybridoma-derived antibodies often cannot distinguish between highly homologous members of the same protein family or proteins with significant posttranslational modifications such as glycosylation (175). Antibody phage display is a powerful technique that can rapidly identify recombinant monoclonal antibodies for challenging targets where traditional hybridoma technology has failed. Since it is an in vitro technology, the selection process in antibody phage display can be modified to enrich for highly unique clones that bind to specific epitopes. Here, we used antibody phage display to select for an antibody fragment that bound to a glycosylation-independent epitope on the protein backbone of CD133. The unique antibody discovered through this selection process, HA10, was able to detect CD133 in cell lines and fixed tissues.

Since its discovery in the late 1990s, CD133 has been viewed as a marker for stem cells of the healthy prostate as well as cancer (117, 155). The isolation

and analysis of CD133 expressing cells has primarily been conducted using the AC133 antibody. It is has been established that the AC133 epitope, but not CD133 protein, is lost when stem cells differentiate (83). Splice variants of CD133 are also known to exist that could potentially affect the epitopes used for detection (176). Based on this evidence, it is plausible that the AC133 epitope represents a population of CD133 that is only found in undifferentiated stem cells. As the basal stem cells in the prostate differentiate into transit-amplifying cells and ultimately luminal cells, the AC133 epitope is lost, but CD133 variants with de novo epitopes are present in the progeny. These new CD133 populations cannot be detected by AC133 or AC141, but can by antibodies, such as HA10, that recognize non-glycosylated epitopes that are consistently exposed on non-truncated protein domains. This hypothesis could potentially explain our flow cytometry data and the staining patterns that were observed by IHC.

By flow cytometry, both HA10 and AC133 bound to immortalized cancer cell lines that were engineered to artificially express full-length CD133. In the endogenously expressing CaCo-2 and PPT2 cells, HA10 recognized a greater population of positive cells than AC133. CaCo-2 cells differentiate and lose the AC133 epitope upon continuous coculturing suggesting that the cells used for flow cytometry had several CD133 epitope populations that could only be detected by HA10. The same can be argued for PPT2, which is a recently discovered PCa stem cell line that can form three-dimensional spheroids over prolonged passages. Most interestingly, only HA10 was able to detect CD133 on the surface of E006AA-

hT cells. E006AA-hT is a subline of E006AA, a cell line that was originally isolated from a primary Gleason 3 + 3 tumor of an African-American patient (177, 178). These cells possess hallmarks of terminally differentiated luminal cells that have undergone oncogenic transformation such as AR expression. Based on these findings, it is possible to say that E006AA-hT cells harbor several CD133 epitope populations, none of which display the AC133 epitope.

Previous IHC studies using the AC133 antibody discovered that CD133 was a marker for a truly rare basal cell type with less than 1% of all basal cells staining positive for CD133 (117). No report has ever documented the staining of luminal epithelial cells with AC133 in the prostate. Another antibody for CD133, 80B258, which recognized an epitope on the polypeptide backbone, was immunoreactive with basal cells and the apical side of luminal cells (137). Our findings with HA10 align with the 80B258 data and not AC133. Basal cell staining was observed with HA10 and was indeed found to be quite rare since only one section out of 150 was unequivocally positive. HA10 also reacted with luminal epithelial cells, staining the apical side of those cells. In contrast to other antibodies, however, HA10 also stained epithelial cells distant from the lumen and closer to the basement membrane. This pattern of staining was not observed with 80B258 and has never been documented before for CD133 in the prostate. The same group that analyzed 80B258 staining in healthy prostate tissues found no immunoreactivity in adenocarcinoma sections. With HA10, we did observe weak staining in adenocarcinoma sections, but it too was extremely rare.

CD133 expression in the LuCaP TMA further highlighted the differences between AC133 and HA10. Immunoreactivity was not observed with AC133 in any of the models, but CD133 expression was detected by HA10 in three models. The three positive LuCaP models were all originally derived from metastatic AR^{neg} neuroendocrine PCa with LuCaP 145.1 and LuCaP 145.2 originating from the same patient. A fourth neuroendocrine model that was derived from a TURP specimen, LuCaP 93, was not positive for CD133. Using HA10, we were also able to detect CD133 in liver biopsies of a patient who failed second-generation anti-androgen therapy with abiraterone. As with the CD133pos LuCaP models, the metastatic lesions from this patient displayed neuroendocrine differentiation based on the expression of CHGA. It is not possible to arrive at any formal conclusions about the biology of CD133 based on our findings with the LuCaP TMA and patient biopsy, except that its biology appears to be complex. The AC133 epitope was not present in the LuCaP models and staining with HA10 in the liver biopsies was strong and uniform in contrast to healthy prostate and adenocarcinoma sections. It appears that lack of an AR by itself does not necessarily correlate with CD133 expression and other factors are involved with the induction of CD133. To illustrate this point, both DU145 and PC3 are AR^{neg} yet only possess a minor population of $CD133^{pos}$ cells similar to that of LNCaP. E006AA-hT cells express both CD133 and AR, though the AR of this cell line has an S599G mutation that renders it inactive and the cells indifferent to castrate levels of androgen (179). The absence of CD133 in the original TURP specimen of the patient suggests that the CD133 in

the liver biopsies may originate from divergent clonal evolution, but it is difficult to say since biopsies at multiple stages of the disease were not taken (180). In order to come to any conclusion about the expression of CD133 in AR^{neg} cancer with neuroendocrine differentiation, more samples from a number of metastatic sites need to be analyzed.

CHAPTER III: Exploitation of CD133 for the Targeted Imaging of Lethal Prostate Cancer

Introduction

The management of patients with metastatic PCa initially relies on inhibiting the AR signaling axis by ADT through surgical castration or gonadotropin-releasing hormone agonists. The therapeutic benefit of ADT is transient and patients inevitably develop disease recurrence, also known as CRPC, which can occur as early as 18 months after the initiation of ADT (181-183). Driven by aberrant AR signaling, second-generation anti-androgens have had a profound effect in extending the lifespan of patients with CRPC (183). Unfortunately, many patients present with *de novo* resistance to these therapies and those that receive an initial benefit often develop acquired resistance quite rapidly through mechanisms such as AR amplification, mutation, and splice variant expression. Similarly, many men with *de novo* or acquired resistance to AR-signaling inhibitors may display a non-AR driven form of disease referred to as AVPC (182, 184, 185). AVPC broadly encompasses CRPC that is non-AR driven and may express neuroendocrine markers or possess small cell morphology (22, 186-188). This lethal subset of PCa is characterized by high metastatic burden in both the bone and viscera, minimal response to therapy, and poor overall prognosis (21, 23).

Effective treatment options for AVPC currently do not exist and novel therapies are urgently needed. Critical to the development of novel therapies for AVPC is the ability to accurately image this disease in patients. For decades now, bone scintigraphy using ^{99m}Tc methylene diphosphonate (^{99m}Tc-MDP) has been considered the most cost-effective and accurate imaging modality for metastatic

PCa patients despite its limited sensitivity and specificity for cancerous lesions (42, 47). Furthermore, recent studies using the PET tracer, NaF, have demonstrated superior sensitivity for detecting bone lesions in PCa patients (37, 42). While this is successful for the majority of AVPC patients who present with bone metastases, a striking 20% also present with visceral disease, rendering bone scintigraphy and NaF-PET imaging inadequate (189, 190). Other PET imaging agents, such as ^{11}C-acetate, ^{11}C/^{18}F-choline, and ^{18}F-fluciclovine, have been employed to image PCa biochemical recurrence (37, 58, 60, 191), however, these agents have yet to be investigated for AVPC. Recently, there has been much success imaging PSMA in bone and visceral metastases of patients with prostate adenocarcinoma using small molecule PET radioligand probes (76). Several PSMA imaging studies have documented a lack of probe uptake in AR^{neg} metastatic lesions suggesting that AVPC does not express PSMA (180, 192, 193). As such, there is currently no accurate imaging modality available for AVPC patients.

The lack of targetable antigens specific to AVPC has complicated the development of an imaging agent for this disease subtype. The heavily glycosylated pentaspan transmembrane protein, CD133, has often been described as an antigen on the surface of both stem cells and CSCs (98). In a previous study, we used human antibody phage display to identify a novel antibody for CD133, termed HA10 (194). Herein, we show that CD133 is highly overexpressed at the mRNA and protein level in a multitude of patients possessing AVPC with an AR^{neg}, neuroendocrine marker-positive (AR-/NE+) phenotype. By microarray analysis, we

confirmed that CD133 and PSMA expression were inversely related and that AVPC is $PSMA^{neg}$. Moreover, we used a full-length human IgG version of HA10 to selectivity identify $CD133^{pos}$ cancer cells by near-infrared (NIR) optical and ^{89}Zr-PET imaging in subcutaneous tumor and metastatic mouse models of AVPC. Our findings identified CD133 as a novel, previously unknown marker of AR-/NE+ AVPC that can be exploited as an imaging target to assess and monitor disease progression. Additionally, CD133-targeted imaging agents could aid in the development of novel therapeutics for a subtype of PCa that is currently incurable by monitoring patient response to therapy.

Materials & Methods

Cell Culture

HEK293T cells were purchased from the ATCC and were maintained according to ATCC guidelines. CWR-R1 cells and luciferase-expressing CWR-R1-EnzR cells were obtained from Dr. Scott Dehm (Masonic Cancer Center, University of Minnesota) and Dr. Donald Vander Griend (Department of Pathology/Surgery, University of Illinois at Chicago), respectively. All parental cell lines were authenticated by short tandem repeat profiling prior to manipulation. Parental CWR-R1 and CWR-R1-EnzR cells were lentivirally transduced to express CD133 as previously described (194). Expression of CD133 in transduced cell lines (CWR-R1^{CD133} and CWR-R1-EnzR^{CD133}) was confirmed via qPCR and western blot and compared to CD133^{neg} parental cell lines. All cells were grown in DMEM supplemented with 10% fetal bovine serum, 1% antibiotic-antimycotic, and 1% glutamax and incubated at 37°C and 5% CO_2. Additionally, CD133 expressing cells were continuously supplemented with 3 µg/mL puromycin to ensure stable levels of CD133 expression.

Antibody Production

The protocols for biopanning, ELISA screening, scFv expression and purification, as well as affinity/specificity characterization of the isolated scFv clone, HA10, were followed as previously described (194). The heavy chain (354 bp) and light chain (318 bp) variable domains of the HA10 sequence were cloned separately into pFUSE2ss derived human IgG expression vectors (InvivoGen) and

co-transfected into HEK293T cells according to manufacturer's guidelines. Following incubation, the serum was collected, filtered through a 0.45-µm filter, and purified using a 1 mL HiTrap Protein A HP column (GE Healthcare). The column was equilibrated with 20 mM sodium phosphate, pH 7.4 prior to loading the serum sample. The column was washed with equilibration buffer for 20 column volumes and bound protein was eluted with 0.1 M citric acid, pH 3. The eluate was collected and concentrated using a 50-kDa centrifugal filter. A final buffer exchange was performed into 1x PBS using a Sephadex G-25 PD-10 desalting column (GE Healthcare). The purity of the final HA10 human IgG was analyzed by reduced and non-reduced SDS-PAGE and the concentration was measured based on absorbance at 280 nm using a NanoDrop™ One UV-Vis Spectrophotometer (Thermo Fisher).

DNA Microarray

PCa patient tissue samples were obtained from patients who died of metastatic CRPC and who signed written informed consent for a rapid autopsy performed within 6 hours of death as part of the Prostate Cancer Donor Program at the University of Washington. A total of 171 tumors from 63 patients were collected for profiling by expression microarray using the protocol previously described in Kumar *et al*. (195). LuCaP xenografts were also profiled using the same protocol.

Immunohistochemistry

Curated samples for analysis were obtained from the PCBN and the University of Minnesota Masonic Cancer Center using a University of Minnesota Human Subjects Division approved IRB protocol for tissue acquisition (IRB#1604M86269) and with patient consent. The tissue sections were stained for CD133 using a previously described procedure (194). A pathologist reviewed the slides and assigned IHC scores as previously reported (196). The AR-/CHGA+ (n=25) soft-tissue metastases were liver (n=14), lymph node (n=3), lung (n=2), retroperitoneal (n=4) and pleural (n=2) while the AR+/CHGA adenocarcinoma sections (n=10) were liver (n=6), lymph node (n=2) and lung (n=2).

Fluorescent Microscopy

CWR-R1-EnzR and CWR-R1-EnzR^{CD133} were seeded on borosilicate coverglass slides (Nunc) and grown to 50% confluence. An internalization staining protocol was used to determine whether the HA10 IgG exhibited cellular uptake. The living cells were first treated with 1 µM of HA10 IgG in 1% bovine serum albumin (BSA) in 1x PBS for 15 m at 37°C. Following primary antibody removal, the cells were washed twice with 1xPBS, fixed with 4% paraformaldehyde for 10 m at room temperature, washed twice with 0.2 M glycine (pH 2.4), permeabilized with 0.25% Triton X-100 for 15 m at 37°C, and washed twice with 1x PBS prior to secondary antibody application. The fixed cells were treated with 10 µg/mL of Alexa Fluor 488-labeled goat anti-human IgG (Invitrogen) in 1% BSA in 1x PBS for 30 m at 37°C. After removal of the secondary antibody, the cells were washed

twice, counterstained with 0.3 μM DAPI, and washed two more times prior to analysis via confocal microscopy (Olympus).

Animal Models

All animal studies were performed in athymic nu/nu mice (Envigo) following Institutional Animal Care and Use Committee (IACUC) approval at the University of Minnesota. For subcutaneous tumor implantation, animals (n=3-4/group) received unilateral injections on the right shoulder of $1x10^6$ CWR-R1 or CWR-$R1^{CD133}$ cells (in 100 μL) in a 1:1 dilution of Matrigel (Corning) to 1x PBS. Tumors were measured twice weekly with calipers and volumes were calculated as length x width x height. For the intracardiac dissemination model, animals (n=4/group) received injections of $2x10^5$ CWR-R1-EnzR or CWR-R1-$EnzR^{CD133}$ cells (in 100 μL) in 1x PBS directly into the left ventricle of the heart, with a 75% accuracy rate. Following the intracardiac injections, mice were weighed twice/week to assess overall health and bioluminescent imaging was performed once/week to evaluate tumor formation and growth.

In Vivo Fluorescent Imaging

HA10 IgG was labeled with IRDye 800CW NHS Ester (LI-COR Biosciences) according to the manufacturer's instructions to develop a near-infrared (NIR) imaging agent (NIR-HA10 IgG). Mice bearing subcutaneous tumors were imaged when all tumors in each group reached a threshold of 100 mm^3. Each mouse was administered 1 nmol (155 μg) of NIR-HA10 IgG via tail vein and imaged at 1, 5, 24, 48, 72, 96, 120, and 144 h post-injection. Following intracardiac dissemination,

mice exhibiting sizeable metastatic lesions as indicated by bioluminescent imaging (BLI) were administered 1 nmol (155 µg) of NIR-HA10 IgG via tail vein and imaged at 24, 48, 72, and 144 h. In both studies, animals were imaged using an IVIS Spectrum scanner (Perkin Elmer) and euthanized at a fixed endpoint 6 days after the NIR-HA10 IgG injection or monitored for overall health and terminated when tumor volumes reached 1,000 mm^3 or weight decreased more than 15%. To determine fluorescent intensity of subcutaneous xenografts, manually drawn regions-of-interest (ROIs) were normalized to a background level of fluorescence on each mouse. To account for variability in size and luciferase expression of intracardiac tumors, a relative radiance unit was determined by dividing the total radiant efficiency of the NIR imaging by the total counts of the BLI signal and used to quantify differences in signal between $CD133^{pos}$ and $CD133^{neg}$ mice.

Bioconjugation and Radiochemistry

For nuclear imaging studies, HA10 IgG was conjugated to p-SCN-Bn-Deferoxamine (DFO, Macrocyclic) as previously described (197). Zirconium-89 (^{89}Zr) was produced and purchased from the University of Wisconsin Medical Physics Department. Once received, ^{89}Zr-oxalate (7.5 mCi) in 1.0 M oxalic acid (600 µL) was adjusted to pH 6.8–7.5 with 1.0 M Na_2CO_3. To radiolabel the IgG, the DFO-HA10 IgG conjugate (400 µL, 3.49 mg/ml, 1.4 mg of mAb) in 0.5 M HEPES (pH 7.5) was added to the neutralized ^{89}Zr-oxalate solution and incubated at room temperature with gentle agitation for 1 h. The labeled product was purified using a PD-10 column pre-equilibrated with PBS buffer. Crude and purified

samples were analyzed by radio-TLC using 50 mM EDTA (pH 5.0) as the eluent. The specific activity of ^{89}Zr-HA10 IgG was calculated to be 2.3 mCi/mg and the radiochemical purity was >98%.

Immunoreactivity

The immunoreactivity of 89Zr-HA10 IgG was assessed by using antigen-specific cellular binding assays using the CD133-transduced cell line (CWR-R1-EnzRCD133) and the non-CD133 expressing parental cell line (CWR-R1-EnzR). CWR-R1-EnzR and CWR-R1-EnzRCD133 cells were suspended in micro-centrifuge tubes at concentrations of 0.5, 1, 2, 3, 4, and 5 x 106 cells/mL in 500 µL of 1x PBS. Aliquots of 89Zr-HA10 IgG (50 µL, 25 µCi) in 1% bovine serum albumin were added to each cell suspension (final volume 550 µL) and incubated at room temperature with gentle agitation for 1 h. Cells were resuspended and washed twice with ice-cold 1x PBS. The supernatant was removed and the 89Zr radioactivity of the cell pellets were counted using a HIDEX automatic gamma counter (HIDEX, Finland). The count data was background corrected and the immunoreactive fraction of ^{89}Zr-HA10 IgG was assessed by comparing the total number of counts in the cell suspensions by control samples.

Stability Studies

The stability of ^{89}Zr-HA10 IgG with respect to change in radiochemical purity was evaluated at 0, 48, 96, and 144 h following purification. For the stability studies, 35 µCi of ^{89}Zr-HA10 IgG was added to 500 µL of 1% BSA in 1x PBS and

incubated at room temperature. The radiochemical purity of 5 µL of ^{89}Zr-HA10 IgG was assessed at each time point by radio-TLC.

In Vivo PET/CT Imaging

PET imaging experiments were conducted on an Inveon µPET/CT scanner (Siemens Medical Solutions). Mice were administered ^{89}Zr-HA10 IgG formulations (150-200 µCi, 25-30 µg of mAb, in 200 µL of 1x PBS) via tail vein injection. Approximately 5 minutes prior to recording PET/CT images, mice were anesthetized by inhalation of 2% isoflurane and placed in the scanner bed in the prone position. PET images were recorded at various time-points between 24–144 h post-injection. PET list-mode data were acquired for 30 min using a γ-ray energy window of 350–650 keV and a coincidence timing window of 3.438 ns. CT acquisition was performed for 5 mins at 80 kVp, 500 µA, 384 ms per step, and 340 steps covering 220 degrees. CT images were reconstructed using a Hu scaled Feldkamp algorithm resulting in 192 × 192 matrix and PET utilized Ordered Subset Expectation Maximization (OSEM-3D) with 18 subsets and 2 iterations resulting in a 128 × 128 matrix. 2D images were prepared in Inveon Research Workplace and quantified using AMIDE. An empirically determined system calibration factor was used to convert voxel count rates to activity concentrations and the resulting image data were normalized to the administered activity to parameterize images in terms of %ID/g. Manually drawn ellipsoid ROIs were used to determine the mean %ID/g in various tumors.

Statistical Analysis

All statistical analyses were performed using Graphpad 7.04. Quantitative RT-PCR and luciferase assay experiments prior to xenograft implantation were repeated three times with three technical replicates each time; all results were represented as mean ± SEM. IHC scores were compared using a Mann-Whitney t-test to account for differences in sample size. Patient microarray data was analyzed using a one-way ANOVA which was corrected for multiple comparisons using Sidak hypothesis testing and LuCaP microarray data was analyzed using a Welch t-test. Pearson's correlation coefficient was used to study the relationships between the genes shown in scatterplots. Animal studies were performed with n=3-4 and signals intensities were quantified as mean ± SEM in bar charts or mean ± min/max in box plots. Statistical significance was determined using a two-way ANOVA and corrected for multiple comparisons using Sidak hypothesis testing.

Results

CD133 is overexpressed in AR-/NE+ PCa

Our initial studies on CD133 suggested an inverse relationship between AR and CD133 expression in a limited number of samples by immunohistochemistry (194). To assess whether CD133 mRNA overexpression was associated with a particular PCa phenotype, 171 tumor samples resected from 63 rapid autopsy subjects were analyzed for CD133 expression as well as gene signatures which demonstrate the AR status and NE differentiation of each tumor sample (Figure 12A) (180, 186, 195). The gene that encodes CD133, *PROM1*, displayed the highest level of expression in AR-/NE+ tissues ($p<0.0001$, Figure 12B). CD133 and AR expression exhibited a moderate inverse correlation (Pearson correlation = -0.5989, Figure 12C). Similarly, expression of the prototypical AR related genes, *FOLH1* and *KLK3*, which encode for PSMA and PSA respectively, were also inversely correlated to CD133 expression (Pearson correlation=-0.5042, Figure 12D; Pearson correlation=-0.4789, Figure 12E).

Since early passages of PDX models display similar morphology to the original tumors from which they are derived (198), 24 early-passage LuCaP xenografts were investigated for expression of CD133. Only four PDX models displayed an AR-/NE+ gene signature and three (75%) of these models showed overexpression of PROM1 (Figure 13A), which was statistically significant when compared to the AR+/NE- PDX models ($p<0.0001$, Figure 13B). Complimentary to the gene expression in patient samples, CD133 exhibited a very strong inverse

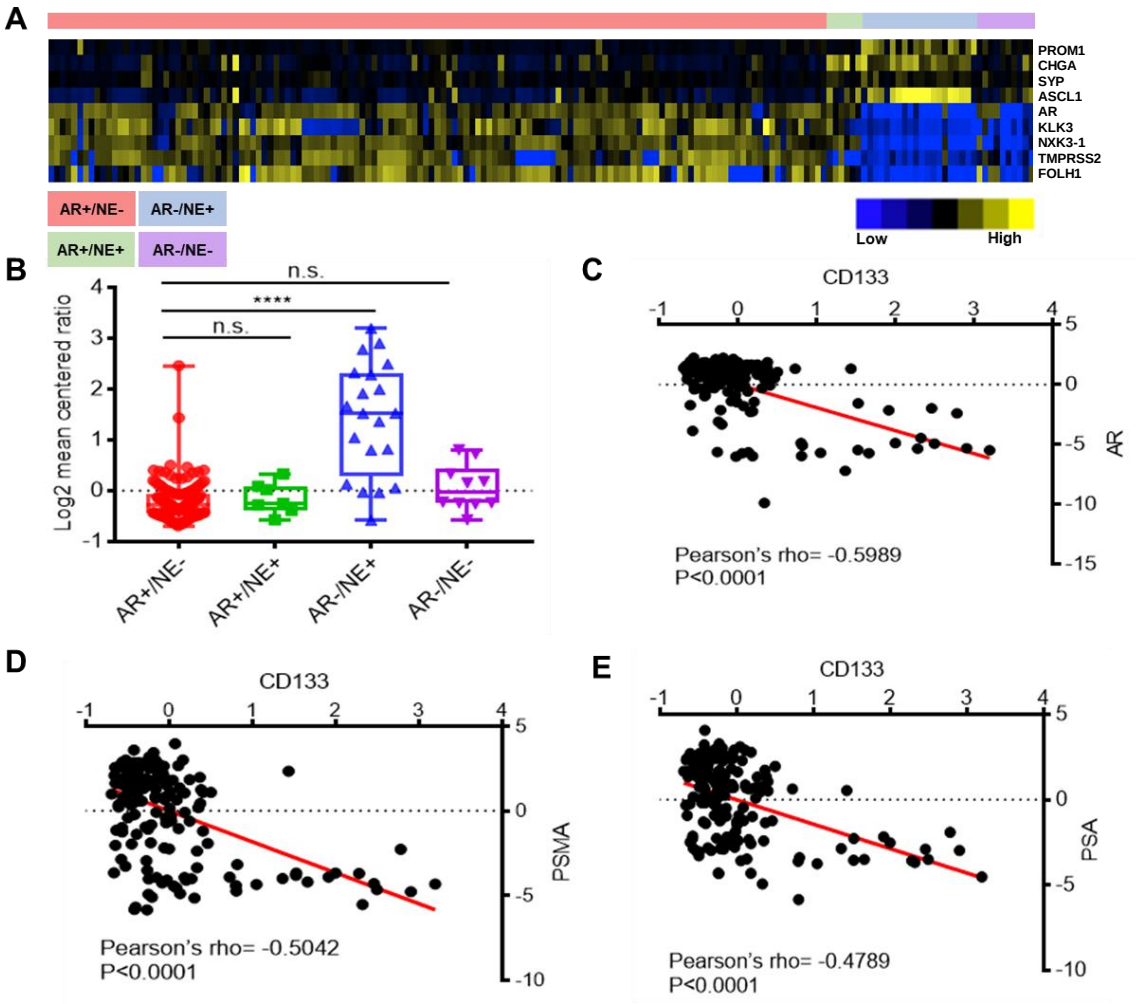

Figure 12. Gene signatures demonstrate that CD133 is overexpressed in an AR-/NE+ PCa phenotype in patient tissue samples. A) CD133 (*PROM1*) expression was evaluated across PCa tumors that displayed gene signatures signifying AR and NE status. **B)** CD133 expression in PCa patient samples was significantly increased in AR-/NE+ AVPC patients compared to other subtypes. **C)** Graph documenting a negative overall correlation between CD133 and AR expression in patient tumors. **D)** A negative overall correlation was also observed between CD133 and PSMA expression in patient tumors, and **E)** there was a negative overall correlation between CD133 and PSA expression (Pearson correlation, r=-0.4789) in patient tumors.

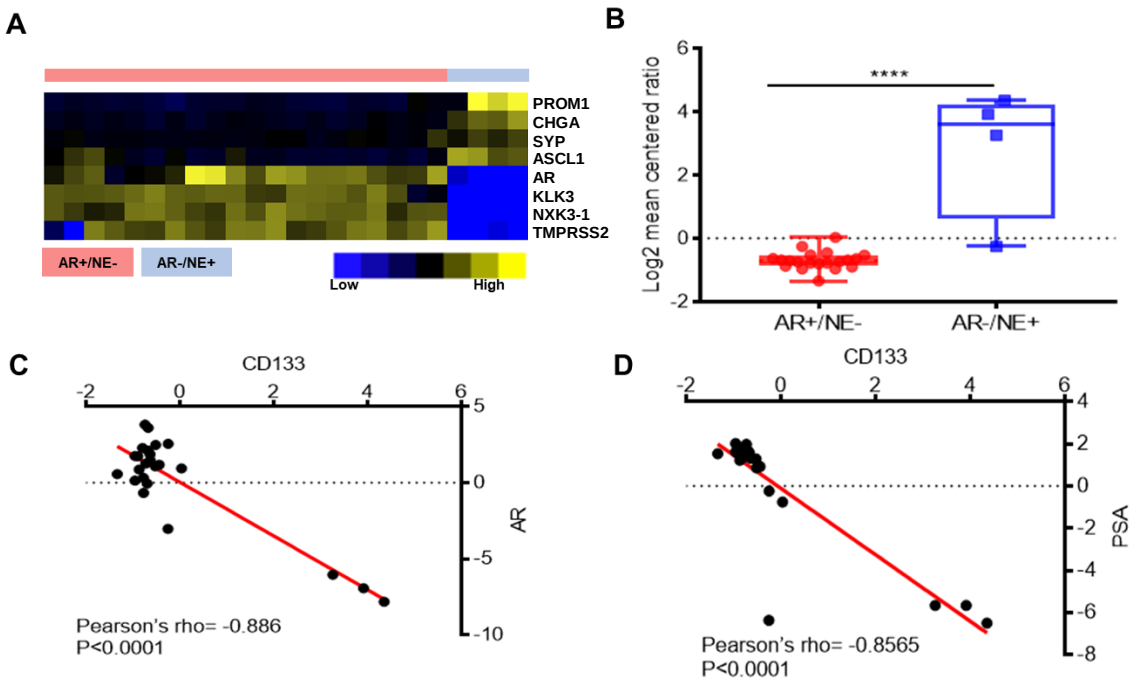

Figure 13. Gene signatures demonstrate that CD133 is overexpressed in an AR-/NE+ PCa phenotype in PDX models. A) CD133 expression was evaluated across 24 LuCaP PDX models. **B)** Quantification of CD133 expression in LuCaP PDX models was significantly increased in AR-/NE+ samples compared to AR+/NE- xenografts. **C)** A negative overall correlation was identified between CD133 and AR expression in the LuCaP PDX models. **D)** There was a negative overall correlation between CD133 and PSA expression (Pearson correlation, r=-0.8565) in LuCaP PDX models.

correlation to both AR and KLK3 in the PDX models (Pearson correlation=-0.886, Figure 13C; Pearson correlation=-0.8565, Figure 13D).

Having elucidated the relationship between AR status, NE differentiation and CD133 at the mRNA level, we next used immunohistochemistry to investigate CD133 protein expression in soft-tissue metastases. Patient tissues (n=35) were classified as either adenocarcinoma (n=10) when sections were AR+/CHGA- or neuroendocrine AVPC (n=25) when sections were AR-/CHGA+. All of the adenocarcinoma tissue sections were negative when stained for CD133 (Figure 14A). Contrarily, 92% (23/25) of the neuroendocrine AVPC tissue sections displayed intense staining and the remaining 8% (2/25) displayed moderate staining for CD133 (Figure 14B). Scoring of the staining intensity in all samples revealed that CD133 expression was significantly different between adenocarcinoma and neuroendocrine AVPC patients ($p<0.0001$, Figure 14C).

Detecting CD133 in vivo by near-infrared optical imaging

In the study described in Chapter II, we identified a human scFv, termed HA10, that specifically bound to CD133 expressed on the cell surface by flow cytometry (194). HA10 was expressed as a full-length bivalent human IgG (IgG1 scaffold) and labeled with the NIR fluorophore IRDye 800CW (NIR-HA10 IgG) for NIR optical imaging. NIR optical imaging was initially used as a proof-of-concept to document the specific localization of the antibody and acquire pharmacokinetic properties allowing for the informed selection of the appropriate radioisotope for PET imaging. Since no immortalized PCa cells lines uniformly express CD133,

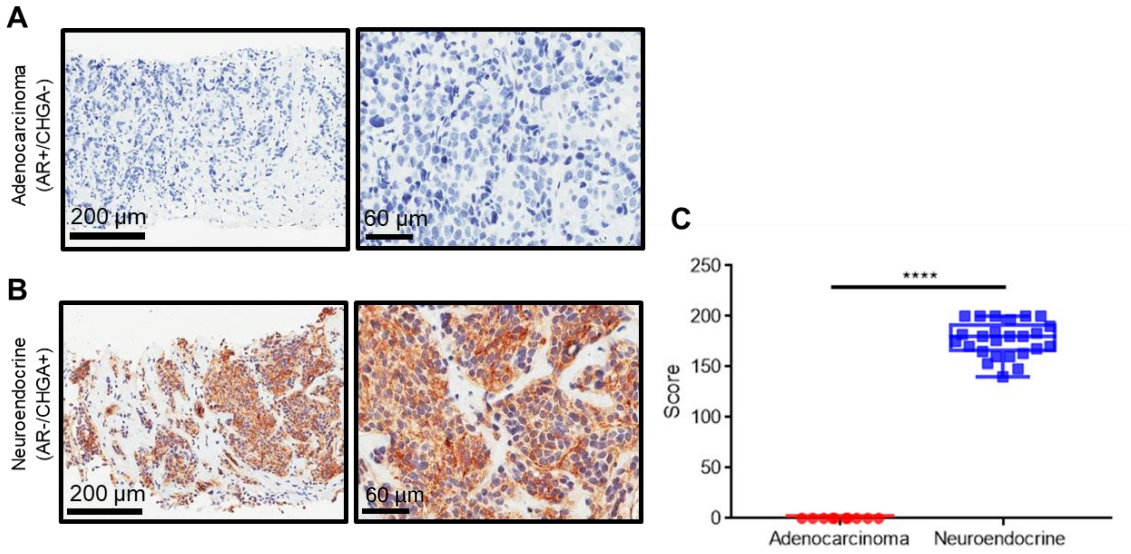

Figure 14. Immunohistochemistry shows CD133 overexpression in neuroendocrine-differentiated AVPC tissue sections. A) Representative images of CD133 expression in adenocarcinoma tissue sections at 200 µm and 60 µm. **B)** Representative images of CD133 expression in neuroendocrine-differentiated tissue sections at 200 µm and 60 µm. **C)** Quantitative analysis showed a significant increase in CD133 staining intensity from adenocarcinoma to neuroendocrine-differentiated tissue sections.

model systems were developed as previously described (194). The human PCa cells lines CWR-R1 and luciferase-expressing CWR-R1-EnzR were transduced to express CD133. CD133 expression in each cell line was quantified by qPCR (Figure 15).

Additionally, cellular uptake assays were performed to assess whether HA10 would serve as an ideal imaging probe prior to *in vivo* studies. For these assays, CWR-R1-EnzR and CWR-R1-EnzR^{CD133} cells were fixed to coverglass slides prior to or after HA10 IgG incubation to allow for surface or internalized staining, respectively. Cellular uptake was monitored using fluorescent microscopy (Figure 16). Both staining protocols revealed high fluorescent signals in the CD133^{pos} cells upon imaging. In contrast, no signal was observed in the CD133^{neg} cells in either protocol. Moreover, the different staining protocols demonstrated that HA10 IgG binds to the cell membrane and is internalized in the CD133^{pos} cells.

Mice bearing either subcutaneous CWR-R1 (n=4) or CWR-R1^{CD133} (n=4) tumors were administered 1 nmol of NIR-HA10 IgG via tail vein and imaged at 1, 5, 24, 48, 72, 96, 120, and 144 h. As early as 24 h post-injection of NIR-HA10 IgG, increased uptake in the CD133^{pos} CWR-R1^{CD133} tumors was observed compared to the CD133^{neg} tumors (Figure17A). Localization of the antibody to CD133^{pos} tumor remained present up to 144h. A small amount of non-specific localization due to the enhanced permeability retention effect was observed in the CWR-R1 tumors, however, the antibody cleared by 72 h post-injection. Similar EPR effects have been observed with the PSMA-targeted antibody and it is still considered

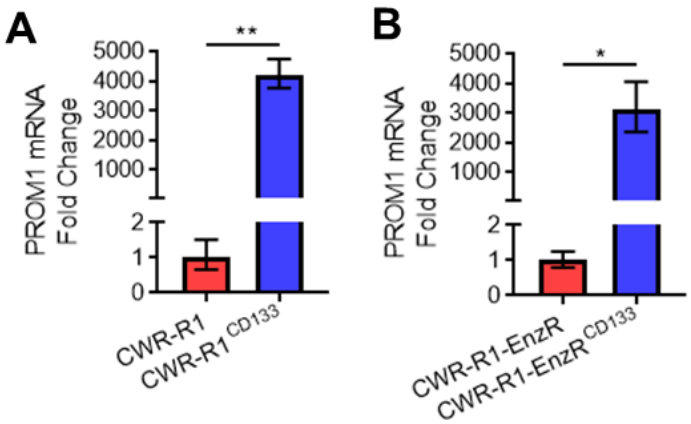

Figure 15. Confirmation of CD133 in cells prior to xenograft implantation. **A)** CD133 is artificially overexpressed in transduced CWR-R1 cells, and **B)** CD133 is artificially overexpressed in transduced luciferase-expressing CWR-R1-EnzR cells.

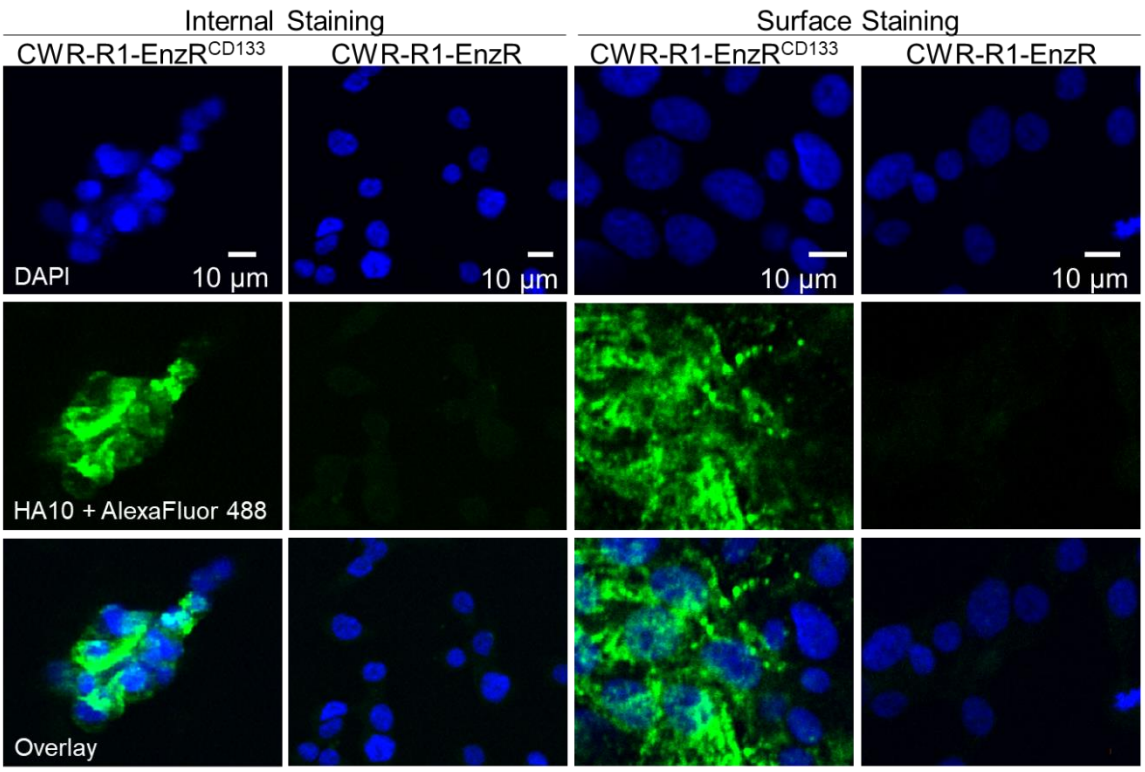

Figure 16. CD133 is internalized into CD133-expressing cells. An internalization staining protocol revealed cellular uptake of HA10 into CD133^{pos} CWR-R1-EnzR PCa cells. For the internalized staining protocol, both cell lines were treated with 1 µM of HA10 IgG for 15 minutes prior to fixation. For the surface staining protocol, both cell lines were treated with 1 µM of HA10 IgG for 15 minutes after fixation. Fixed cells were incubated with an Alexa Fluor 488-labeled anti-human IgG (green) and counterstained with DAPI.

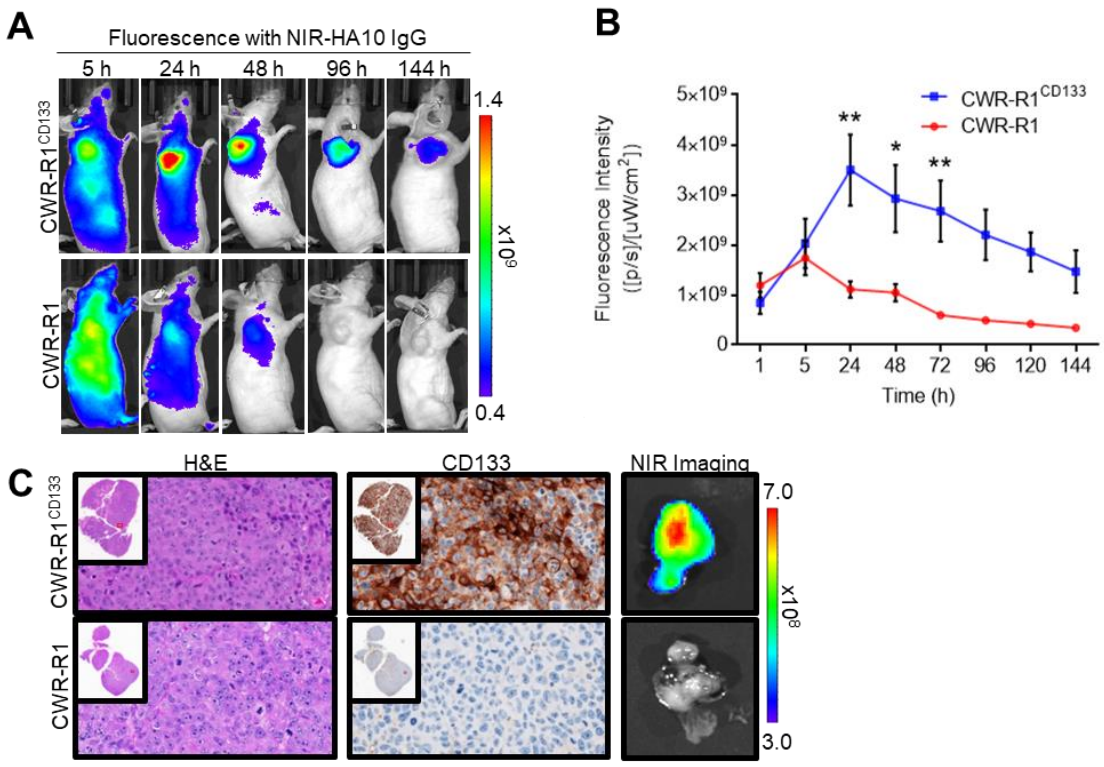

Figure 17. NIR-HA10 IgG is selective for CD133-positive subcutaneous tumors. A) NIR imaging of mice bearing either CD133-positive (CWR-R1^{CD133}) or CD133-negative (CWR-R1) subcutaneous tumors. Mice received 1 nmol of NIR-HA10 IgG via tail vein and then were imaged serially at the designated times. **B)** Quantitative analysis of the subcutaneous tumors from the NIR optical imaging experiment displayed significantly higher signals between 24-72 h post-injection. Values represent mean ± SEM of 4 animals/group. **C)** *Ex vivo* IHC (40X) and NIR image of representative mouse tumors at 144 h post-injection of NIR-HA10 IgG. Values represent mean ± SEM of 3-4 animals/group.

specific enough for clinical translation as a theranostic agent (199). Average fluorescent intensity in $CD133^{pos}$ tumors remained significantly higher than $CD133^{neg}$ tumors from 24 to 72h (Figure 17B). After the final 144 h time point, the tumors were excised from the mice, imaged by NIR and stained for CD133 expression (Figure 17C). The CWR-$R1^{CD133}$ tumors displayed high levels of CD133 expression across the entire tumor by IHC, indicating stable CD133 expression following xenograft implantation, while immunoreactivity was absent in the CWR-R1 tumor sections. Similarly, NIR imaging demonstrated a strong signal in the CWR-$R1^{CD133}$ tumors which was not present in the CWR-R1 tumors, verifying that the NIR-HA10 IgG was retained by the tumor and able to selectively detect CD133 up to 144h post-injection.

The ability of NIR-HA10 IgG to detect small, dispersed CD133-postive lesions in complex microenvironments was next tested in a metastasis model. To create an appropriate spontaneous metastasis model, mice received intracardiac injections of either luciferase-expressing CWR-R1-EnzR (n=4) or luciferase-expressing CWR-R1-$EnzR^{CD133}$ (n=3) cells. The luciferase activity of the cells was assessed 1-3 days prior to injection in all mouse models (Figure 18A). Bioluminescent imaging was performed on the mice once per week to assess lesion formation and size. Once mice in each group had at least one sizeable tumor ($>3x10^5$ total counts), they received 1 nmol of NIR-HA10 IgG via tail vein. NIR optical imaging was then conducted at 24, 48, 72, and 144 h post-injection (Figure 18B). Comparable to the subcutaneous model, the signal was highly visible and

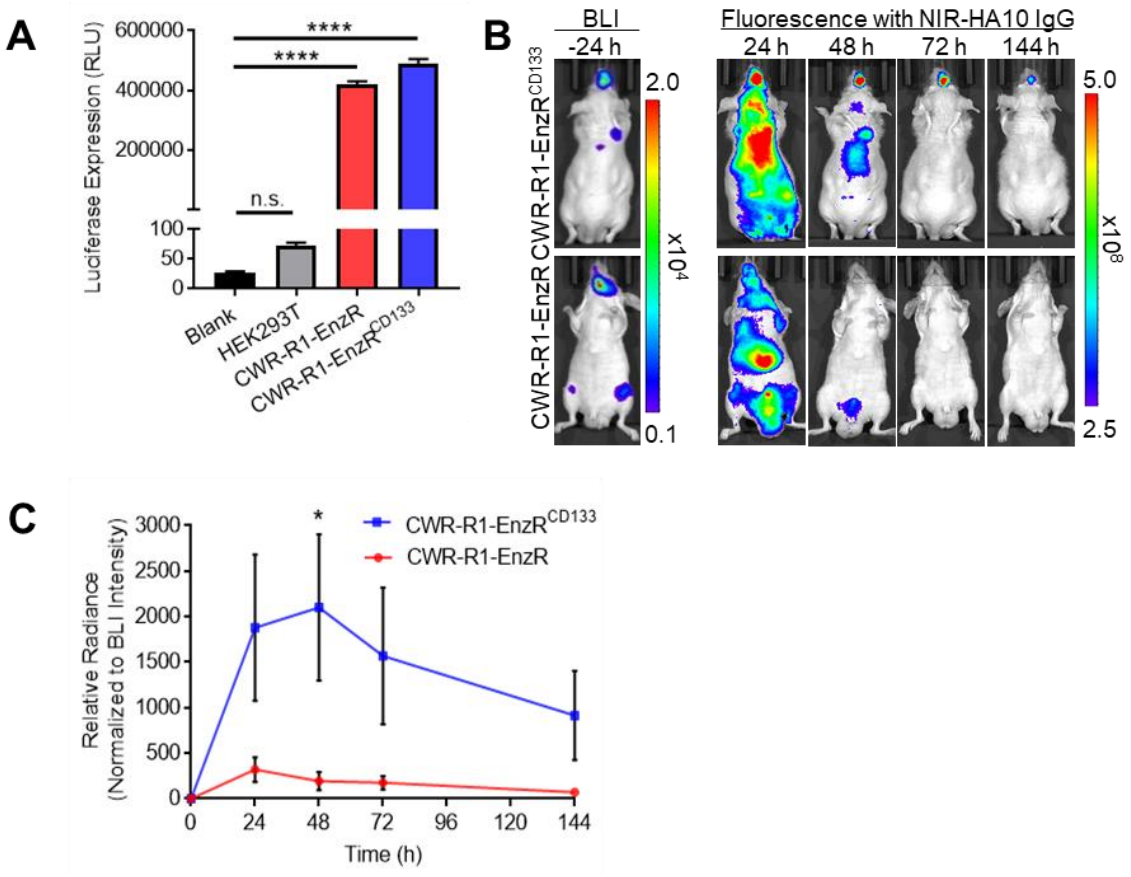

Figure 18. NIR-HA10 IgG is selective for CD133-positive metastatic tumors. **A)** Verification of luciferase expression in CWR-R1-EnzR derived cell lines. **B)** NIR imaging of representative mice possessing either CD133-positive (CWR-R1-EnzR^{CD133}) or CD133-negative (CWR-R1-EnzR) metastatic tumors. Mice received 1 nmol of NIR-HA10 IgG via tail vein and then were images at the designated times. **C)** Quantitative analysis of metastatic tumors from mice used in D displayed a significantly higher signal at 48 h post-injection. Values represent mean ± SEM of 3-4 animals/group.

specific for $CD133^{pos}$ tumors at 24 h, remained high for up to 72 h, and was still detectable at 144 h. The quantitative analysis supported this observation demonstrating a significant difference in relative radiance at 48 h (p=0.0383) and a noticeable decline in signal between 72 and 144 h in $CD133^{pos}$ tumors (Figure 18C). Furthermore, the relative radiance signal remained low in the all of the $CD133^{neg}$ tumors with minimal tumor or mouse variability, suggesting that the NIR-HA10 IgG is highly selective for $CD133^{pos}$ tumors.

PET/CT imaging of CD133

The results of the NIR optical imaging studies suggested that longitudinal PET imaging studies could be possible using radiolabeled HA10 IgG. Therefore, we decided to use the long-lived positron emitting radioisotope ^{89}Zr ($t_{1/2}$ - 3.3 d) for PET imaging. Additionally, PET imaging with ^{89}Zr-DFO conjugated antibodies, including studies with the PSMA-targeted antibody J591, are commonplace in the clinic (199-202). HA10 IgG was first conjugated to DFO and radiolabeled with ^{89}Zr-oxalate at room temperature under slightly alkaline conditions using modified methods from Zeglis *et al*. (197). Purity was assessed by radio-TLC and peaks were compared to a pure $^{89}Zr^{4+}$ standard (Figure 19A). Only ^{89}Zr-HA10 IgG sample preparations which resulted in a purity of >98% and a specific activity of >2mCi/mg were used for future analyses.

The stability of ^{89}Zr-HA10 IgG was determined by radio-TLC after incubation in 1% BSA in PBS for up to 144 h at room temperature (Figure 19B). The radiochemical purity remained above 96% at all the time points, indicating a <2%

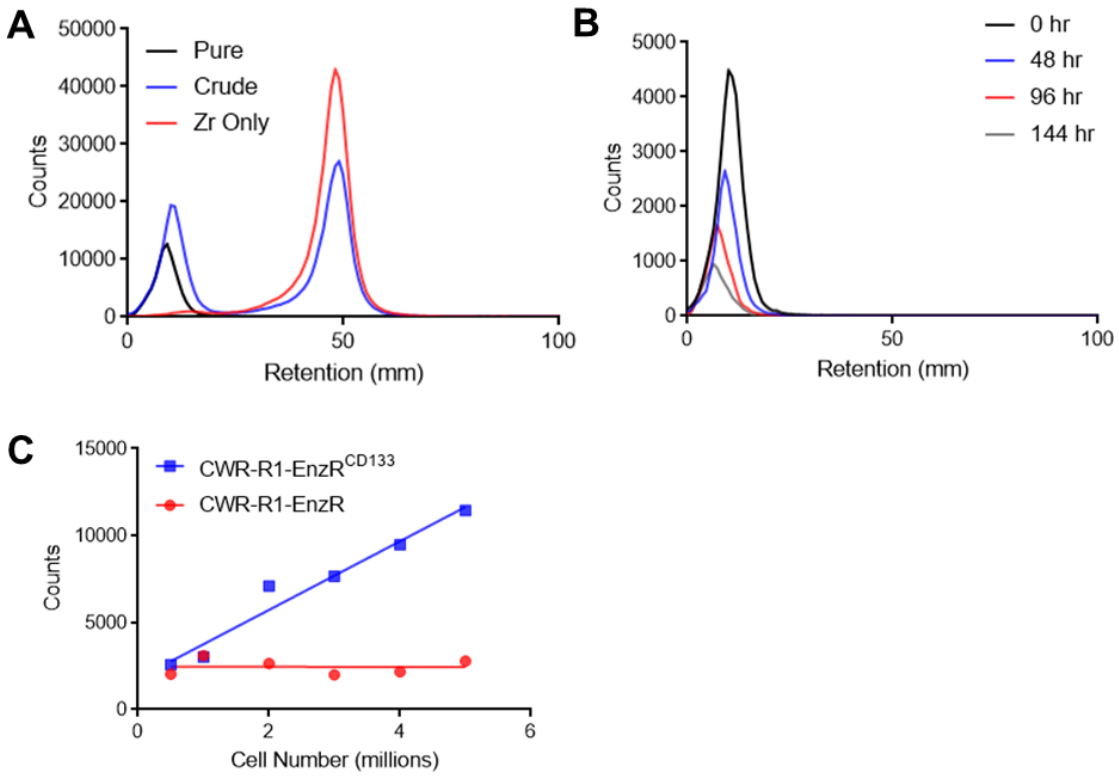

Figure 19. Characterization of ^{89}Zr-HA10 IgG. A) A representative radio-TLC chromatogram of a sample preparation including un-conjugated $^{89}Zr^{4+}$ standard, crude ^{89}Zr-HA10 IgG, and pure ^{89}Zr-HA10 IgG. **B)** Overlayed radio-TLC chromatograms of ^{89}Zr-HA10 IgG in 1% BSA in PBS at 0, 48, 96, and 144 h post-preparation (purity >96% in all samples). **C)** The immunoreactivity of ^{89}Zr-HA10 IgG was assessed by using antigen-specific cellular binding assays using CD133-positive cells (CWR-R1-EnzR^{CD133}) and CD133-negative cells (CWR-R1-EnzR). The CD133-positive cell line demonstrated a concentration-dependent increase in immunoreactive fraction compared to the CD133-negative cell line, indicating high specificity of ^{89}Zr-HA10 IgG for the CD133 antigen (p=0.0006).

decrease at any given time. Thus, ^{89}Zr-HA10 IgG was expected to remain intact *in vivo* on the time-scale described in our PET imaging studies. Similarly, immunoreactivity was measured by an antigen-specific *in vitro* cellular association assay using CWR-R1-EnzR and CWR-R1-EnzR^{CD133} cells (Figure 19C). The immunoreactive fraction of ^{89}Zr-HA10 IgG was directly proportional to the number of CD133^{pos} cells in the sample and displayed a strong linear relationship in the CD133^{pos} cell line (R^2=0.9588). CD133^{neg} control cells showed no binding to ^{89}Zr-HA10 IgG (R^2=0.0003), further demonstrating the specificity of ^{89}Zr-HA10 IgG for CD133-expressing cells.

The ability of ^{89}Zr-HA10 IgG to detect CD133-postive cancer cells in vivo was first tested in mice bearing subcutaneous CWR-R1^{CD133} (n=3) or parental CWR-R1 (n=3) tumors. Mice were injected with 150 µCi (67 µg, 2.22 mCi/mg) via tail vein and imaged by µPET/CT at 24, 48, 72, and 144 h (Figure 20A). Transverse 2D images of the CWR-R1^{CD133} xenografts showed the highest signals in the tumor compared to the CWR-R1 xenografts which showed high liver uptake. Additionally, 3D reconstructions were generated to assess ^{89}Zr-HA10 IgG uptake across multiple planes. Tumor margins were well defined in CWR-R1^{CD133} images between 24 and 72 h, which was not observed in the CD133^{neg} xenografts. Both groups of mice displayed nearly complete clearance at 144 h. Time activity curves were generated from the PET images to display the mean %ID/g of ^{89}Zr uptake in the CD133^{pos} versus CD133^{neg} groups of tumor-bearing mice (Figure 20B). A significant difference was observed at the 24 and 48 h time points with mean %ID/g

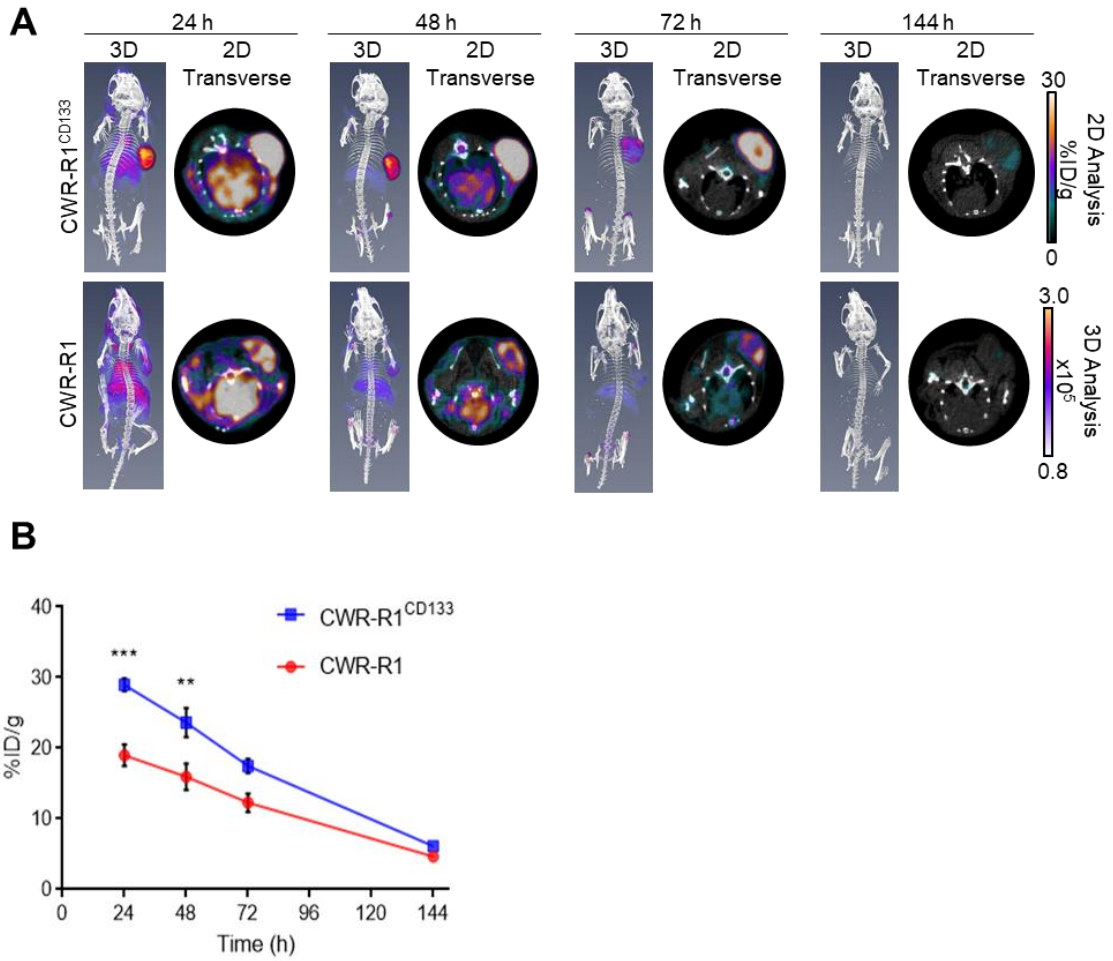

Figure 20. ^{89}Zr-HA10 IgG displays significantly higher tumoral uptake in CD133-positive tumors. A) Reconstructed 3D and 2D PET/CT images of mice bearing either CD133-positive (CWR-R1^{CD133}) or CD133-negative (CWR-R1) subcutaneous tumors. Mice received 150 µCi of ^{89}Zr-HA10 IgG via tail vein and then were imaged at the designated times. **B)** Quantitative analysis of subcutaneous tumors from mice used in A displayed significantly higher signals at 24 and 48 h post-injection. Values represent mean ± SEM of 3 animals/group. **C)** *Ex vivo* biodistribution of ^{89}Zr-HA10 IgG in all tissues of mice bearing subcutaneous CWR-R1-EnzR^{CD133} or CWR-R1-EnzR tumors. Mice were injected with 10-15 µCi of ^{89}Zr-HA10 IgG via tail vein prior to sacrifice at the designated time points. Values represent mean ± SEM of 3-4 animals.

values averaging 28.96 ± 0.92 (CWR-R1^{CD133}) and 18.97 ± 1.56 (CWR-R1) at 24 h (p=0.0003) and 23.60 ± 2.04 (CWR-R1^{CD133}) and 15.94 ± 1.89 (CWR-R1) at 48 h (p=0.0041).

Ex vivo biodistribution was performed to evaluate overall distribution and potential off-target effects of ^{89}Zr-HA10 IgG (Figure 21 and Table 3). The data reveal that distribution of ^{89}Zr-HA10 IgG was comparable in all organs between the two groups, with the exception of the tumors. At 24 h, ^{89}Zr uptake was higher in CD133^{pos} tumors at a level which was considered insignificant, but at 72 h the average %ID/g of ^{89}Zr uptake was approximately 3-fold higher in CD133^{pos} tumors at a level which was considered insignificant, but at 72 h the average %ID/g of ^{89}Zr uptake was approximately 3-fold higher in CD133^{pos} tumors (p<0.0001). Similarly, minimal ^{89}Zr uptake was observed in various other organs. This data correlates well with the PET imaging data and suggests that CD133 is a promising antigen that can be selectively targeted for the imaging of CD133-expressing tumors.

The diagnostic potential of ^{89}Zr-HA10 IgG was further investigated by µPET/CT imaging in mice bearing spontaneous metastatic lesions. Following intracardiac injection with luciferase expressing CWR-R1-EnzR^{CD133} or CWR-R1-EnzR cells, mice underwent bioluminescent imaging once per week to monitor spontaneous lesion development and growth. At approximately 3.5 weeks post-injection, the remaining healthy CD133^{pos} (n=2) and CD133^{neg} (n=2) mice had developed multiple metastatic lesions in or around the bone (Figure 22A). Mice were injected with 200 µCi (22 µg, 9.5 mCi/mg) of ^{89}Zr-HA10 IgG via tail vein and

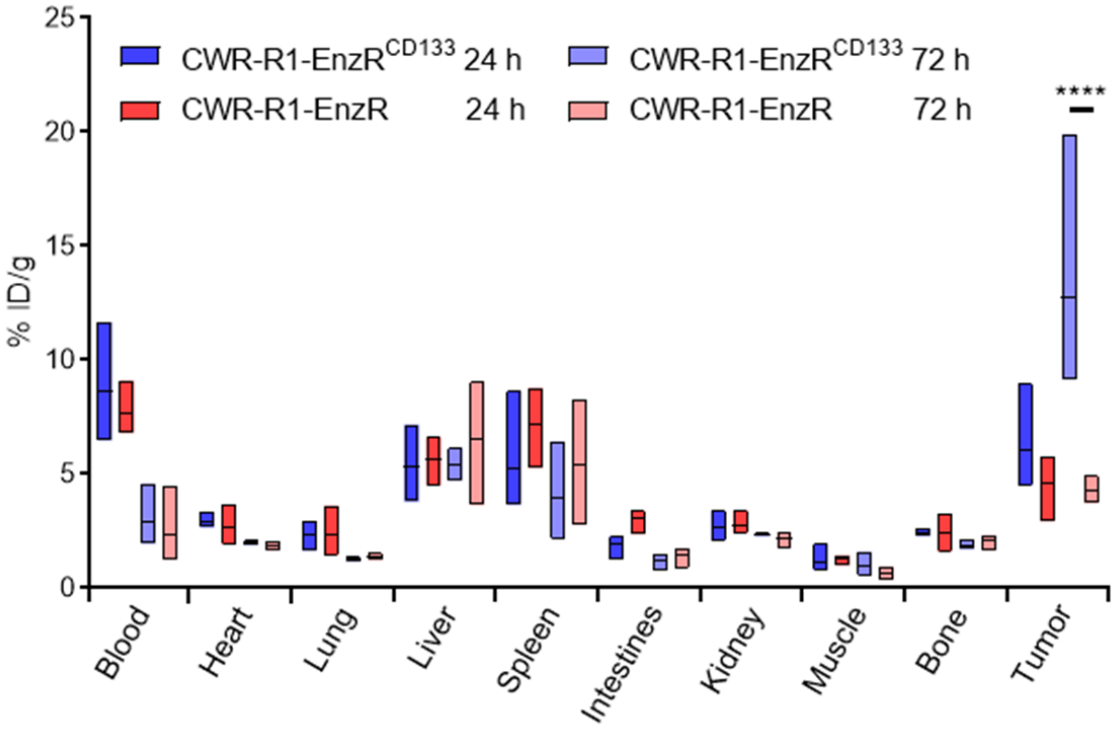

Figure 21. *Ex vivo* biodistribution of ^{89}Zr-HA10 IgG in all tissues of mice bearing subcutaneous CWR-R1-EnzR^{CD133} or CWR-R1-EnzR tumors. Mice were injected with 10-15 µCi of ^{89}Zr-HA10 IgG via tail vein prior to sacrifice at the designated time points. Values represent mean ± min/max of 3-4 animals.

Table 3. Ex vivo biodistribution data. Complete biodistribution of ^{89}Zr-HA10 IgG administered via tail vein into mice bearing subcutaneous CWR-R1-EnzR^{CD133} or CWR-R1-EnzR xenografts.

	CWR-R1-EnzR^{CD133}		**CWR-R1-EnzR**	
Organ	**24 h (n=4)**	**72 h (n=3)**	**24 h (n=4)**	**72 h (n=4)**
Blood	8.64 ± 2.39	2.87 ± 1.49	7.64 ± 1.01	2.30 ± 1.47
Heart	2.87 ± 0.33	1.99 ± 0.12	2.65 ± 0.73	1.87 ± 0.17
Lung	2.36 ± 0.56	1.26 ± 0.12	2.32 ± 0.92	1.36 ± 0.13
Liver	5.31 ± 1.39	5.38 ± 0.73	5.63 ± 1.02	6.56 ± 2.27
Spleen	5.21 ± 2.32	3.97 ± 2.20	7.18 ± 1.57	5.40 ± 2.25
Intestines	1.91 ± 0.45	1.23 ± 0.40	3.04 ± 0.48	1.45 ± 0.41
Kidney	2.68 ± 0.55	2.34 ± 0.08	2.74 ± 0.46	2.15 ± 0.30
Muscle	1.14 ± 0.54	0.96 ± 0.58	1.27 ± 0.20	0.63 ± 0.25
Bone	2.46 ± 0.14	1.88 ± 0.24	2.44 ± 0.68	2.10 ± 0.32
Tumor	6.06 ± 2.00	12.74 ± 6.19	4.58 ± 1.25	4.30 ± 0.50
Tumor/Blood	0.70 ± 0.12	5.56 ± 4.24	0.60 ± 0.13	2.40 ± 1.16
Tumor/Muscle	5.52 ± 0.64	18.51 ± 16.50	3.60 ± 0.82	7.52 ± 2.96

*The data are expressed as the mean %ID/g ± SD. The errors for tumor/blood and tumor/muscle ratios are calculated as the geometric mean of the standard deviations.

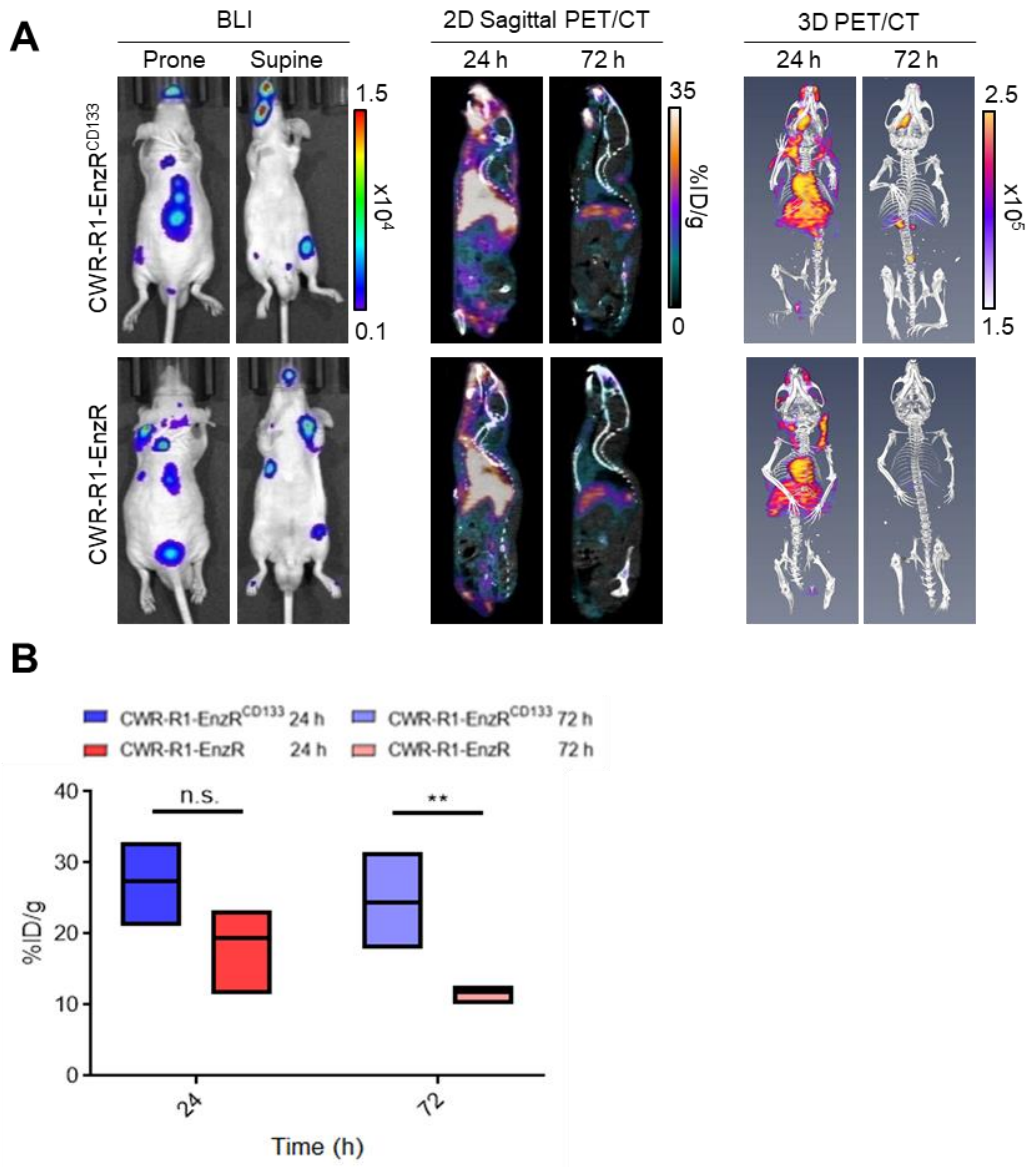

Figure 22. ^{89}Zr-HA10 IgG can selectively detect CD133-positive metastatic PCa tumors by PET/CT imaging. A) PET/CT imaging of representative mice bearing either CD133-positive (CWR-R1-EnzR^{CD133}) or CD133-negative (CWR-R1-EnzR) metastatic tumors. Mice received 200 µCi of ^{89}Zr-HA10 IgG via tail vein and then were images at the designated times. **B)** Quantitative analysis of metastatic tumors from mice used in A displayed significantly higher signals at 72 h post-injection. Values represent mean ± min/max of 4 tumors/group from 2 animals/group.

imaged by μPET/CT at 24 and 72 h. 2D and 3D images revealed a high level of ^{89}Zr distribution at 24 h in both groups of mice, while ^{89}Zr uptake at 72 h was exclusively observed in the tumors of CD133^{pos} mice. Quantification of the mean %ID/g of ^{89}Zr uptake in the tumors confirmed these results by showing that there was no significant difference at 24 h despite higher signals in the CD133^{pos} tumors, 27.41 ± 2.50 versus 19.35 ± 2.63 (Figure 22B). At 72 h, the mean %ID/g in the tumors was significantly different among the two groups, 24.30 ± 3.19 and 11.82 ± 0.57, respectively ($p=0.0069$).

Discussion

The emergence of non-AR driven disease in patients with CRPC has steadily increased after the introduction of AR-signaling inhibitors such as abiraterone and enzalutamide (181, 186, 203). At this stage of disease, survival is poor and therapies that dramatically prolong life do not exist. While new therapies are in demand, new imaging agents to monitor disease progression and response to therapy are also needed. PSMA-targeted radiotracers that have shown promise at detecting bone and visceral metastases in patients with adenocarcinoma are ineffective due to the lack of PSMA expression in non-AR driven PCa. As such, novel antigens and targeted imaging agents are needed to aid in the detection and monitoring of this subtype of disease. In this study, we have identified CD133 as a new targetable antigen that is overexpressed in one of these non-PSMA expressing patient populations and developed a novel antibody-based imaging agent that can accurately detect CD133 in preclinical models of PCa. To our knowledge, this is the first study demonstrating that CD133 is a promising marker for AR-/NE+ AVPC. Furthermore, despite the use of preclinical CD133-targeted PET imaging in other cancers (204), this is the first time that CD133 has been targeted for imaging of PCa.

Our targeted agent, HA10 IgG, showed significant selectivity and sensitivity for CD133-expressing tumors using multiple imaging modalities and cancer models, verifying the specificity of the antibody-antigen interaction. Interestingly, subcutaneous xenograft models in both the NIR and PET imaging studies

displayed better tumoral uptake at earlier time points (between 24-48 h, Figure 17A and 20A), whereas, metastatic xenografts displayed better uptake at slightly later time points (between 48-72 h, Figure 18B and 22A). It has been shown that different PCa xenografts exhibit varying degrees of vasculature as determined by tumor-stromal interaction, size, and site of the tumor (205). Differences in these factors are likely to account for the slightly different uptake kinetics exhibited by the HA10 IgG. Additionally, PET imaging revealed that ^{89}Zr-HA10 IgG tumoral uptake varied within the CD133^{pos} metastatic tumors. While all CD133^{pos} tumors were visible at 72 h in the 2D images, only some tumors were visible in the 3D reconstruction after background normalization, suggesting there was less ^{89}Zr-HA10 IgG uptake in some of the metastatic lesions. Due to the high signals in the small spinal tumor and large mandibular tumor, we postulated that size and anatomical location were not the primary causes of this occurrence. We also determined that CD133 expression is stable following implantation of the xenografts, however, we did not rule out that the metastatic process and tumor microenvironment of the secondary site may have altered the tumor phenotype and resulted in less ^{89}Zr-HA10 IgG uptake. Multiple studies have suggested that preclinical metastatic models may lack the ability to faithfully mimic the tumor microenvironment during metastasis (206-208), which may explain the reduced PET signal in some of the CD133^{pos} metastatic lesions.

In conclusion, this study illustrates the importance of identifying new antigens for targeted imaging and treatment monitoring of AVPC patients. Our data

show that AVPC patients with an AR-/NE+ phenotype possess high levels of the surface protein, CD133. Our previous studies show that the epitope our antibody recognizes on CD133 is not highly expressed in early stages of PCa or healthy tissues (194), demonstrating its promise as targetable biomarker for late-stage AVPC patients. Furthermore, our data show that CD133 can be exploited for improved imaging using a novel antibody developed by our lab. HA10 IgG was specific for $CD133^{pos}$ tumors by various imaging modalities, including clinically relevant modality PET/CT imaging. These encouraging results indicate that ^{89}Zr-HA10 IgG displays high potential as a radiotracer for non-invasive immunoPET imaging of AR-/NE+ AVPC patients.

CHAPTER IV: Conclusions and Future Directions

Conclusions

CD133 is an unreliable CSC marker in PCa but is likely an effective biomarker for a subset of AVPC

CD133 has been postulated to identify CSCs in numerous solid cancers including brain cancer (209), PCa (148), and colon cancer (210). In many of these studies, CD133-expressing CSCs exhibited self-renewal potential and the ability to regenerate a histologically similar tumor mass following transplantation into immunodeficient mice. However, using CD133 to identify and isolate CSCs has recently become controversial for the following reasons: 1) it is frequently identified in the glandular epithelium in some tissues which could make it difficult to differentiate between CSCs and non-stem like cancer cells, 2) a few studies have documented the inability of $CD133^{pos}$ cell populations to recapitulate the original tumor morphology when xenotransplanted suggesting that CD133 may also be expressed on differentiated cells, and 3) some studies have shown $CD133^{neg}$ populations are able to recapitulate the original tumor morphology suggesting that CD133 may not uniquely mark CSCs (98). Despite the unreliable nature of CD133 as a CSC marker, studies in brain, colon, and renal cancer have indicated that CD133 overexpression is correlated to shorter patient survival and more aggressive disease (211-213), suggesting its role as a biomarker of cancer progression rather than stemness directly. This research encompasses the first studies to establish and define CD133 as a biomarker of aggressive disease in PCa.

CD133 is overexpressed in AR-/NE+ AVPC patients

The first evidence of CD133 overexpression in PCa patients was identified in a case study described in Chapter II. This patient presented with high-risk regional PCa and underwent a TURP and ADT therapy which initially caused a reduction in PSA, however, the cancer had progressed after 1 year of treatment. The patient immediately began second-generation anti-androgen therapy and displayed some level of biochemical regression, but also developed clinical progression in the form of extensive liver metastases, indicating a shift from AR-driven CRPC to non-AR driven AVPC. Interestingly, the liver metastases showed strong staining for CD133, while the original TURP biopsy exhibited no CD133 expression. Our studies also revealed that the non-AR expressing liver metastasis biopsy displayed high staining for the neuroendocrine marker, CHGA, indicating that CD133 may be specific to a particular phenotype of AVPC which is AR-/NE+.

In Chapter III, we tested this hypothesis using DNA microarrays from 171 CRPC patient tumor samples. Each sample was evaluated for markers of AR gene regulation, neuroendocrine differentiation, and CD133 expression. The gene signatures for AR and NE status were chosen according to previously published literature. These results revealed that only the AR-/NE+ phenotype of AVPC patients exhibited significantly elevated levels of CD133 expression. Similarly, these results indicated that there was an inverse relationship between CD133 expression and PSMA expression in this patient population, suggesting that this is a valuable biomarker for patients that do not express PSMA. These data were

confirmed by immunohistochemistry of 35 PCa patient tissue samples (25 AR-/NE+ samples and 10 AR+/NE- samples). All 25 AR-/NE+ patients displayed moderate to high staining for CD133, while the 10 AR+/NE- patients showed no staining for CD133, concluding that CD133 is a selective biomarker for AR-/NE+ AVPC.

Development of the novel antibody, HA10 IgG, facilitated better CD133 detection than commercially available antibodies

The most frequently used commercially available antibodies for CD133 bind to glycosylated epitopes of the EC3 domain. Since CD133 is known to be structurally complex, we hypothesized that detecting deglycosylated CD133 may provide a more accurate and effective approach to targeting CD133 for imaging and therapy of lethal AVPC. To develop an improved antibody, we used antibody phage display to identify a human scFv, termed HA10. HA10 is selective for a glycosylation-independent epitope on the EC2 domain of CD133, providing the ability to detect both glycosylated and deglycosylated CD133. When compared to the commercial antibody, AC133, HA10 detected CD133 at similar or better levels in all assays tested to date. Notably, HA10 identified more CD133 in assays which relied heavily on maintaining the natural antigen structure, such as flow cytometry, suggesting that there is a small population of cells that are masked by glycosylation and are undetectable using commercial antibodies. After characterization, HA10 was further developed into a full-length human IgG, termed HA10 IgG, and used for imaging preclinical models of PCa.

HA10 IgG displayed diagnostic potential in CD133-expressing preclinical models of PCa

HA10 IgG was labeled with a NIR probe or ^{89}Zr and used for fluorescent imaging or PET imaging, respectively. Fluorescent imaging and PET imaging were performed in subcutaneous and metastatic tumor models. In the subcutaneous model, both probes displayed high selectivity and specificity for CD133^{pos} tumors between 2 to 3 days post-injection. Tumor localization was observed at 24 hours post-injection, however, there was still a significant amount of probe in circulation at that time which leads to decreased contrast in the image. Alternatively, majority of the background signal was distributed or cleared between 48-72 hours, indicating that there is an optimal time frame for imaging after probe administration. *Ex vivo* biodistribution with the PET imaging probe confirmed these results by demonstrating a high concentration of ^{89}Zr remaining in the blood at 24 hours post-injection.

Similar selectivity for CD133 was observed in the metastatic models, however, there were some metastatic lesions during the PET imaging studies that exhibited much lower tumoral uptake signals compared to other lesions within the same mouse. In general, spinal and mandibular lesions displayed better uptake than limb lesions. Since CD133 expression was confirmed by IHC after imaging and tumor size between mandibular tumors and spinal tumors was highly variable, we believe that vascularization and/or the tumor microenvironment may play a critical role in determining how well the probe is distributed to the lesion and will

likely affect the efficacy of the probe. Additionally, since ^{89}Zr is known to be bone seeking, it is possible that the tumor signal is masked by non-specific accumulation of the radioisotope to the bone. Other radioisotopes will need to be investigated to assess whether the bone-seeking nature of ^{89}Zr is interfering with the diagnostic potential of HA10 IgG.

Future Directions

What is the therapeutic potential of HA10 IgG?

Numerous clinical trials using alpha- and beta- particle radiolabeled J591 to treat CRPC are currently underway (75, 214-218), however, our studies show that PSMA is not expressed in a subset of advanced CRPC patients. Thus, we hypothesize that a proportion of the patients in these trials which display an AR-/NE+ phenotype will not respond to a PSMA-targeted therapy. Alternatively, our preliminary analyses of HA10 IgG suggest that its ability to fill the void of targeted agents for AR-/NE+ AVPC patients. The selectivity and specificity of HA10 IgG provides a rationale for studying it as a radioimmunotherapy agent for targeted treatment of AR-/NE+ AVPC. At this time, there is no evidence that HA10 IgG induces any antibody-dependent cellular cytotoxicity, although this phenomenon was never thoroughly investigated in these studies. Short term exposure to the labeled HA10 IgG for imaging studies revealed no decline in overall mouse health *in vivo* or cell toxicity *in vitro*. Additionally, previous research in CD133 knockout mice showed that the antigen CD133 was not critical to the overall viability of the mouse (93, 219), however, these same studies also indicated that CD133 is expressed in hematopoietic stem cells and may be critical for retinal function. Future therapeutic studies are needed to assess the therapeutic potential of HA10 IgG and should adequately monitor adverse effects related to myelosuppression and vision loss.

Similarly, despite the fact that CD133 represents a promising target for imaging and therapeutic intervention of AR-/NE+ AVPC, it is still subject to various resistance mechanisms like any other protein. For example, since CD133 is not essential for cell viability (93) and $CD133^{pos}$ cells are documented to give rise to $CD133^{neg}$ cell populations (149), it is reasonable to assume that a tumor which originally expressed CD133 would adapt to preferentially produce HA10 IgG-resistant $CD133^{neg}$ tumors. Furthermore, CD133 currently has 7 different defined isoforms and 6 more potential isoforms that are produced by alternative splicing (220). Mechanisms of antibody resistance may also emerge through alterations on the epitope in which the antibody binds. Future studies are required to directly identify where HA10 IgG is binding on the EC2 domain of CD133 and determine whether any of the previously described isoforms are already lacking this associated epitope.

<u>How is CD133 regulated and does it directly drive more aggressive disease?</u>

The physiologic function of CD133 in normal biology and the progression of cancer remains elusive. Understanding the molecular underpinnings of how CD133 is regulated and drives aggressive disease would provide more insight into the diagnostic and therapeutic potential of CD133-targeted agents such as HA10 IgG. While this research did not focus on understanding CD133 regulation and signaling, some preliminary research was performed to investigate which pathways may affect CD133 expression. The first and most frequently referenced pathway was the Wnt signaling pathway. To interrogate this pathway, PC3 and

CWR-R1-EnzR cells were treated for 72 hours with 20 ng/ml of Wnt3a. RNA was extracted from these cell lines and qPCR was performed to evaluate CD133 expression. Interestingly, CD133 expression was significantly increased in CWR-R1-EnzR cells (Figure 23A), but not PC3 cells (Figure 23B), indicating that differences in these cell lines results in different CD133 regulation. Similar results were observed when cells were transduced with the BAMBI gene which encodes for a transmembrane glycoprotein related to the type I receptors of the transforming growth factor-beta (TGFβ) family (Figure 24A and 24B). Despite the fact that TGFβ has been documented to induce CD133 expression in colon cancer and PCa (221, 222), this is the first evidence to suggest that BAMBI specifically may play a role in CD133 regulation. More research is needed to investigate these pathways and identify if they are directly regulating CD133 expression and how this all correlates to more aggressive disease.

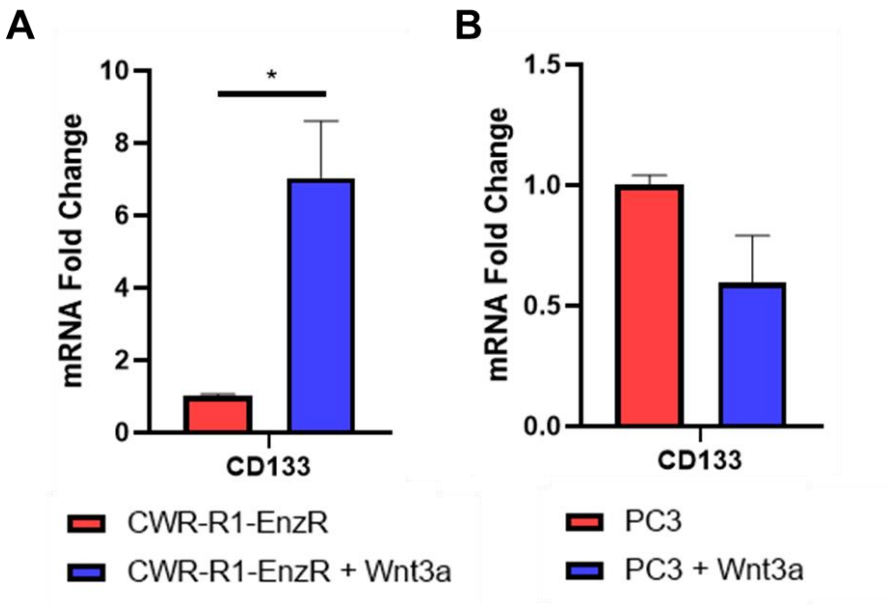

Figure 23. Addition of Wnt3a to PCa cell lines produces variable CD133 expression in different PCa cell lines. A) CWR-R1-EnzR cells and **B)** PC3 cells were stimulated with 20 ng/mL Wnt3a for 72 hours. qPCR was used to determine relative mRNA levels of CD133.

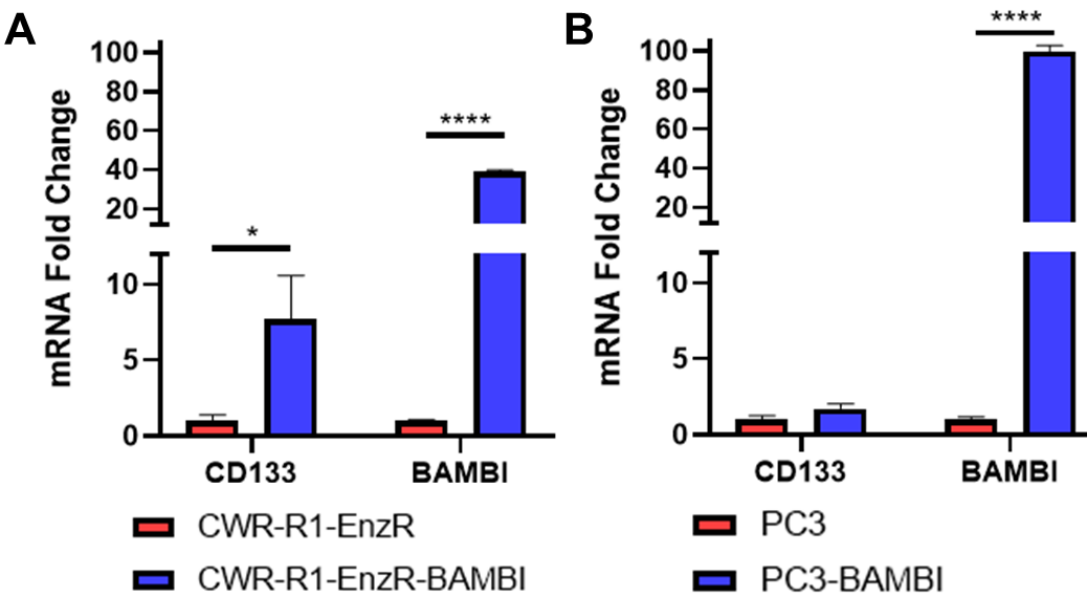

Figure 24. Transduction of BAMBI into PCa cell lines produces variable CD133 expression in different PCa cell lines. **A)** CWR-R1-EnzR cells and **B)** PC3 cells were stably transduced with lentivirus to produce BAMBI. qPCR was used to determine relative mRNA levels of CD133 and verify BAMBI expression.

References

1. Facts & Figures 2019 Atlanta, GA: American Cancer Society 2019 [Available from: https://www.cancer.org/cancer/prostate-cancer/about/key-statistics.html#references.
2. Howlader N, Noone AM, Krapcho M, Miller D, Brest A, Yu M, et al. SEER Cancer Statistics Review, 1975-2016 Bethesda, MD: National Cancer Institute; 2019 [Available from: https://seer.cancer.gov/csr/1975_2016/.
3. Chang S, Schapira L, Williams M, Meyerhardt J, Loprinzi C, Mulrooney DA, et al. Prostate Cancer: Types of Treatment Cancer.Net; 2018 [Available from: https://www.cancer.net/about-us/cancernet-editorial-board.
4. Watchful Waiting or Active Surveillance for Prostate Cancer: American Cancer Society 2016 [Available from: https://www.cancer.org/cancer/prostate-cancer/treating/watchful-waiting.html#references.
5. Heidenreich A, Bastian PJ, Bellmunt J, Bolla M, Joniau S, van der Kwast T, et al. EAU guidelines on prostate cancer. part 1: screening, diagnosis, and local treatment with curative intent-update 2013. Eur Urol. 2014;65(1):124-37.
6. Kinsella N, Helleman J, Bruinsma S, Carlsson S, Cahill D, Brown C, et al. Active surveillance for prostate cancer: a systematic review of contemporary worldwide practices. Transl Androl Urol. 2018;7(1):83-97.
7. Bekelman JE, Rumble RB, Chen RC, Pisansky TM, Finelli A, Feifer A, et al. Clinically Localized Prostate Cancer: ASCO Clinical Practice Guideline Endorsement of an American Urological Association/American Society for Radiation Oncology/Society of Urologic Oncology Guideline. J Clin Oncol. 2018:JCO1800606.
8. Harris WP, Mostaghel EA, Nelson PS, Montgomery B. Androgen deprivation therapy: progress in understanding mechanisms of resistance and optimizing androgen depletion. Nat Clin Pract Urol. 2009;6(2):76-85.
9. Hormone Therapy for Prostate Cancer: American Cancer Society 2018 [Available from: https://www.cancer.org/cancer/prostate-cancer/treating/hormone-therapy.html#written_by.
10. Balk SP. Androgen receptor functions in prostate cancer development and progression. Asian J Androl. 2014;16(4):561-4.
11. Huggins C, Hodges CV. Studies on prostatic cancer. I. The effect of castration, of estrogen and androgen injection on serum phosphatases in metastatic carcinoma of the prostate. CA Cancer J Clin. 1972;22(4):232-40.
12. Cookson MS, Roth BJ, Dahm P, Engstrom C, Freedland SJ, Hussain M, et al. Castration-resistant prostate cancer: AUA Guideline. J Urol. 2013;190(2):429-38.
13. Saad F, Hotte SJ. Guidelines for the management of castrate-resistant prostate cancer. Can Urol Assoc J. 2010;4(6):380-4.
14. El-Amm J, Aragon-Ching JB. The Current Landscape of Treatment in Non-Metastatic Castration-Resistant Prostate Cancer. Clin Med Insights Oncol. 2019;13:1179554919833927.

15. James ND, de Bono JS, Spears MR, Clarke NW, Mason MD, Dearnaley DP, et al. Abiraterone for Prostate Cancer Not Previously Treated with Hormone Therapy. N Engl J Med. 2017;377(4):338-51.
16. Feldman BJ, Feldman D. The development of androgen-independent prostate cancer. Nat Rev Cancer. 2001;1(1):34-45.
17. Burgess S. FDA Approves Provenge: U.S. Food and Drug Administration; 2010 [Available from: https://www.drugs.com/newdrugs/fda-approves-provenge-cellular-immunotherapy-men-advanced-prostate-cancer-2130.html.
18. Cheever MA, Higano CS. PROVENGE (Sipuleucel-T) in prostate cancer: the first FDA-approved therapeutic cancer vaccine. Clin Cancer Res. 2011;17(11):3520-6.
19. Kantoff PW, Higano CS, Shore ND, Berger ER, Small EJ, Penson DF, et al. Sipuleucel-T immunotherapy for castration-resistant prostate cancer. N Engl J Med. 2010;363(5):411-22.
20. Small EJ, Schellhammer PF, Higano CS, Redfern CH, Nemunaitis JJ, Valone FH, et al. Placebo-controlled phase III trial of immunologic therapy with sipuleucel-T (APC8015) in patients with metastatic, asymptomatic hormone refractory prostate cancer. J Clin Oncol. 2006;24(19):3089-94.
21. Aparicio AM, Harzstark AL, Corn PG, Wen S, Araujo JC, Tu SM, et al. Platinum-based chemotherapy for variant castrate-resistant prostate cancer. Clin Cancer Res. 2013;19(13):3621-30.
22. Beltran H, Tomlins S, Aparicio A, Arora V, Rickman D, Ayala G, et al. Aggressive variants of castration-resistant prostate cancer. Clin Cancer Res. 2014;20(11):2846-50.
23. Vlachostergios PJ, Puca L, Beltran H. Emerging Variants of Castration-Resistant Prostate Cancer. Curr Oncol Rep. 2017;19(5):32.
24. Davies AH, Beltran H, Zoubeidi A. Cellular plasticity and the neuroendocrine phenotype in prostate cancer. Nat Rev Urol. 2018;15(5):271-86.
25. Should I Be Screened? : Prostate Cancer Foundation 2019 [Available from: https://www.pcf.org/about-prostate-cancer/what-is-prostate-cancer/the-psa-test/should-i-be-screened/.
26. Force USPST, Grossman DC, Curry SJ, Owens DK, Bibbins-Domingo K, Caughey AB, et al. Screening for Prostate Cancer: US Preventive Services Task Force Recommendation Statement. JAMA. 2018;319(18):1901-13.
27. Gulati R, Gore JL, Etzioni R. Comparative effectiveness of alternative prostate-specific antigen--based prostate cancer screening strategies: model estimates of potential benefits and harms. Ann Intern Med. 2013;158(3):145-53.
28. Ahmed HU, Arya M, Freeman A, Emberton M. Do low-grade and low-volume prostate cancers bear the hallmarks of malignancy? Lancet Oncol. 2012;13(11):e509-17.
29. Eggener SE, Badani K, Barocas DA, Barrisford GW, Cheng JS, Chin AI, et al. Gleason 6 Prostate Cancer: Translating Biology into Population Health. J Urol. 2015;194(3):626-34.

30. Loeb S, Bjurlin MA, Nicholson J, Tammela TL, Penson DF, Carter HB, et al. Overdiagnosis and overtreatment of prostate cancer. Eur Urol. 2014;65(6):1046-55.
31. Balk SP, Ko YJ, Bubley GJ. Biology of prostate-specific antigen. J Clin Oncol. 2003;21(2):383-91.
32. What are Some Other Causes of a High PSA? : Prostate Cancer Foundation; 2019 [Available from: https://www.pcf.org/what-are-some-other-causes-of-a-high-psa/?gclid=Cj0KCQjw6IfoBRCiARIsAF6q06tP8gggsOk08tWvAQusDNjn5_STHJxnGoKfkCGKf0prJ6D_GF24o38aAlynEALw_wcB.
33. Palmerola R, Smith P, Elliot V, Reese CT, Mahon FB, Harpster LE, et al. The digital rectal examination (DRE) remains important - outcomes from a contemporary cohort of men undergoing an initial 12-18 core prostate needle biopsy. Can J Urol. 2012;19(6):6542-7.
34. Tests for Prostate Cancer: American Cancer Society 2017 [Available from: https://www.cancer.org/cancer/prostate-cancer/detection-diagnosis-staging/how-diagnosed.html#written_by.
35. Prostate Cancer Prevention and Early Detection: American Cancer Society 2019 [Available from: https://www.cancer.org/cancer/prostate-cancer/early-detection.html.
36. Epstein JI, Zelefsky MJ, Sjoberg DD, Nelson JB, Egevad L, Magi-Galluzzi C, et al. A Contemporary Prostate Cancer Grading System: A Validated Alternative to the Gleason Score. Eur Urol. 2016;69(3):428-35.
37. Lindenberg L, Choyke P, Dahut W. Prostate Cancer Imaging with Novel PET Tracers. Curr Urol Rep. 2016;17(3):18.
38. Den RB, George D, Pieczonka C, McNamara M. Ra-223 Treatment for Bone Metastases in Castrate-Resistant Prostate Cancer: Practical Management Issues for Patient Selection. Am J Clin Oncol. 2019;42(4):399-406.
39. Gandaglia G, Abdollah F, Schiffmann J, Trudeau V, Shariat SF, Kim SP, et al. Distribution of metastatic sites in patients with prostate cancer: A population-based analysis. Prostate. 2014;74(2):210-6.
40. Inoue T, Segawa T, Kamba T, Yoshimura K, Nakamura E, Nishiyama H, et al. Prevalence of skeletal complications and their impact on survival of hormone refractory prostate cancer patients in Japan. Urology. 2009;73(5):1104-9.
41. Subramanian G, McAfee JG, Blair RJ, Kallfelz FA, Thomas FD. Technetium-99m-methylene diphosphonate--a superior agent for skeletal imaging: comparison with other technetium complexes. J Nucl Med. 1975;16(8):744-55.
42. Wondergem M, van der Zant FM, Knol RJJ, Burgers AMG, Bos SD, de Jong IJ, et al. (99m)Tc-HDP bone scintigraphy and (18)F-sodiumfluoride PET/CT in primary staging of patients with prostate cancer. World J Urol. 2018;36(1):27-34.

43. McGregor B, Tulloch AG, Quinlan MF, Lovegrove F. The role of bone scanning in the assessment of prostatic carcinoma. Br J Urol. 1978;50(3):178-81.
44. O'Donoghue EP, Constable AR, Sherwood T, Stevenson JJ, Chisholm GD. Bone scanning and plasma phosphatases in carcinoma of the prostate. Br J Urol. 1978;50(3):172-7.
45. Juweid ME, Cheson BD. Positron-emission tomography and assessment of cancer therapy. N Engl J Med. 2006;354(5):496-507.
46. Rohren EM, Turkington TG, Coleman RE. Clinical applications of PET in oncology. Radiology. 2004;231(2):305-32.
47. Sheikhbahaei S, Jones KM, Werner RA, Salas-Fragomeni RA, Marcus CV, Higuchi T, et al. (18)F-NaF-PET/CT for the detection of bone metastasis in prostate cancer: a meta-analysis of diagnostic accuracy studies. Ann Nucl Med. 2019;33(5):351-61.
48. Hillner BE, Siegel BA, Hanna L, Duan F, Shields AF, Coleman RE. Impact of 18F-fluoride PET in patients with known prostate cancer: initial results from the National Oncologic PET Registry. J Nucl Med. 2014;55(4):574-81.
49. Hillner BE, Siegel BA, Hanna L, Duan F, Shields AF, Quinn B, et al. Impact of (18)F-Fluoride PET on Intended Management of Patients with Cancers Other Than Prostate Cancer: Results from the National Oncologic PET Registry. J Nucl Med. 2014;55(7):1054-61.
50. Dyrberg E, Hendel HW, Huynh THV, Klausen TW, Logager VB, Madsen C, et al. (68)Ga-PSMA-PET/CT in comparison with (18)F-fluoride-PET/CT and whole-body MRI for the detection of bone metastases in patients with prostate cancer: a prospective diagnostic accuracy study. Eur Radiol. 2019;29(3):1221-30.
51. Evans JD, Jethwa KR, Ost P, Williams S, Kwon ED, Lowe VJ, et al. Prostate cancer-specific PET radiotracers: A review on the clinical utility in recurrent disease. Pract Radiat Oncol. 2018;8(1):28-39.
52. Fraum TJ, Ludwig DR, Kim EH, Schroeder P, Hope TA, Ippolito JE. Prostate cancer PET tracers: essentials for the urologist. Can J Urol. 2018;25(4):9371-83.
53. Spratt DE, McHugh DJ, Morris MJ, Morgans AK. Management of Biochemically Recurrent Prostate Cancer: Ensuring the Right Treatment of the Right Patient at the Right Time. Am Soc Clin Oncol Educ Book. 2018;38:355-62.
54. Wallitt KL, Khan SR, Dubash S, Tam HH, Khan S, Barwick TD. Clinical PET Imaging in Prostate Cancer. Radiographics. 2017;37(5):1512-36.
55. Schuster DM, Nanni C, Fanti S. PET Tracers Beyond FDG in Prostate Cancer. Semin Nucl Med. 2016;46(6):507-21.
56. Giovacchini G, Picchio M, Garcia-Parra R, Briganti A, Abdollah F, Gianolli L, et al. 11C-choline PET/CT predicts prostate cancer-specific survival in patients with biochemical failure during androgen-deprivation therapy. J Nucl Med. 2014;55(2):233-41.
57. Piccardo A, Paparo F, Piccazzo R, Naseri M, Ricci P, Marziano A, et al. Value of fused 18F-Choline-PET/MRI to evaluate prostate cancer relapse in

patients showing biochemical recurrence after EBRT: preliminary results. Biomed Res Int. 2014;2014:103718.
58. Dusing RW, Peng W, Lai SM, Grado GL, Holzbeierlein JM, Thrasher JB, et al. Prostate-specific antigen and prostate-specific antigen velocity as threshold indicators in 11C-acetate PET/CTAC scanning for prostate cancer recurrence. Clin Nucl Med. 2014;39(9):777-83.
59. Mohsen B, Giorgio T, Rasoul ZS, Werner L, Ali GR, Reza DK, et al. Application of C-11-acetate positron-emission tomography (PET) imaging in prostate cancer: systematic review and meta-analysis of the literature. BJU Int. 2013;112(8):1062-72.
60. Turkbey B, Mena E, Shih J, Pinto PA, Merino MJ, Lindenberg ML, et al. Localized prostate cancer detection with 18F FACBC PET/CT: comparison with MR imaging and histopathologic analysis. Radiology. 2014;270(3):849-56.
61. Odewole OA, Tade FI, Nieh PT, Savir-Baruch B, Jani AB, Master VA, et al. Recurrent prostate cancer detection with anti-3-[(18)F]FACBC PET/CT: comparison with CT. Eur J Nucl Med Mol Imaging. 2016;43(10):1773-83.
62. Nanni C, Schiavina R, Boschi S, Ambrosini V, Pettinato C, Brunocilla E, et al. Comparison of 18F-FACBC and 11C-choline PET/CT in patients with radically treated prostate cancer and biochemical relapse: preliminary results. Eur J Nucl Med Mol Imaging. 2013;40 Suppl 1:S11-7.
63. Nanni C, Schiavina R, Brunocilla E, Boschi S, Borghesi M, Zanoni L, et al. 18F-Fluciclovine PET/CT for the Detection of Prostate Cancer Relapse: A Comparison to 11C-Choline PET/CT. Clin Nucl Med. 2015;40(8):e386-91.
64. Parent EE, Schuster DM. Update on (18)F-Fluciclovine PET for Prostate Cancer Imaging. J Nucl Med. 2018;59(5):733-9.
65. Beattie BJ, Smith-Jones PM, Jhanwar YS, Schoder H, Schmidtlein CR, Morris MJ, et al. Pharmacokinetic assessment of the uptake of 16beta-18F-fluoro-5alpha-dihydrotestosterone (FDHT) in prostate tumors as measured by PET. J Nucl Med. 2010;51(2):183-92.
66. Rathkopf DE, Morris MJ, Fox JJ, Danila DC, Slovin SF, Hager JH, et al. Phase I study of ARN-509, a novel antiandrogen, in the treatment of castration-resistant prostate cancer. J Clin Oncol. 2013;31(28):3525-30.
67. Bouchelouche K, Choyke PL, Capala J. Prostate specific membrane antigen- a target for imaging and therapy with radionuclides. Discov Med. 2010;9(44):55-61.
68. Wright GL, Jr., Haley C, Beckett ML, Schellhammer PF. Expression of prostate-specific membrane antigen in normal, benign, and malignant prostate tissues. Urol Oncol. 1995;1(1):18-28.
69. ProstaScint Product Approval Information - Licensing Action Rockville, MD: U.S. Food and Drug Administration 1996 [Available from: https://www.accessdata.fda.gov/drugsatfda_docs/appletter/1996/capcyt102896L.htm.

70. Wilkinson S, Chodak G. The role of 111indium-capromab pendetide imaging for assessing biochemical failure after radical prostatectomy. J Urol. 2004;172(1):133-6.
71. Lamb HM, Faulds D. Capromab pendetide. A review of its use as an imaging agent in prostate cancer. Drugs Aging. 1998;12(4):293-304.
72. Bander NH, Milowsky MI, Nanus DM, Kostakoglu L, Vallabhajosula S, Goldsmith SJ. Phase I trial of 177lutetium-labeled J591, a monoclonal antibody to prostate-specific membrane antigen, in patients with androgen-independent prostate cancer. J Clin Oncol. 2005;23(21):4591-601.
73. Milowsky MI, Nanus DM, Kostakoglu L, Vallabhajosula S, Goldsmith SJ, Bander NH. Phase I trial of yttrium-90-labeled anti-prostate-specific membrane antigen monoclonal antibody J591 for androgen-independent prostate cancer. J Clin Oncol. 2004;22(13):2522-31.
74. Osborne JR, Green DA, Spratt DE, Lyashchenko S, Fareedy SB, Robinson BD, et al. A prospective pilot study of (89)Zr-J591/prostate specific membrane antigen positron emission tomography in men with localized prostate cancer undergoing radical prostatectomy. J Urol. 2014;191(5):1439-45.
75. Tagawa ST, Milowsky MI, Morris M, Vallabhajosula S, Christos P, Akhtar NH, et al. Phase II study of Lutetium-177-labeled anti-prostate-specific membrane antigen monoclonal antibody J591 for metastatic castration-resistant prostate cancer. Clin Cancer Res. 2013;19(18):5182-91.
76. Pandit-Taskar N, O'Donoghue JA, Durack JC, Lyashchenko SK, Cheal SM, Beylergil V, et al. A Phase I/II Study for Analytic Validation of 89Zr-J591 ImmunoPET as a Molecular Imaging Agent for Metastatic Prostate Cancer. Clin Cancer Res. 2015;21(23):5277-85.
77. Bouchelouche K, Choyke PL. Prostate-specific membrane antigen positron emission tomography in prostate cancer: a step toward personalized medicine. Curr Opin Oncol. 2016;28(3):216-21.
78. Bakht MK, Derecichei I, Li Y, Ferraiuolo RM, Dunning M, Oh SW, et al. Neuroendocrine differentiation of prostate cancer leads to PSMA suppression. Endocr Relat Cancer. 2018;26(2):131-46.
79. Liu T, Wu LY, Fulton MD, Johnson JM, Berkman CE. Prolonged androgen deprivation leads to downregulation of androgen receptor and prostate-specific membrane antigen in prostate cancer cells. Int J Oncol. 2012;41(6):2087-92.
80. Corbeil D, Karbanova J, Fargeas CA, Jaszai J. Prominin-1 (CD133): Molecular and Cellular Features Across Species. Adv Exp Med Biol. 2013;777:3-24.
81. Liu Y, Ren S, Xie L, Cui C, Xing Y, Liu C, et al. Mutation of N-linked glycosylation at Asn548 in CD133 decreases its ability to promote hepatoma cell growth. Oncotarget. 2015;6(24):20650-60.
82. Elsaba TM, Martinez-Pomares L, Robins AR, Crook S, Seth R, Jackson D, et al. The stem cell marker CD133 associates with enhanced colony formation and cell motility in colorectal cancer. PLoS One. 2010;5(5):e10714.

83. Kemper K, Sprick MR, de Bree M, Scopelliti A, Vermeulen L, Hoek M, et al. The AC133 epitope, but not the CD133 protein, is lost upon cancer stem cell differentiation. Cancer Res. 2010;70(2):719-29.
84. Thamm K, Graupner S, Werner C, Huttner WB, Corbeil D. Monoclonal Antibodies 13A4 and AC133 Do Not Recognize the Canine Ortholog of Mouse and Human Stem Cell Antigen Prominin-1 (CD133). PLoS One. 2016;11(10):e0164079.
85. Bidlingmaier S, Zhu X, Liu B. The utility and limitations of glycosylated human CD133 epitopes in defining cancer stem cells. J Mol Med (Berl). 2008;86(9):1025-32.
86. Shmelkov SV, Jun L, St Clair R, McGarrigle D, Derderian CA, Usenko JK, et al. Alternative promoters regulate transcription of the gene that encodes stem cell surface protein AC133. Blood. 2004;103(6):2055-61.
87. Grosse-Gehling P, Fargeas CA, Dittfeld C, Garbe Y, Alison MR, Corbeil D, et al. CD133 as a biomarker for putative cancer stem cells in solid tumours: limitations, problems and challenges. J Pathol. 2013;229(3):355-78.
88. Fargeas CA, Joester A, Missol-Kolka E, Hellwig A, Huttner WB, Corbeil D. Identification of novel Prominin-1/CD133 splice variants with alternative C-termini and their expression in epididymis and testis. J Cell Sci. 2004;117(Pt 18):4301-11.
89. Corbeil D, Roper K, Fargeas CA, Joester A, Huttner WB. Prominin: a story of cholesterol, plasma membrane protrusions and human pathology. Traffic. 2001;2(2):82-91.
90. Su YJ, Lin WH, Chang YW, Wei KC, Liang CL, Chen SC, et al. Polarized cell migration induces cancer type-specific CD133/integrin/Src/Akt/GSK3beta/beta-catenin signaling required for maintenance of cancer stem cell properties. Oncotarget. 2015;6(35):38029-45.
91. Roper K, Corbeil D, Huttner WB. Retention of prominin in microvilli reveals distinct cholesterol-based lipid micro-domains in the apical plasma membrane. Nat Cell Biol. 2000;2(9):582-92.
92. Simons K, Toomre D. Lipid rafts and signal transduction. Nat Rev Mol Cell Biol. 2000;1(1):31-9.
93. Zacchigna S, Oh H, Wilsch-Brauninger M, Missol-Kolka E, Jaszai J, Jansen S, et al. Loss of the cholesterol-binding protein prominin-1/CD133 causes disk dysmorphogenesis and photoreceptor degeneration. J Neurosci. 2009;29(7):2297-308.
94. Kosodo Y, Roper K, Haubensak W, Marzesco AM, Corbeil D, Huttner WB. Asymmetric distribution of the apical plasma membrane during neurogenic divisions of mammalian neuroepithelial cells. EMBO J. 2004;23(11):2314-24.
95. Bauer N, Wilsch-Brauninger M, Karbanova J, Fonseca AV, Strauss D, Freund D, et al. Haematopoietic stem cell differentiation promotes the release of prominin-1/CD133-containing membrane vesicles--a role of the endocytic-exocytic pathway. EMBO Mol Med. 2011;3(7):398-409.

96. Marzesco AM, Janich P, Wilsch-Brauninger M, Dubreuil V, Langenfeld K, Corbeil D, et al. Release of extracellular membrane particles carrying the stem cell marker prominin-1 (CD133) from neural progenitors and other epithelial cells. J Cell Sci. 2005;118(Pt 13):2849-58.
97. Bauer N, Fonseca AV, Florek M, Freund D, Jaszai J, Bornhauser M, et al. New insights into the cell biology of hematopoietic progenitors by studying prominin-1 (CD133). Cells Tissues Organs. 2008;188(1-2):127-38.
98. Glumac PM, LeBeau AM. The role of CD133 in cancer: a concise review. Clin Transl Med. 2018;7(1):18.
99. Li Z. CD133: a stem cell biomarker and beyond. Exp Hematol Oncol. 2013;2(1):17.
100. Wu Y, Wu PY. CD133 as a marker for cancer stem cells: progresses and concerns. Stem Cells Dev. 2009;18(8):1127-34.
101. Jaksch M, Munera J, Bajpai R, Terskikh A, Oshima RG. Cell cycle-dependent variation of a CD133 epitope in human embryonic stem cell, colon cancer, and melanoma cell lines. Cancer Res. 2008;68(19):7882-6.
102. Bussolati B, Moggio A, Collino F, Aghemo G, D'Armento G, Grange C, et al. Hypoxia modulates the undifferentiated phenotype of human renal inner medullary CD133+ progenitors through Oct4/miR-145 balance. Am J Physiol Renal Physiol. 2012;302(1):F116-28.
103. Maeda K, Ding Q, Yoshimitsu M, Kuwahata T, Miyazaki Y, Tsukasa K, et al. CD133 Modulate HIF-1alpha Expression under Hypoxia in EMT Phenotype Pancreatic Cancer Stem-Like Cells. Int J Mol Sci. 2016;17(7).
104. Soeda A, Park M, Lee D, Mintz A, Androutsellis-Theotokis A, McKay RD, et al. Hypoxia promotes expansion of the CD133-positive glioma stem cells through activation of HIF-1alpha. Oncogene. 2009;28(45):3949-59.
105. Iida H, Suzuki M, Goitsuka R, Ueno H. Hypoxia induces CD133 expression in human lung cancer cells by up-regulation of OCT3/4 and SOX2. Int J Oncol. 2012;40(1):71-9.
106. Griguer CE, Oliva CR, Gobin E, Marcorelles P, Benos DJ, Lancaster JR, Jr., et al. CD133 is a marker of bioenergetic stress in human glioma. PLoS One. 2008;3(11):e3655.
107. Yang C, Yang Y, Gupta N, Liu X, He A, Liu L, et al. Pentaspan membrane glycoprotein, prominin-1, is involved in glucose metabolism and cytoskeleton alteration. Biochemistry (Mosc). 2007;72(8):854-62.
108. Bourseau-Guilmain E, Griveau A, Benoit JP, Garcion E. The importance of the stem cell marker prominin-1/CD133 in the uptake of transferrin and in iron metabolism in human colon cancer Caco-2 cells. PLoS One. 2011;6(9):e25515.
109. Bisson I, Prowse DM. WNT signaling regulates self-renewal and differentiation of prostate cancer cells with stem cell characteristics. Cell Res. 2009;19(6):683-97.
110. Rappa G, Mercapide J, Anzanello F, Le TT, Johlfs MG, Fiscus RR, et al. Wnt interaction and extracellular release of prominin-1/CD133 in human malignant melanoma cells. Exp Cell Res. 2013;319(6):810-9.

111. Mak AB, Nixon AM, Kittanakom S, Stewart JM, Chen GI, Curak J, et al. Regulation of CD133 by HDAC6 promotes beta-catenin signaling to suppress cancer cell differentiation. Cell Rep. 2012;2(4):951-63.
112. Brossa A, Papadimitriou E, Collino F, Incarnato D, Oliviero S, Camussi G, et al. Role of CD133 Molecule in Wnt Response and Renal Repair. Stem Cells Transl Med. 2018;7(3):283-94.
113. Dubrovska A, Kim S, Salamone RJ, Walker JR, Maira SM, Garcia-Echeverria C, et al. The role of PTEN/Akt/PI3K signaling in the maintenance and viability of prostate cancer stem-like cell populations. Proc Natl Acad Sci U S A. 2009;106(1):268-73.
114. Sahlberg SH, Spiegelberg D, Glimelius B, Stenerlow B, Nestor M. Evaluation of cancer stem cell markers CD133, CD44, CD24: association with AKT isoforms and radiation resistance in colon cancer cells. PLoS One. 2014;9(4):e94621.
115. Wei Y, Jiang Y, Zou F, Liu Y, Wang S, Xu N, et al. Activation of PI3K/Akt pathway by CD133-p85 interaction promotes tumorigenic capacity of glioma stem cells. Proc Natl Acad Sci U S A. 2013;110(17):6829-34.
116. Shmelkov SV, Butler JM, Hooper AT, Hormigo A, Kushner J, Milde T, et al. CD133 expression is not restricted to stem cells, and both CD133+ and CD133- metastatic colon cancer cells initiate tumors. J Clin Invest. 2008;118(6):2111-20.
117. Richardson GD, Robson CN, Lang SH, Neal DE, Maitland NJ, Collins AT. CD133, a novel marker for human prostatic epithelial stem cells. J Cell Sci. 2004;117(Pt 16):3539-45.
118. Leong KG, Wang BE, Johnson L, Gao WQ. Generation of a prostate from a single adult stem cell. Nature. 2008;456(7223):804-8.
119. Signoretti S, Waltregny D, Dilks J, Isaac B, Lin D, Garraway L, et al. p63 is a prostate basal cell marker and is required for prostate development. Am J Pathol. 2000;157(6):1769-75.
120. Brawer MK, Peehl DM, Stamey TA, Bostwick DG. Keratin immunoreactivity in the benign and neoplastic human prostate. Cancer Res. 1985;45(8):3663-7.
121. De Marzo AM, Meeker AK, Epstein JI, Coffey DS. Prostate stem cell compartments: expression of the cell cycle inhibitor p27Kip1 in normal, hyperplastic, and neoplastic cells. Am J Pathol. 1998;153(3):911-9.
122. Alam TN, O'Hare MJ, Laczko I, Freeman A, Al-Beidh F, Masters JR, et al. Differential expression of CD44 during human prostate epithelial cell differentiation. J Histochem Cytochem. 2004;52(8):1083-90.
123. Bello-DeOcampo D, Kleinman HK, Deocampo ND, Webber MM. Laminin-1 and alpha6beta1 integrin regulate acinar morphogenesis of normal and malignant human prostate epithelial cells. Prostate. 2001;46(2):142-53.
124. Knox JD, Cress AE, Clark V, Manriquez L, Affinito KS, Dalkin BL, et al. Differential expression of extracellular matrix molecules and the alpha 6-integrins in the normal and neoplastic prostate. Am J Pathol. 1994;145(1):167-74.

125. Lawson DA, Xin L, Lukacs RU, Cheng D, Witte ON. Isolation and functional characterization of murine prostate stem cells. Proc Natl Acad Sci U S A. 2007;104(1):181-6.
126. Goldstein AS, Lawson DA, Cheng D, Sun W, Garraway IP, Witte ON. Trop2 identifies a subpopulation of murine and human prostate basal cells with stem cell characteristics. Proc Natl Acad Sci U S A. 2008;105(52):20882-7.
127. Petkova N, Hennenlotter J, Sobiesiak M, Todenhofer T, Scharpf M, Stenzl A, et al. Surface CD24 distinguishes between low differentiated and transit-amplifying cells in the basal layer of human prostate. Prostate. 2013;73(14):1576-90.
128. Wang Y, Hayward S, Cao M, Thayer K, Cunha G. Cell differentiation lineage in the prostate. Differentiation. 2001;68(4-5):270-9.
129. Wang X, Kruithof-de Julio M, Economides KD, Walker D, Yu H, Halili MV, et al. A luminal epithelial stem cell that is a cell of origin for prostate cancer. Nature. 2009;461(7263):495-500.
130. Wang W, Epstein JI. Small cell carcinoma of the prostate. A morphologic and immunohistochemical study of 95 cases. Am J Surg Pathol. 2008;32(1):65-71.
131. Beltran H, Rickman DS, Park K, Chae SS, Sboner A, MacDonald TY, et al. Molecular characterization of neuroendocrine prostate cancer and identification of new drug targets. Cancer Discov. 2011;1(6):487-95.
132. Jaworska D, Krol W, Szliszka E. Prostate Cancer Stem Cells: Research Advances. Int J Mol Sci. 2015;16(11):27433-49.
133. Taylor RA, Toivanen R, Risbridger GP. Stem cells in prostate cancer: treating the root of the problem. Endocr Relat Cancer. 2010;17(4):R273-85.
134. Toivanen R, Shen MM. Prostate organogenesis: tissue induction, hormonal regulation and cell type specification. Development. 2017;144(8):1382-98.
135. Collins AT, Habib FK, Maitland NJ, Neal DE. Identification and isolation of human prostate epithelial stem cells based on alpha(2)beta(1)-integrin expression. J Cell Sci. 2001;114(Pt 21):3865-72.
136. Schmelz M, Moll R, Hesse U, Prasad AR, Gandolfi JA, Hasan SR, et al. Identification of a stem cell candidate in the normal human prostate gland. Eur J Cell Biol. 2005;84(2-3):341-54.
137. Missol-Kolka E, Karbanova J, Janich P, Haase M, Fargeas CA, Huttner WB, et al. Prominin-1 (CD133) is not restricted to stem cells located in the basal compartment of murine and human prostate. Prostate. 2011;71(3):254-67.
138. Wei X, Orjalo AV, Xin L. CD133 does not enrich for the stem cell activity in vivo in adult mouse prostates. Stem Cell Res. 2016;16(3):597-606.
139. Immervoll H, Hoem D, Sakariassen PO, Steffensen OJ, Molven A. Expression of the "stem cell marker" CD133 in pancreas and pancreatic ductal adenocarcinomas. BMC Cancer. 2008;8:48.

140. Lardon J, Corbeil D, Huttner WB, Ling Z, Bouwens L. Stem cell marker prominin-1/AC133 is expressed in duct cells of the adult human pancreas. Pancreas. 2008;36(1):e1-6.
141. Rountree CB, Ding W, Dang H, Vankirk C, Crooks GM. Isolation of CD133+ liver stem cells for clonal expansion. J Vis Exp. 2011(56).
142. Schmelzer E, Zhang L, Bruce A, Wauthier E, Ludlow J, Yao HL, et al. Human hepatic stem cells from fetal and postnatal donors. J Exp Med. 2007;204(8):1973-87.
143. Feng HL, Liu YQ, Yang LJ, Bian XC, Yang ZL, Gu B, et al. Expression of CD133 correlates with differentiation of human colon cancer cells. Cancer Biol Ther. 2010;9(3):216-23.
144. Karbanova J, Missol-Kolka E, Fonseca AV, Lorra C, Janich P, Hollerova H, et al. The stem cell marker CD133 (Prominin-1) is expressed in various human glandular epithelia. J Histochem Cytochem. 2008;56(11):977-93.
145. Jaszai J, Janich P, Farkas LM, Fargeas CA, Huttner WB, Corbeil D. Differential expression of Prominin-1 (CD133) and Prominin-2 in major cephalic exocrine glands of adult mice. Histochem Cell Biol. 2007;128(5):409-19.
146. Sagrinati C, Netti GS, Mazzinghi B, Lazzeri E, Liotta F, Frosali F, et al. Isolation and characterization of multipotent progenitor cells from the Bowman's capsule of adult human kidneys. J Am Soc Nephrol. 2006;17(9):2443-56.
147. Fukamachi H, Shimada S, Ito K, Ito Y, Yuasa Y. CD133 is a marker of gland-forming cells in gastric tumors and Sox17 is involved in its regulation. Cancer Sci. 2011;102(7):1313-21.
148. Collins AT, Berry PA, Hyde C, Stower MJ, Maitland NJ. Prospective identification of tumorigenic prostate cancer stem cells. Cancer Res. 2005;65(23):10946-51.
149. Vander Griend DJ, Karthaus WL, Dalrymple S, Meeker A, DeMarzo AM, Isaacs JT. The role of CD133 in normal human prostate stem cells and malignant cancer-initiating cells. Cancer Res. 2008;68(23):9703-11.
150. Zhou J, Wang H, Cannon V, Wolcott KM, Song H, Yates C. Side population rather than CD133(+) cells distinguishes enriched tumorigenicity in hTERT-immortalized primary prostate cancer cells. Mol Cancer. 2011;10:112.
151. Wang L, Huang X, Zheng X, Wang X, Li S, Zhang L, et al. Enrichment of prostate cancer stem-like cells from human prostate cancer cell lines by culture in serum-free medium and chemoradiotherapy. Int J Biol Sci. 2013;9(5):472-9.
152. Reyes EE, Gillard M, Duggan R, Wroblewski K, Kregel S, Isikbay M, et al. Molecular analysis of CD133-positive circulating tumor cells from patients with metastatic castration-resistant prostate cancer. J Transl Sci. 2015;1(1).
153. Isaacs JT. Prostate stem cells and benign prostatic hyperplasia. Prostate. 2008;68(9):1025-34.
154. Chen X, Rycaj K, Liu X, Tang DG. New insights into prostate cancer stem cells. Cell Cycle. 2013;12(4):579-86.
155. Corbeil D. Prominin-1 (CD133): New Insights on Stem & Cancer Stem Cell Biology. Advances in Experimental Medicine and Biology: Springer; 2013.

156. Jang JW, Song Y, Kim SH, Kim J, Seo HR. Potential mechanisms of CD133 in cancer stem cells. Life Sci. 2017;184:25-9.
157. Miraglia S, Godfrey W, Yin AH, Atkins K, Warnke R, Holden JT, et al. A novel five-transmembrane hematopoietic stem cell antigen: isolation, characterization, and molecular cloning. Blood. 1997;90(12):5013-21.
158. Yin AH, Miraglia S, Zanjani ED, Almeida-Porada G, Ogawa M, Leary AG, et al. AC133, a novel marker for human hematopoietic stem and progenitor cells. Blood. 1997;90(12):5002-12.
159. Maitland NJ, Collins AT. Prostate cancer stem cells: a new target for therapy. J Clin Oncol. 2008;26(17):2862-70.
160. Green CL, Loken M, Buck D, Deeg HJ. Discordant expression of AC133 and AC141 in patients with myelodysplastic syndrome (MDS) and acute myelogeneous leukemia (AML). Leukemia. 2000;14(4):770-2.
161. Mallard BW, Tiralongo J. Cancer stem cell marker glycosylation: Nature, function and significance. Glycoconj J. 2017;34(4):441-52.
162. Barrantes-Freer A, Renovanz M, Eich M, Braukmann A, Sprang B, Spirin P, et al. CD133 Expression Is Not Synonymous to Immunoreactivity for AC133 and Fluctuates throughout the Cell Cycle in Glioma Stem-Like Cells. PLoS One. 2015;10(6):e0130519.
163. Osmond TL, Broadley KW, McConnell MJ. Glioblastoma cells negative for the anti-CD133 antibody AC133 express a truncated variant of the CD133 protein. Int J Mol Med. 2010;25(6):883-8.
164. Hermansen SK, Christensen KG, Jensen SS, Kristensen BW. Inconsistent immunohistochemical expression patterns of four different CD133 antibody clones in glioblastoma. J Histochem Cytochem. 2011;59(4):391-407.
165. Reyes EE, Kunovac SK, Duggan R, Kregel S, Vander Griend DJ. Growth kinetics of CD133-positive prostate cancer cells. Prostate. 2013;73(7):724-33.
166. Kim J, Stroud RM, Craik CS. Rapid identification of recombinant Fabs that bind to membrane proteins. Methods. 2011;55(4):303-9.
167. Schmittgen TD, Livak KJ. Analyzing real-time PCR data by the comparative C(T) method. Nat Protoc. 2008;3(6):1101-8.
168. Wang S, Zheng C, Liu Y, Zheng H, Wang Z. Construction of multiform scFv antibodies using linker peptide. J Genet Genomics. 2008;35(5):313-6.
169. Arndt KM, Muller KM, Pluckthun A. Factors influencing the dimer to monomer transition of an antibody single-chain Fv fragment. Biochemistry. 1998;37(37):12918-26.
170. Botchkina GI, Zuniga ES, Rowehl RH, Park R, Bhalla R, Bialkowska AB, et al. Prostate cancer stem cell-targeted efficacy of a new-generation taxoid, SBT-1214 and novel polyenolic zinc-binding curcuminoid, CMC2.24. PLoS One. 2013;8(9):e69884.
171. Ren F, Sheng WQ, Du X. CD133: a cancer stem cells marker, is used in colorectal cancers. World J Gastroenterol. 2013;19(17):2603-11.
172. Smith SA, Crowe JE, Jr. Use of Human Hybridoma Technology To Isolate Human Monoclonal Antibodies. Microbiol Spectr. 2015;3(1):AID-0027-2014.

173. Baker M. Reproducibility crisis: Blame it on the antibodies. Nature. 2015;521(7552):274-6.
174. Marx V. Finding the right antibody for the job. Nat Methods. 2013;10(8):703-7.
175. Laffly E, Sodoyer R. Monoclonal and recombinant antibodies, 30 years after. Hum Antibodies. 2005;14(1-2):33-55.
176. Fargeas CA, Huttner WB, Corbeil D. Nomenclature of prominin-1 (CD133) splice variants - an update. Tissue Antigens. 2007;69(6):602-6.
177. Koochekpour S, Maresh GA, Katner A, Parker-Johnson K, Lee TJ, Hebert FE, et al. Establishment and characterization of a primary androgen-responsive African-American prostate cancer cell line, E006AA. Prostate. 2004;60(2):141-52.
178. Koochekpour S, Willard SS, Shourideh M, Ali S, Liu C, Azabdaftari G, et al. Establishment and characterization of a highly tumorigenic African American prostate cancer cell line, E006AA-hT. Int J Biol Sci. 2014;10(8):834-45.
179. D'Antonio JM, Vander Griend DJ, Antony L, Ndikuyeze G, Dalrymple SL, Koochekpour S, et al. Loss of androgen receptor-dependent growth suppression by prostate cancer cells can occur independently from acquiring oncogenic addiction to androgen receptor signaling. PLoS One. 2010;5(7):e11475.
180. Beltran H, Prandi D, Mosquera JM, Benelli M, Puca L, Cyrta J, et al. Divergent clonal evolution of castration-resistant neuroendocrine prostate cancer. Nat Med. 2016;22(3):298-305.
181. Nevedomskaya E, Baumgart SJ, Haendler B. Recent Advances in Prostate Cancer Treatment and Drug Discovery. Int J Mol Sci. 2018;19(5).
182. Rickman DS, Beltran H, Demichelis F, Rubin MA. Biology and evolution of poorly differentiated neuroendocrine tumors. Nat Med. 2017;23(6):1-10.
183. Wadosky KM, Koochekpour S. Molecular mechanisms underlying resistance to androgen deprivation therapy in prostate cancer. Oncotarget. 2016;7(39):64447-70.
184. Yap TA, Smith AD, Ferraldeschi R, Al-Lazikani B, Workman P, de Bono JS. Drug discovery in advanced prostate cancer: translating biology into therapy. Nat Rev Drug Discov. 2016;15(10):699-718.
185. Nouri M, Caradec J, Lubik AA, Li N, Hollier BG, Takhar M, et al. Therapy-induced developmental reprogramming of prostate cancer cells and acquired therapy resistance. Oncotarget. 2017;8(12):18949-67.
186. Bluemn EG, Coleman IM, Lucas JM, Coleman RT, Hernandez-Lopez S, Tharakan R, et al. Androgen Receptor Pathway-Independent Prostate Cancer Is Sustained through FGF Signaling. Cancer Cell. 2017;32(4):474-89 e6.
187. Ather MH, Abbas F, Faruqui N, Israr M, Pervez S. Correlation of three immunohistochemically detected markers of neuroendocrine differentiation with clinical predictors of disease progression in prostate cancer. BMC Urol. 2008;8:21.
188. Gupta K, Gupta S. Neuroendocrine differentiation in prostate cancer: key epigenetic players. Transl Cancer Res. 2017;6(Suppl 1):S104-S8.

189. Lindenberg ML, Turkbey B, Mena E, Choyke PL. Imaging Locally Advanced, Recurrent, and Metastatic Prostate Cancer: A Review. JAMA Oncol. 2017;3(10):1415-22.
190. Halabi S, Kelly WK, Ma H, Zhou H, Solomon NC, Fizazi K, et al. Meta-Analysis Evaluating the Impact of Site of Metastasis on Overall Survival in Men With Castration-Resistant Prostate Cancer. J Clin Oncol. 2016;34(14):1652-9.
191. Umbehr MH, Muntener M, Hany T, Sulser T, Bachmann LM. The role of 11C-choline and 18F-fluorocholine positron emission tomography (PET) and PET/CT in prostate cancer: a systematic review and meta-analysis. Eur Urol. 2013;64(1):106-17.
192. Tosoian JJ, Gorin MA, Rowe SP, Andreas D, Szabo Z, Pienta KJ, et al. Correlation of PSMA-Targeted (18)F-DCFPyL PET/CT Findings With Immunohistochemical and Genomic Data in a Patient With Metastatic Neuroendocrine Prostate Cancer. Clin Genitourin Cancer. 2017;15(1):e65-e8.
193. Parimi V, Goyal R, Poropatich K, Yang XJ. Neuroendocrine differentiation of prostate cancer: a review. Am J Clin Exp Urol. 2014;2(4):273-85.
194. Glumac PM, Forster CL, Zhou H, Murugan P, Gupta S, LeBeau AM. The identification of a novel antibody for CD133 using human antibody phage display. Prostate. 2018;78(13):981-91.
195. Kumar A, Coleman I, Morrissey C, Zhang X, True LD, Gulati R, et al. Substantial interindividual and limited intraindividual genomic diversity among tumors from men with metastatic prostate cancer. Nat Med. 2016;22(4):369-78.
196. Roudier MP, Winters BR, Coleman I, Lam HM, Zhang X, Coleman R, et al. Characterizing the molecular features of ERG-positive tumors in primary and castration resistant prostate cancer. Prostate. 2016;76(9):810-22.
197. Zeglis BM, Lewis JS. The bioconjugation and radiosynthesis of 89Zr-DFO-labeled antibodies. J Vis Exp. 2015(96).
198. Nguyen HM, Vessella RL, Morrissey C, Brown LG, Coleman IM, Higano CS, et al. LuCaP Prostate Cancer Patient-Derived Xenografts Reflect the Molecular Heterogeneity of Advanced Disease an--d Serve as Models for Evaluating Cancer Therapeutics. Prostate. 2017;77(6):654-71.
199. Holland JP, Divilov V, Bander NH, Smith-Jones PM, Larson SM, Lewis JS. 89Zr-DFO-J591 for immunoPET of prostate-specific membrane antigen expression in vivo. J Nucl Med. 2010;51(8):1293-300.
200. Borjesson PK, Jauw YW, Boellaard R, de Bree R, Comans EF, Roos JC, et al. Performance of immuno-positron emission tomography with zirconium-89-labeled chimeric monoclonal antibody U36 in the detection of lymph node metastases in head and neck cancer patients. Clin Cancer Res. 2006;12(7 Pt 1):2133-40.
201. Perk LR, Stigter-van Walsum M, Visser GW, Kloet RW, Vosjan MJ, Leemans CR, et al. Quantitative PET imaging of Met-expressing human cancer xenografts with 89Zr-labelled monoclonal antibody DN30. Eur J Nucl Med Mol Imaging. 2008;35(10):1857-67.

202. Dijkers EC, Oude Munnink TH, Kosterink JG, Brouwers AH, Jager PL, de Jong JR, et al. Biodistribution of 89Zr-trastuzumab and PET imaging of HER2-positive lesions in patients with metastatic breast cancer. Clin Pharmacol Ther. 2010;87(5):586-92.
203. Kita Y, Goto T, Akamatsu S, Yamasaki T, Inoue T, Ogawa O, et al. Castration-Resistant Prostate Cancer Refractory to Second-Generation Androgen Receptor Axis-Targeted Agents: Opportunities and Challenges. Cancers (Basel). 2018;10(10).
204. Gaedicke S, Braun F, Prasad S, Machein M, Firat E, Hettich M, et al. Noninvasive positron emission tomography and fluorescence imaging of CD133+ tumor stem cells. Proc Natl Acad Sci U S A. 2014;111(6):E692-701.
205. Burrell JS, Walker-Samuel S, Boult JK, Baker LC, Jamin Y, Halliday J, et al. Investigating the Vascular Phenotype of Subcutaneously and Orthotopically Propagated PC3 Prostate Cancer Xenografts Using Combined Carbogen Ultrasmall Superparamagnetic Iron Oxide MRI. Top Magn Reson Imaging. 2016;25(5):237-43.
206. Song H, Shahverdi K, Huso DL, Wang Y, Fox JJ, Hobbs RF, et al. An immunotolerant HER-2/neu transgenic mouse model of metastatic breast cancer. Clin Cancer Res. 2008;14(19):6116-24.
207. Werbeck JL, Thudi NK, Martin CK, Premanandan C, Yu L, Ostrowksi MC, et al. Tumor microenvironment regulates metastasis and metastasis genes of mouse MMTV-PymT mammary cancer cells in vivo. Vet Pathol. 2014;51(4):868-81.
208. Wang M, Zhao J, Zhang L, Wei F, Lian Y, Wu Y, et al. Role of tumor microenvironment in tumorigenesis. J Cancer. 2017;8(5):761-73.
209. Singh SK, Hawkins C, Clarke ID, Squire JA, Bayani J, Hide T, et al. Identification of human brain tumour initiating cells. Nature. 2004;432(7015):396-401.
210. O'Brien CA, Pollett A, Gallinger S, Dick JE. A human colon cancer cell capable of initiating tumour growth in immunodeficient mice. Nature. 2007;445(7123):106-10.
211. Saeednejad Zanjani L, Madjd Z, Abolhasani M, Andersson Y, Rasti A, Shariftabrizi A, et al. Cytoplasmic expression of CD133 stemness marker is associated with tumor aggressiveness in clear cell renal cell carcinoma. Exp Mol Pathol. 2017;103(2):218-28.
212. Yan X, Ma L, Yi D, Yoon JG, Diercks A, Foltz G, et al. A CD133-related gene expression signature identifies an aggressive glioblastoma subtype with excessive mutations. Proc Natl Acad Sci U S A. 2011;108(4):1591-6.
213. Chen S, Song X, Chen Z, Li X, Li M, Liu H, et al. CD133 expression and the prognosis of colorectal cancer: a systematic review and meta-analysis. PLoS One. 2013;8(2):e56380.
214. Tagawa ST. Neoadjuvant J591 Treatment for Prostate Cancer New York, NY: Weill Cornell Medical College; 2019 [Available from: https://ClinicalTrials.gov/show/NCT02693860.

215. Tagawa ST. Radioimmunotherapy in Prostate Cancer Using 177Lu-J591 Antibody New York, NY: Weill Cornell Medical College-New York Presbyterian Hospital; 2019 [Available from: https://ClinicalTrials.gov/show/NCT00538668.
216. Tagawa ST. Docetaxel/Prednisone Plus Fractionated 177Lu- J591 Antibody for Metastatic, Castrate-resistant Prostate Cancer New York, NY: Weill Cornell Medical College; 2018 [Available from: https://ClinicalTrials.gov/show/NCT00916123.
217. Tagawa ST. 177Lu Radiolabeled Monoclonal Antibody HuJ591 (177Lu-J591) and Ketoconazole in Patients With Prostate Cancer New York, NY: Weill Medical College of Cornell University; 2019 [Available from: https://ClinicalTrials.gov/show/NCT00859781.
218. Tagawa ST. Phase I Trial of 225Ac−J591 in Patients With mCRPC New York, NY: Weill Cornell Medical College; 2018 [Available from: https://ClinicalTrials.gov/show/NCT03276572.
219. Arndt K, Grinenko T, Mende N, Reichert D, Portz M, Ripich T, et al. CD133 is a modifier of hematopoietic progenitor frequencies but is dispensable for the maintenance of mouse hematopoietic stem cells. Proc Natl Acad Sci U S A. 2013;110(14):5582-7.
220. O43490 (PROM1_HUMAN) [Internet]. Available from: https://www.uniprot.org/uniprot/O43490#cross_references.
221. You H, Ding W, Rountree CB. Epigenetic regulation of cancer stem cell marker CD133 by transforming growth factor-beta. Hepatology. 2010;51(5):1635-44.
222. Sheng X, Li Z, Wang DL, Li WB, Luo Z, Chen KH, et al. Isolation and enrichment of PC-3 prostate cancer stem-like cells using MACS and serum-free medium. Oncol Lett. 2013;5(3):787-92.